CONFIDENTIAL

~~537~~

~~Consolidated Vultee~~

~~KAY 4/11~~

~~CONFIDENTIAL~~

~~FILE~~

NATIONAL ADVISORY COMMITTEE FOR AERONAUTICS

RESEARCH MEMORANDUM

for the

Bureau of Aeronautics, Navy Department

HIGH-SPEED LONGITUDINAL-STABILITY AND -CONTROL CHARACTERISTICS OF THE CONSOLIDATED VULTEE LARK MISSILE AS PREDICTED FROM WIND-TUNNEL TESTS (TED No. NACA 2391)

By John A. Axelson and Andrew Martin

Ames Aeronautical Laboratory
Moffett Field, Calif.

12-13-46

NATIONAL ADVISORY COMMITTEE FOR AERONAUTICS

RESEARCH MEMORANDUM

for the

Bureau of Aeronautics, Navy Department

HIGH-SPEED LONGITUDINAL-STABILITY AND -CONTROL CHARACTERISTICS OF THE CONSOLIDATED VULTEE LARK MISSILE AS PREDICTED FROM WIND-TUNNEL TESTS (TED No. NACA 2391)

By John A. Axelson and Andrew Martin

SUMMARY

A high-speed wind-tunnel investigation of the aerodynamic characteristics of a full-scale model of the Consolidated Vultee Lark indicates that the missile possesses satisfactory longitudinal-stability and -control characteristics throughout the Mach number range from 0.2 to 0.85, but that the maximum lift coefficients developed are not high enough to insure interception of the target at high altitudes. A reduction in wing loading appears advisable. Although the static longitudinal stability at zero angle of attack changes with Mach number and with lift coefficient, satisfactory control should be possible at all times as the tails retain their relatively large effectiveness throughout the range of Mach numbers and lift coefficients tested. Minimum stability and maximum maneuverability occur around 0.80 Mach number and 0.2 lift coefficient, which corresponds to level flight

conditions of the missile. The optimum ratio of tail-to-wing deflection is 0.4.

INTRODUCTION

At the request of the Bureau of Aeronautics, Navy Department, high-speed wind-tunnel tests were conducted to determine the high-speed longitudinal-stability and -control characteristics of a full-scale model of the Consolidated Vultee Lark, bearing the Navy designation KAY-1.

The model KAY-1 Lark, a pilotless winged missile intended for use as an anti-aircraft weapon, is shown in figure 1. It is powered by two liquid-fuel rocket motors of 200- and 400-pound thrust. The missile attains a speed corresponding to a Mach number of 0.8 and has a flight duration of approximately 4 minutes.

In the performance of a mission, several different conditions of operation are encountered. These occur during the various phases of flight as follows:

1. For the launching phase, the missile, supported on a cradle, is catapulted into the air at an angle of 20° to 30° and is assisted by two 1000-pound thrust jato units. The missile and carriage accelerate to a speed of approximately 220 feet per second (150 mph) in approximately 0.55 second. The carriage decelerates because of drag and drops free.

2. The transition phase is the period of flight from the end of the launching to the attainment of controlled

flight conditions or jettisoning of the jato rockets whichever occurs later. The jato rockets jettison approximately 12 seconds after their start. For the remainder of the transition phase the aircraft is accelerated to a speed sufficiently high for maneuvering flight.

3. During climb and approach to the target, the missile is to be radio-controlled from the point of launching until the target is within target-seeker operating range.

4. The pursuit phase starts when the aircraft target-seeking equipment picks up the target. At this time the target seeker takes over in the missile and guides it on a homing course towards the target. When the missile is within 50 feet of the target, the fragmentation bomb in the nose is detonated.

The missile is controlled in flight by vertical and horizontal wings of variable incidence, each wing having full-span, plain flaps of 20 percent chord, and by two tails inclined at 45° to the horizontal. The wings, flaps, and tails, being linked together, deflect simultaneously. The wing and flap deflections bear the following relationship:

Wing incidence	Flap deflection
0°	0°
2	5.6
4	11.1
6	16.5
8	21.8
10	26.9
12	32

The ratio of tail deflection to wing deflection has been tentatively set at 0.4, but additional deflection of the tail is provided for in order to obtain balance. Small vanes protruding from the fuselage midway between the nose and wing actuate the tail mechanism to maintain zero angles of attack and yaw. Intelligence equipment within the missile keeps the horizontal wings level, preventing any roll. The vertical and horizontal wings operate independently. Aileron control is provided by differential operation of the vertical wing flaps. All turns are made at a set rate of turn; that is, for a desired angle of turn a definite time of application of control is required.

MODEL AND APPARATUS

The full-scale model of the Consolidated Vultee Lark was furnished by the Consolidated Vultee Aircraft Corporation. The dimensions of the model are presented in figure 1 and listed as follows:

Wing area, square feet	8.75
Wing chord (constant), feet	1.562
Wing span, feet	5.61
Flap area aft of hinge line (one flap), square foot	0.637
Flap chord aft of hinge line, foot	0.312
Tail chord, feet	1.225
Tail span, feet	4.65

Tail area, square feet 5.69

The model in its standard configuration included the horizontal and vertical wings, horizontal and vertical flaps, fuselage, tail, tail cone, and control fairings. The control fairings were raised portions on the lower sides of the fuselage extending from stations 48 to 159. The rocket of the missile was not simulated in these tests, so the blunt tail of the fuselage was modified in order to avoid the separation which would otherwise occur in the absence of the jet. A tail cone was added aft of station 194.5 to minimize this separation but was short enough to have little effect upon the stability of the model. Two jato units were also tested as shown in figure 2. The model was constructed of steel, dural, and wood. The wings and tails consisted of steel spars covered with dural sheet. The center section of the fuselage was fabricated from a steel tube, while the nose and tail cone were of wood.

The deflections of the vertical wing and flaps were remotely controlled and indicated. The horizontal wing and flaps had to be set manually during tunnel shutdown. Both wings were individually tested up to an incidence of 12°, while the flaps were tested up to deflections of 60°. The tail settings were remotely controlled and indicated and were deflected simultaneously to give a resultant vertical force. The tails were tested through a range of deflections from -10° to 10°.

Hinge moments were measured on both sets of tail surfaces, the vertical wing, and the vertical-wing flaps. The hinge moments were evaluated by measuring electrically the strain of a cantilever beam subjected to the hinge-moment load.

In figure 2 are photographs showing the Lark model mounted in the Ames 16-foot high-speed wind tunnel. The model was supported in the wind tunnel by four 5-percent-thick front struts and one 7-percent-thick rear strut, the latter being tapered over the upper 25 inches from a 20-inch chord to a 10-inch tip chord. The trunnion fittings were mounted 56 inches apart on the 38-percent-chord line of the horizontal wing. Since the fittings protruded outside of the wing contour, it was necessary to house them in wooden fairings on both the upper and lower surfaces of the wing.

Tests were conducted through a Mach number range from 0.20 to 0.875 corresponding to a Reynolds number range from 2.2×10^6 to 6.3×10^6.

SYMBOLS

C_L lift coefficient (lift/qS)

C_D drag coefficient (drag/qS)

C_m pitching-moment coefficient about the 38-percent-chord line of the wing $\left(\frac{\text{pitching moment}}{qSc}\right)$

C_{h_w} wing hinge-moment coefficient about the 38-percent-chord line of the wing $\left(\frac{\text{hinge moment}}{qSc}\right)$

C_{h_f} wing flap hinge-moment coefficient $\left(\frac{\text{hinge moment}}{qS_fc_f}\right)$

C_{h_t} tail hinge-moment coefficient about the 15-percent-chord line of the tail $\left(\frac{\text{hinge moment}}{qS_tc_t}\right)$

q dynamic pressure $(\frac{1}{2}\rho V^2)$, pounds per square foot

S wing area, square feet

c wing chord, feet

b wing span, feet

S_f flap area, aft of hinge line, square feet

c_f flap chord, aft of hinge line, feet

S_t tail area, square feet

c_t tail chord, feet

i_{w_h} incidence of the horizontal wing relative to the fuselage, degrees

i_{w_v} incidence of the vertical wing relative to the fuselage, degrees

δ_{f_h} deflection of the horizontal-wing flap relative to the horizontal wing, degrees

δ_{f_v} deflection of the vertical-wing flap relative to the vertical wing, degrees

δ_t tail deflection, degrees

α angle of attack of the fuselage, degrees

M Mach number, ratio of the free-stream velocity to the velocity of sound

RESULTS AND DISCUSSION

Corrections

Corrections have been applied to the results in this report to account for tare, tunnel-wall, and constriction effects. In determining the tare corrections for the four front struts the model was first tested with the two lower front struts removed and then with all four front struts in place. The increments of lift and drag between the two sets of results were doubled to account for the effects of four struts. Since the struts were not vertical but were inclined and because the attachment points were near the wing tips, lift on the horizontal wings of the model induced lift on each of the four struts. The vertical components of the lift on the four struts were additive. To compensate for this effect, all lift derived from the horizontal wing was reduced accordingly. The tare corrections for the lower rear strut were obtained from tests of the model supported by the upper rear strut shown in figure 2(a) with and without the standard lower strut in place. The tunnel-wall corrections were calculated by the method of reference 1. The constriction corrections were evaluated using a method analogous to that developed in reference 2, except that the blockage due to the fuselage was assumed to vary as $(1-M^2)^{3/2}$.

Order of Presentation

Because of the many control surfaces on the model, there were a great number of possible combinations of control-surface deflections and Mach numbers. Where possible, the effect of each variable was determined, and then only those combinations which might be directly applicable to the performance of the missile were tested. The results have been divided into three main sections: the basic data, the wing-flap linkage data, and the balance linkage data. The basic data include the effects of varying independently the angle of attack, the wing incidence, the flap deflection, the tail setting, and the Mach number on the lift, drag, pitching-moment, and hinge-moment characteristics of the model. Also in this section are the component effects of the tail cone, control fairings, and jatos. The wing-flap linkage data include the lift, drag, pitching-moment, and hinge-moment characteristics of the model with the wing and flaps deflected according to the ratio established by the linkage and with the model at an angle of attack of 0°. The balance linkage data present a complete summary of the aerodynamic characteristics of the model at conditions which might be encountered in flight throughout the Mach number range from 0.20 to 0.875. For all these results the angle of attack and pitching moments are zero, the lift being developed by linked deflections of the wing, flaps, and tails.

Basic Data

Lift and drag.- The effects of varying independently the angle of attack and the flap deflection on the polars for the model with the tail surfaces removed and for the complete model are shown in figures 3 and 4, respectively. Higher lift-to-drag ratios are obtained by varying the angle of attack than by varying the flap deflection. Because the Lark is to maintain zero angle of attack in flight, polars for simultaneous variations of angle of attack, wing incidence, and flap setting are not shown. However, for considerations of range, it is noteworthy that in the determination of the maximum lift-to-drag ratios the polars must represent balance conditions, and the large effect due to the tail setting must be considered.

The variations of lift coefficient with angle of attack, wing incidence, and flap deflection for the model with the tail surfaces removed are shown in figure 5. These results were obtained with the horizontal wing and flaps deflected. Since each wing was pivoted in order to vary its incidence, gaps existed between the inboard ends of the wings and the fuselage. The gaps on the horizontal wing were sealed by the insertion of felt pads glued to the inboard end of the wing. At the larger wing incidences, however, gaps developed at the leading and trailing edges. Since hinge moments were measured on the vertical wing, demanding a minimum of friction, the gap

between the vertical wing and fuselage was not sealed. Further, an annular opening existed around the entrance of the vertical-wing shaft into the fuselage. The leakage resulting from the gap and annular opening effectively reduced the aspect ratio of the wing. Figure 6 presents a comparison of the lift coefficients measured independently on the horizontal and vertical wings. The reduced lift-curve slope, higher maximum lift, and smaller change with Mach number are all characteristics of wings with very low aspect ratios. The lift characteristics of the horizontal wing, however, are subject to effects of the struts, the fairings over the strut fittings, and leakage through the junction, the combined effect of which is to cause earlier stall and a reduction in the maximum lift coefficients.

The variations of lift coefficient with angle of attack, horizontal-wing-flap deflection, and tail setting are presented in figure 7. The lift coefficients in figure 7(c) are based on the wing area and indicate the extent to which the relatively large tail surfaces affect the lift of the model.

Variations of drag coefficient with Mach number are presented in figures 8 and 9 for the model with the tail surfaces removed and for the complete model, respectively. The Mach number of divergence at zero lift is around 0.83.

Pitching moment.- The variations of pitching-moment coefficient with angle of attack and with horizontal-wing-flap deflection are presented in figure 10 for the model with

and without the tail surfaces. The pitching-moment coefficient, being measured about the 38-percent-chord line of the wing, increases rapidly with increasing angle of attack for the model with the tail surfaces removed. The pitching-moment coefficients for the complete model do not exhibit a linear variation with angle of attack above 0.7 Mach number because of the effects on the tail of the changes in the wake and downwash from the wing. The variation of pitching-moment coefficient with flap deflection for the model with the tail surfaces removed indicates forward motion of the center of pressure at the larger deflections due to separation from the flaps. For the complete model, the pitching-moment coefficients increase with flap deflection because of the lift induced on the tails and fuselage by the downwash from the flaps. Figure 11 presents the variation of pitching-moment coefficient with tail deflection and indicates little variation in tail effectiveness throughout the Mach number range from 0.20 to 0.875.

Hinge moments.- The variation of wing hinge-moment coefficient with wing incidence for the vertical wing is shown in figure 12. The increase in hinge-moment coefficient with Mach number at a given wing incidence corresponds to the increase in lift coefficient already shown in figure 5. The variations of wing and flap hinge-moment coefficients with deflection of the vertical flaps are presented in figure 13. Figure 14 presents the variation of tail hinge-moment coefficient with

tail deflection for several angles of attack. Since the tails were mounted at the 15-percent-chord line, the nose portion served as an aerodynamic balance, the effectiveness of which increased with Mach number as indicated by the changes in the slopes of the curves. The nose balance also produced an increase in the parameter $dC_h/d\alpha$ with increasing Mach number as is evident from the wider spacing of the curves.

Rolling moments.- No rolling-moment data are shown in this report. However, a preliminary investigation indicated reduced rolling effectiveness due to the reversed rolling moments produced by the downwash on the large tail surfaces and by the lift induced on the horizontal wing by the aileron motion of the vertical wing flaps. Further investigation of the rolling moments is advisable.

Effects of components.- The increments of drag due to the tail cone and control fairings are presented in figure 15. The removal of the tail cone resulted in an increase in drag of the model because of the separation from the blunt tail of the fuselage. As the Mach number was increased, the boundary layer along the fuselage thickened so that even with the tail cone attached some separation developed at the higher Mach numbers. The increments of drag due to the control fairings were small, but it should be pointed out that when the fairings were removed, four small attachment lugs for the jatos were exposed and probably added some drag.

The increments of lift, drag, and pitching-moment

coefficients produced by the addition of the jato units to the model with the tail surfaces removed are shown in figure 16 for various angles of attack, wing, and flap settings. The results indicate relatively large interference effects at 12° wing incidence because of the close proximity of the wing and jatos. The increments of lift, drag, and pitching-moment coefficients due to the addition of the jato units to the complete model are shown in figures 17, 18, and 19, respectively, for several angles of attack and tail settings. The increments at any given angle of attack and tail setting are the differences between the results for the model with and without the jatos at the same settings of control surfaces and angle of attack. The data for the model with the jatos attached may be obtained by adding the increments to the basic data for the complete model. The variation of tail hinge-moment coefficient with tail deflection at several angles of attack for the model with the jatos is presented in figure 20.

Linkage Data

Lift, drag, and pitching moments.- The lift and drag characteristics of the model with the horizontal wing and flaps deflected according to the established linkage ratio are presented in figure 21 for the model with and without the tail surfaces. The large effects of tail deflection on the lift and drag are evident. The lift-curve slope for the tail-off configuration is greater than that for the complete

model because of the negative lift induced on the tail surfaces by the downwash from the wing. Figure 22 presents the variation with Mach number of the lift-curve slopes over the range of wing incidences for which the lift curves are almost linear. The parameter dC_L/di_w is the ratio of lift coefficient to wing incidence but with the horizontal flaps also deflected.

The variation of pitching-moment coefficient with lift coefficient for linked deflections of the horizontal wing and flaps is shown in figure 23 for the model with and without the tail surfaces. It should be noted that the slopes of these curves at zero pitching moment do not represent the static longitudinal stability of the model, since all the data are for zero angle of attack. Extrapolation of figure 23(g) indicates that at 0.80 Mach number and 12° wing incidence, the maximum lift coefficient at balance is about 0.97. Since the missile will have a relatively high wing loading somewhere between 90 and 130 pounds per square foot during the pursuit phase, a lift coefficient of 0.97 is not high enough to insure interception of the target at high altitudes. A reduction in the wing loading appears desirable. There is an almost linear relationship between the wing incidence and the tail deflection required for balance. The ratio of tail deflection to wing deflection, however, changes with the location of the center of gravity of the missile; the more aft the location the greater the ratio. Figure 24 presents the variation with

lift coefficient of the required tail and wing deflections for balance in level flight corresponding to center-of-gravity locations of 25 percent and 38 percent of the wing chord. It is obvious that no single linkage will provide balance at all lift coefficients or center-of-gravity locations but rather an optimum linkage should be selected based on the conditions expected in normal flight. A ratio of 0.4 appears to be the optimum value. The angle-of-attack mechanism will automatically provide the remaining control necessary for balance.

The variations of wing hinge-moment coefficient and of flap hinge-moment coefficient with linked deflections of the vertical wing and flaps are shown in figure 25. The tail hinge-moment coefficients for the model with the horizontal wing and flaps deflected according to the linkage ratio are presented in figure 26.

Balance Linkage Data

Lift and drag.- Figure 27 and the remaining figures in this report present the data for which the model is balanced (zero pitching moment) and represent the conditions which the missile might actually encounter in flight. The polars are shown in figure 27, while the maximum lift-to-drag ratios and the corresponding lift coefficient and wing incidences for maximum lift-to-drag ratio are summarized in figure 28. The variations of drag coefficient with Mach number for several horizontal-wing incidences and the corresponding flap deflections

are shown in figure 29.

Hinge moments.- The variations of horizontal wing and flap hinge-moment coefficients with lift coefficient at balance are shown in figures 30 and 31. The variations of the tail deflection and the tail hinge-moment coefficient with lift coefficient at balance are presented in figures 32 and 33. It should be noted that these tail data are applicable throughout the large range of lift coefficients regardless of the fact that the flight path may be curvilinear, because the damping moments would be very small due to the relatively short tail length of the missile. Consequently, the additional tail deflection is small enough to be neglected.

Longitudinal stability.- The static longitudinal stability and the stick-fixed neutral-point locations are summarized in figure 34 for the model at or near zero angle of attack. The missile becomes increasingly stable at high lift coefficients and higher Mach numbers and similarly the neutral point moves further aft. Minimum stability occurs around 2° wing incidence slightly above 0.8 Mach number, which approximates level flight of the missile and which promotes maximum maneuverability so essential to the performance of the missile. The variations in stability should not be detrimental because the tail retains its large effectiveness throughout the wide ranges of Mach numbers and lift coefficients.

CONCLUSIONS

The high-speed wind-tunnel tests of the full-scale model of the Consolidated Vultee Lark indicated the following:

1. The maximum lift coefficient obtainable at 0.80 Mach number with the missile balanced at zero angle of attack is around 0.97. For successful operation of the missile at high altitudes, it appears that a reduction in wing loading will be necessary.

2. The static longitudinal stability at zero angle of attack changes with wing incidence and with Mach number, but these changes should not interfere with the performance of the missile because the tails retain their large effectiveness throughout the range of Mach numbers and lift coefficients tested. The minimum stability occurs around 0.80 Mach number and a lift coefficient of 0.20 which corresponds to level flight of the missile where maximum maneuverability is desirable.

3. The optimum ratio of tail-to-wing deflection is 0.4.

Ames Aeronautical Laboratory,
National Advisory Committee for Aeronautics,
Moffett Field, Calif.

John A. Axelson
John A. Axelson,
Mechanical Engineer.

Andrew Martin,
Aeronautical Engineer.

Approved:
Donald H. Wood
Donald H. Wood,
Aeronautical Engineer.

REFERENCES

1. Silverstein, Abe, and White, James A.: Wind-Tunnel Interference with Particular Reference to Off-Center Positions of the Wing and to the Downwash at the Tail. NACA Rep. No. 547, 1935.

2. Thom, A.: Blockage Corrections and Choking in the R.A.E. High Speed Tunnel. Rep. No. Aero. 1891, R.A.E. (British-U.S. Confidential), Nov. 1943.

3. Anon.: Summary of the Model KAY-1 Lark, Monthly Activity as of October 31, 1945. Consolidated Vultee Aircraft Corporation, Nov. 1945.

FIGURE LEGENDS

Figure 1.- Three-view drawing of the full-scale model of the Consolidated Vultee Lark showing alternate configuration with the jato units attached.

Figure 2.- Photographs of the full-scale model of the Consolidated Vultee Lark in the Ames 16-foot high-speed wind tunnel. (a) Front view of the model with the upper rear strut used in the evaluation of tares. (b) Rear view of the model with the upper rear strut.

Figure 2.- Concluded. (c) Front view of the model, less tail surfaces, with the jatos attached and with the standard lower rear strut. (d) Rear view of the model, less tail surfaces, with the jatos attached and with the standard lower rear strut.

Figure 3.- Variation of drag coefficient with lift coefficient for the full-scale model of the Consolidated Vultee Lark, less tail. (a) Variable angle of attack. i_{w_v}, i_{w_h}, δ_{f_v}, δ_{f_h}, 0°.

Figure 3.- Concluded. (b) Variable horizontal wing flap deflection. α, i_{w_v}, i_{w_h}, δ_{f_v}, 0°.

Figure 4.- Variation of drag coefficient with lift coefficient for the Consolidated Vultee Lark.

Figure 5.- Variation of lift coefficient with angle of attack, wing incidence, and flap deflection for the full-scale model of the Consolidated Vultee Lark, less tail. (a) Variable angle of attack. i_{w_v}, i_{w_h}, δ_{f_v}, δ_{f_h}, 0°. (b) Variable horizontal wing incidence. α, i_{w_v}, δ_{f_v}, δ_{f_h}, 0°.

Figure 5.- Concluded. (c) Variable horizontal wing flap deflection. α, i_{w_v}, i_{w_h}, δ_{f_v}, 0°.

Figure 6.- Comparison of the lift characteristics of the horizontal and vertical wings of the full-scale model of the Consolidated Vultee Lark, less tail. α, δ_{f_v}, δ_{f_h}, 0°.

Figure 7.- Variation of lift coefficient with angle of attack, horizontal wing flap deflection, and tail setting for the full-scale model of the Consolidated Vultee Lark. (a) Variable angle of attack. i_{w_v}, i_{w_h}, δ_{f_v}, δ_{f_h}, δ_t, 0°. (b) Variable horizontal wing flap deflection. α, i_{w_v}, i_{w_h}, δ_{f_v}, δ_{f_h}, 0°.

Figure 7.- Concluded. (c) Variable tail setting. α, i_{w_v}, i_{w_h}, δ_{f_v}, δ_{f_h}, 0°.

Figure 8.- Variation of drag coefficient with Mach number for the full-scale model of the Consolidated Vultee Lark, less tail.

Figure 9.- Variation of drag coefficient with Mach number for the full-scale model of the Consolidated Vultee Lark.

Figure 10.- Effects of angle of attack and horizontal wing-flap deflection on the pitching-moment coefficient of the full-scale model of the Consolidated Vultee Lark.

Figure 11.- Variation of pitching-moment coefficient with tail deflection for the full-scale model of the Consolidated Vultee Lark. α, i_{w_v}, i_{w_h}, δ_{f_v}, δ_{f_h}, 0°.

Figure 12.- Variation of wing hinge-moment coefficient with wing incidence for the vertical wing of the full-scale model of the Consolidated Vultee Lark. α, i_{w_h}, δ_{f_v}, δ_{f_h}, 0°.

Figure 13.- Variations of wing and flap hinge-moment coefficients with flap deflection for the vertical wing of the full-scale model of the Consolidated Vultee Lark. α, i_{w_v}, i_{w_h}, δ_{f_h}, 0°.

Figure 14.- Variation of tail hinge-moment coefficient with tail deflection at various angles of attack for the full-scale model of the Consolidated Vultee Lark. i_{w_v}, i_{w_h}, δ_{f_v}, δ_{f_h}, 0°. (a) M, 0.2. (b) M, 0.4. (c) M, 0.6. (d) M, 0.7. (e) M, 0.75. (f) M, 0.775.

Figure 14.- Concluded. (g) M, 0.80. (h) M, 0.825. (i) M, 0.85. (j) M, 0.875.

Figure 15.- Variations of the drag increments of the tail cone and of the control fairings with Mach number for the full-scale model of the Consolidated Vultee Lark. α, i_{w_v}, i_{w_h}, δ_{f_v}, δ_{f_h}, δt, 0°.

Figure 16.- Variation of the increments of lift, drag, and pitching-moment coefficients with Mach number due to the jatos on the full-scale model of the Consolidated Vultee Lark, less tail. i_{w_v}, δ_{f_v}, 0°.

Figure 17.- Variation of the increments of lift coefficient with number due to the jatos on the full-scale model of the Consolidated Vultee Lark. i_{w_v}, i_{w_h}, δ_{f_v}, δ_{f_h}, 0°.

Figure 18.- Variation of the increments of drag coefficient with Mach number due to the jatos on the full-scale model of the Consolidated Vultee Lark. i_{w_v}, i_{w_h}, δ_{f_v}, δ_{f_h}, 0°.

Figure 19.- Variation of the increments of pitching-moment coefficient with Mach number due to the jatos on the full-scale model of the Consolidated Vultee Lark. i_{w_v}, i_{w_h}, δ_{f_v}, δ_{f_h}, 0°.

Figure 20.- Variation of tail hinge-moment coefficient with tail deflection for the full-scale model of the Consolidated Vultee Lark with jatos.

Figure 21.- Variation of lift coefficient with drag coefficient and with linked deflections of the horizontal wing and flaps for the full-scale model of the Consolidated Vultee Lark. α, i_{w_v}, δ_{f_v}, 0°. (a) M, 0.2.

Figure 21.- Continued. (b) M, 0.4.

Figure 21.- Continued. (c) M, 0.6.

Figure 21.- Continued. (d) M, 0.7.

Figure 21.- Continued. (e) M, 0.75.

Figure 21.- Continued. (f) M, 0.775.

Figure 21.- Continued. (g) M, 0.8.

Figure 21.- Continued. (h) M, 0.825.

Figure 21.- Continued. (i) M, 0.85.

Figure 21.- Concluded. (j) M, 0.875.

Figure 22.- Variation with Mach number of the lift-curve slope for linked deflections of the horizontal wing and flaps for the full-scale model of the Consolidated Vultee Lark. α, i_{w_v}, δ_{f_v}, 0°.

Figure 23.- Variation of pitching-moment coefficient with coefficient for linked deflections of the horizontal wing and flaps of the full-scale model of the Consolidated Vultee Lark. α, i_{w_v}, δ_{f_v}, 0°. (a) M, 0.2.

Figure 23.- Continued. (b) M, 0.4.

Figure 23.- Continued. (c) M, 0.6.

Figure 23.- Continued. (d) M, 0.7.

Figure 23.- Continued. (e) M, 0.75.

Figure 23.- Continued. (f) M, 0.775.

Figure 23.- Continued. (g) M, 0.8.

Figure 23.- Continued. (h) M, 0.825.

Figure 23.- Continued. (i) M, 0.85.

Figure 23.- Concluded. (j) M, 0.875.

Figure 24.- Variation of the ratio of tail deflection to wing deflection for balance for the full-scale model of the Consolidated Vultee Lark.

Figure 25.- Variation of wing hinge-moment coefficient and of flap hinge-moment coefficient with linked deflections of the vertical wing and flaps for the full-scale model of the Consolidated Vultee Lark. α, i_{w_h}, δ_{f_h}, 0°.

Figure 26.- Variation of tail hinge-moment coefficient with tail deflection at various linked deflections of the horizontal wing and flap of the full-scale model of the Consolidated Vultee Lark. α, i_{w_v}, δ_{f_v}, 0°. (a) M, 0.2. (b) M, 0.4. (c) M, 0.6. (d) M, 0.7. (e) M, 0.75. (f) M, 0.775.

Figure 26.- Concluded. (g) M, 0.80. (h) M, 0.825. (i) M, 0.85. (j) M, 0.875.

Figure 27.- Variation of drag coefficient with lift coefficient at balance ($C_m = 0$) with linked deflections of the horizontal wing and flaps for the full-scale model of the Consolidated Vultee Lark. α, i_{w_v}, δ_{f_v}, 0°.

Figure 28.- Variation with Mach number of the maximum lift-to-drag ratios and the corresponding lift coefficients and wing incidences at balance ($C_m = 0$) for the full-scale model of the Consolidated Vultee Lark with the wing-flap linkage. α, i_{w_v}, δ_{f_v}, 0°.

Figure 29.- Variation of drag coefficient with Mach number at balance ($C_m = 0^\circ$) for linked deflections of the horizontal wing and flaps for the full-scale model of the Consolidated Vultee Lark. α, i_{w_v}, δ_{f_v}, 0°.

Figure 30.- Variation of wing hinge-moment coefficient with lift coefficient at balance (pitching moment = 0) for linked deflections of horizontal wing and flaps for the full-scale model of the Consolidated Vultee Lark. α, i_{w_v}, δ_{f_v}, 0°.

Figure 31.- Variation of flap hinge-moment coefficient with lift coefficient at balance ($C_m = 0$) for linked deflections of the horizontal wing and flaps for the full-scale model of the Consolidated Vultee Lark. α, i_{w_v}, δ_{f_v}, 0°.

Figure 32.- Variation of tail deflection with lift coefficient at balance ($C_m = 0$) with linked deflections of the horizontal wing and flaps for the full-scale model of the Consolidated Vultee Lark. α, i_{w_v}, δ_{f_v}, 0°.

Figure 33.- Variation of tail hinge-moment coefficient with lift coefficient at balance ($C_m = 0$) with linked deflections of the horizontal wing and flaps for the full-scale model of the Consolidated Vultee Lark. α, i_{w_v}, δ_{f_v}, 0°.

Figure 34.- Static longitudinal stability and neutral-point location at balance ($C_m = 0$) for the full-scale model of the Consolidated Vultee Lark. α, i_{w_v}, δ_{f_v}, 0°.

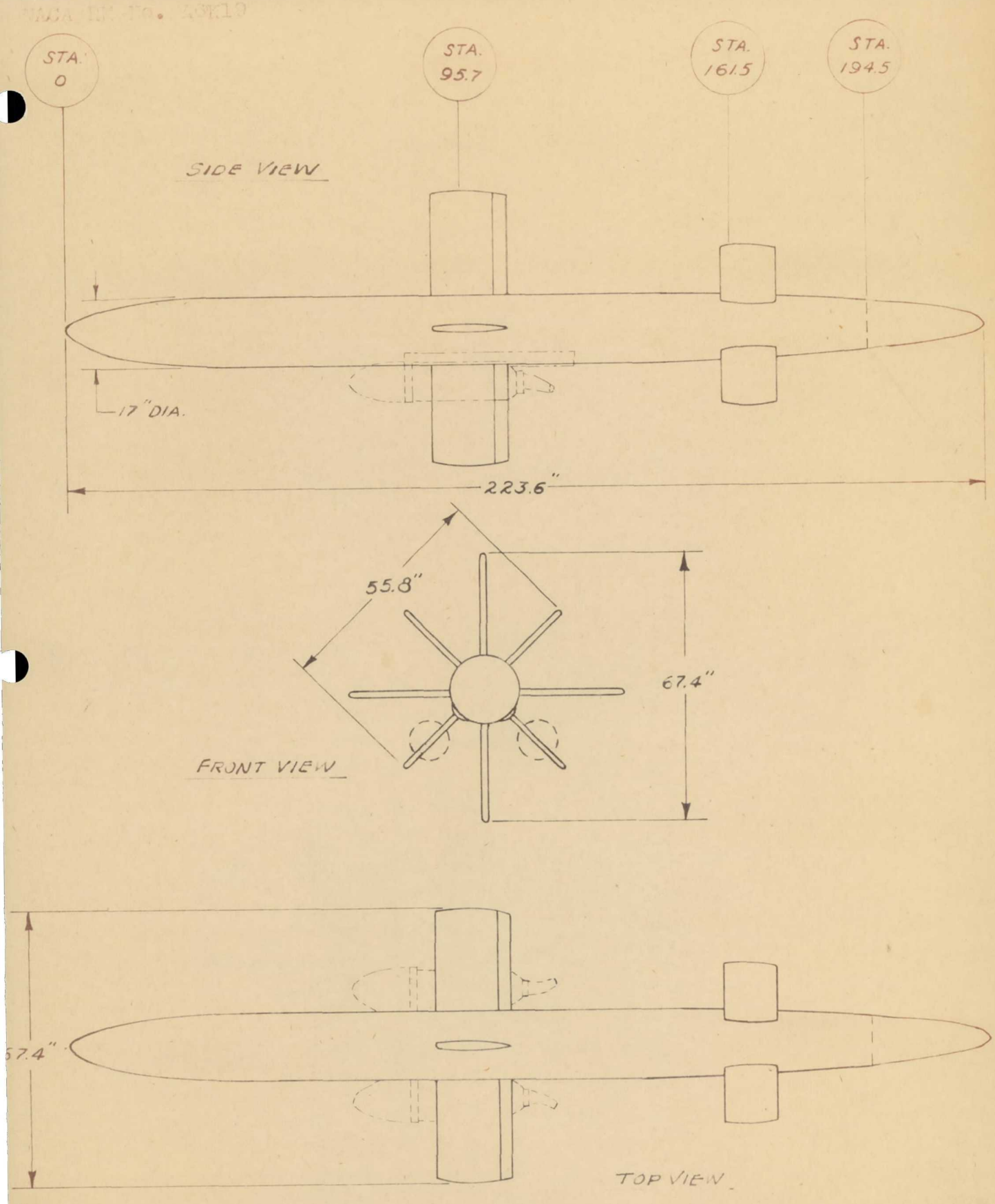

FIGURE 1. - THREE-VIEW DRAWING OF THE FULL-SCALE MODEL OF THE CONSOLIDATED VULTEE LARK SHOWING ALTERNATE CONFIGURATION

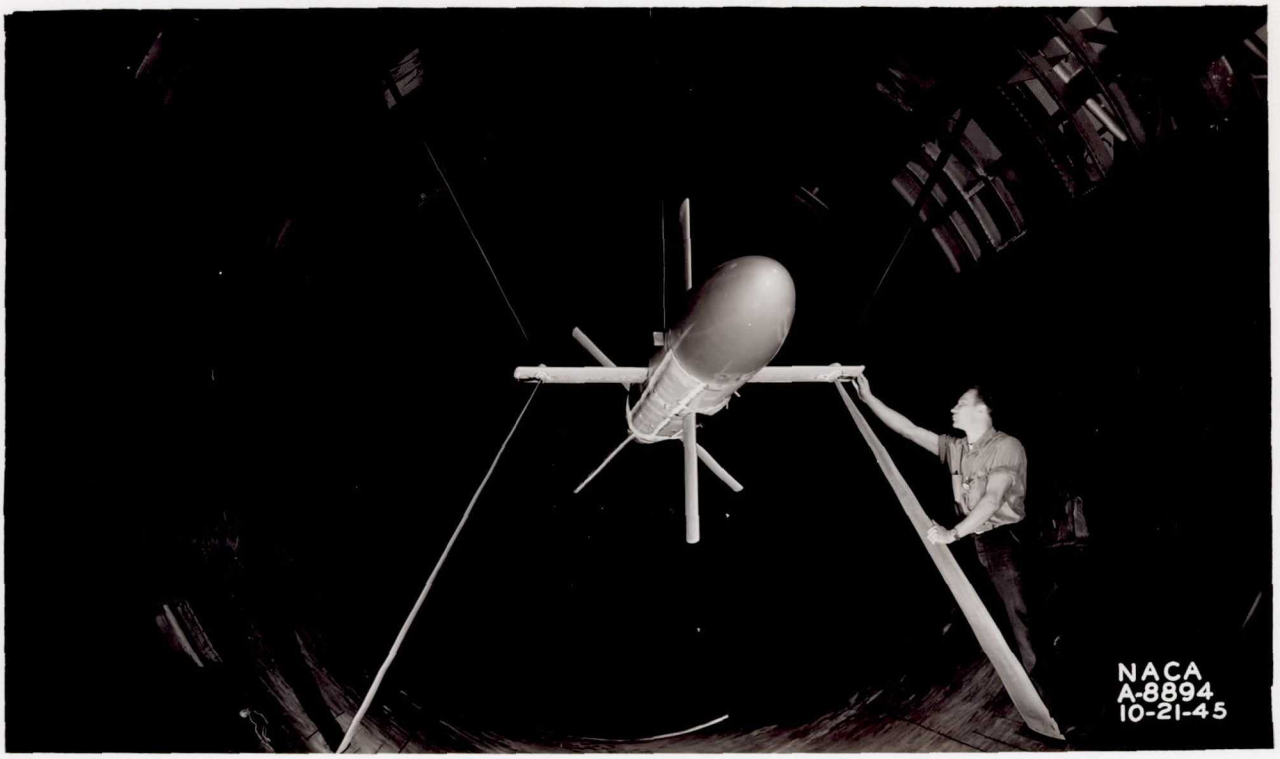

(a) Front view of the model with the upper rear strut used in the evaluation of tares.

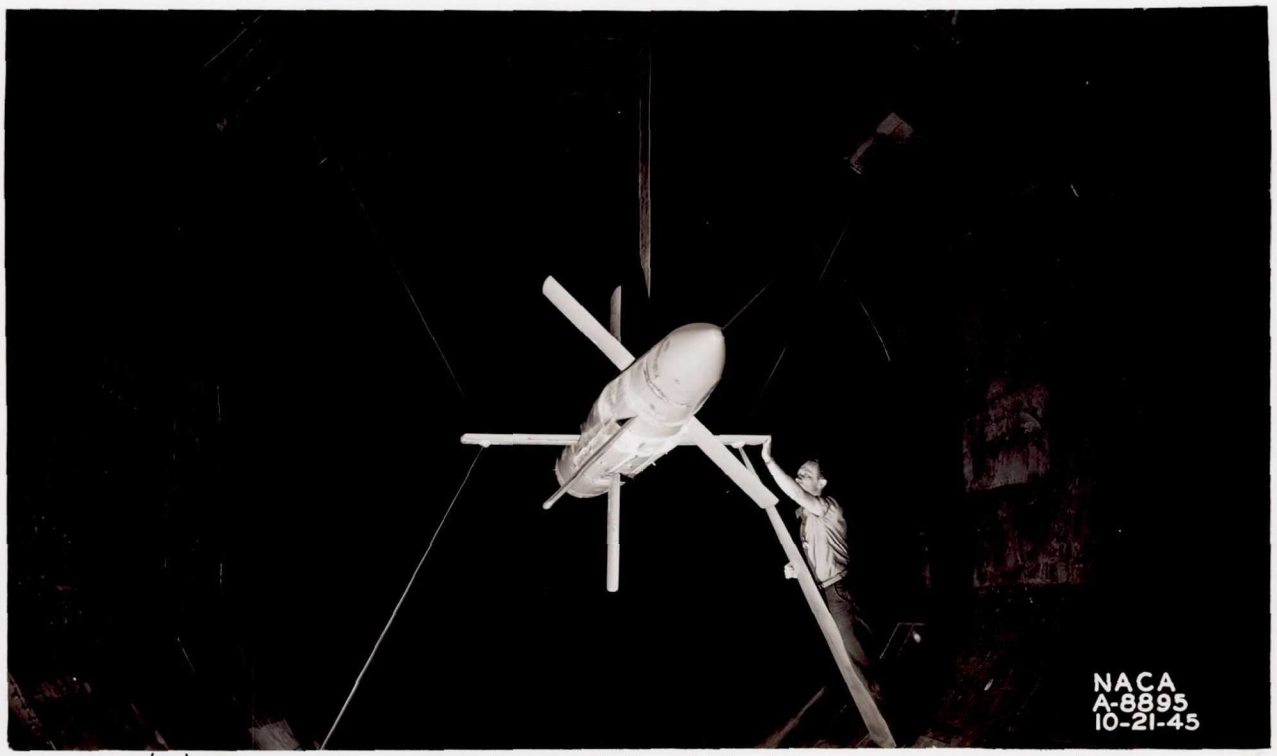

(b) Rear view of the model with the upper rear strut.

Figure 2.- Photographs of the full-scale model of the Consolidated Vultee Lark in the Ames 16-foot high-speed wind tunnel.

(c) Front view of the model, less tail surfaces, with the jatos attached and with the standard lower rear strut.

(d) Rear view of the model, less tail surfaces, with the jatos attached and with the standard lower rear strut.

Figure 2.- Concluded.

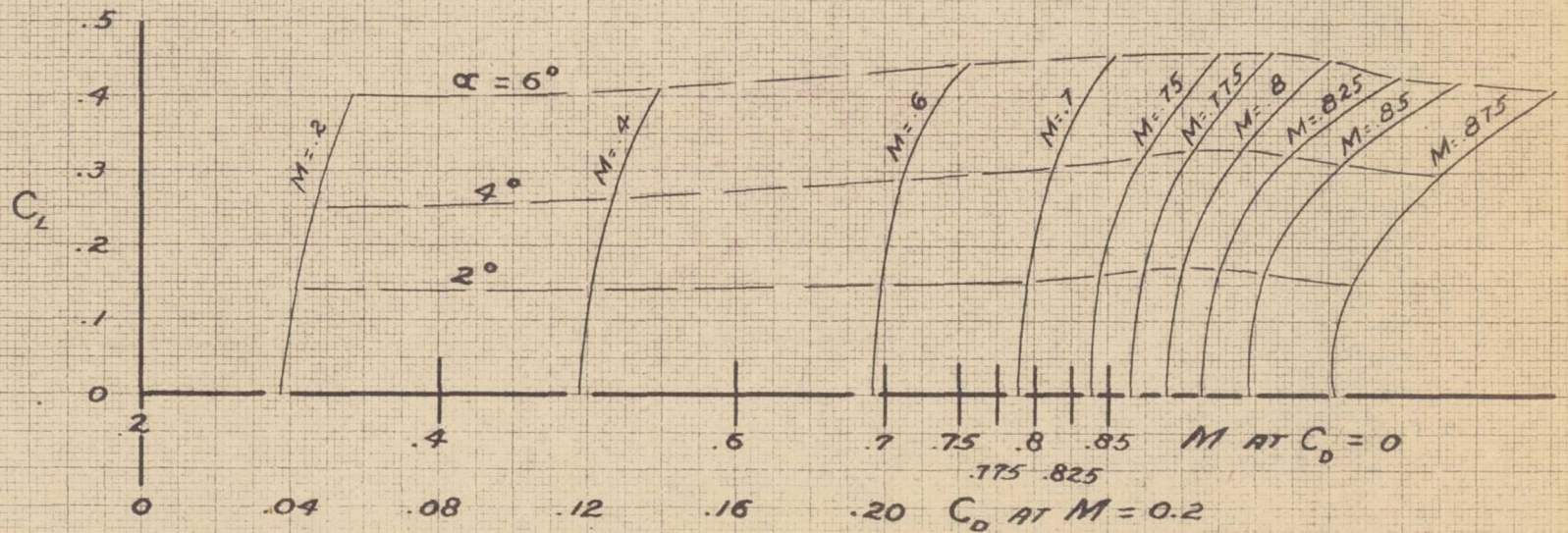

(a) VARIABLE ANGLE OF ATTACK. i_{W_V}, i_{W_H}, d_{t_V}, d_{t_H}, 0°.

FIGURE 3.- VARIATION OF DRAG COEFFICIENT WITH LIFT COEFFICIENT FOR THE FULL-SCALE MODEL OF THE CONSOLIDATED VULTEE LARK, LESS TAIL.

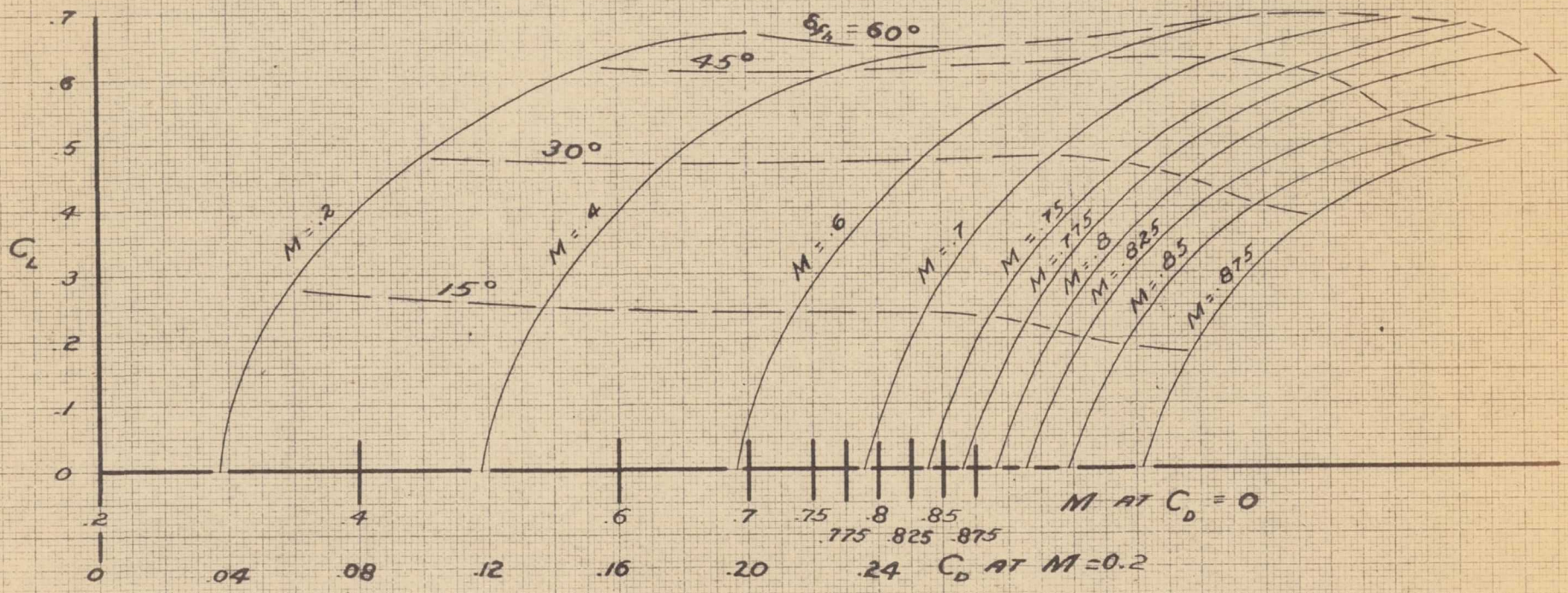

CONFIDENTIAL
NATIONAL ADVISORY COMMITTEE FOR AERONAUTICS

(b) VARIABLE HORIZONTAL WING FLAP DEFLECTION. α, i_{W_V}, i_{W_H}, δ_{f_V}, 0°.

FIGURE 3. - CONCLUDED.

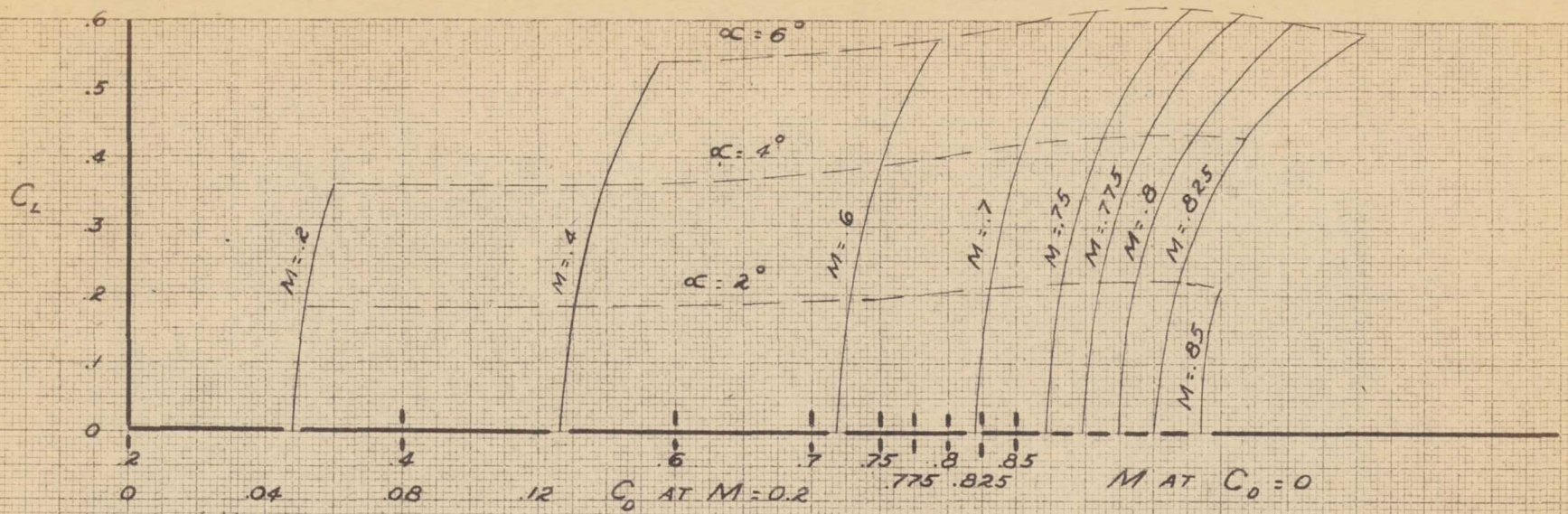

(a) VARIABLE ANGLE OF ATTACK. i_{w_v}, i_{w_h}, δ_{f_v}, δ_{f_h}, δ_t, 0°.

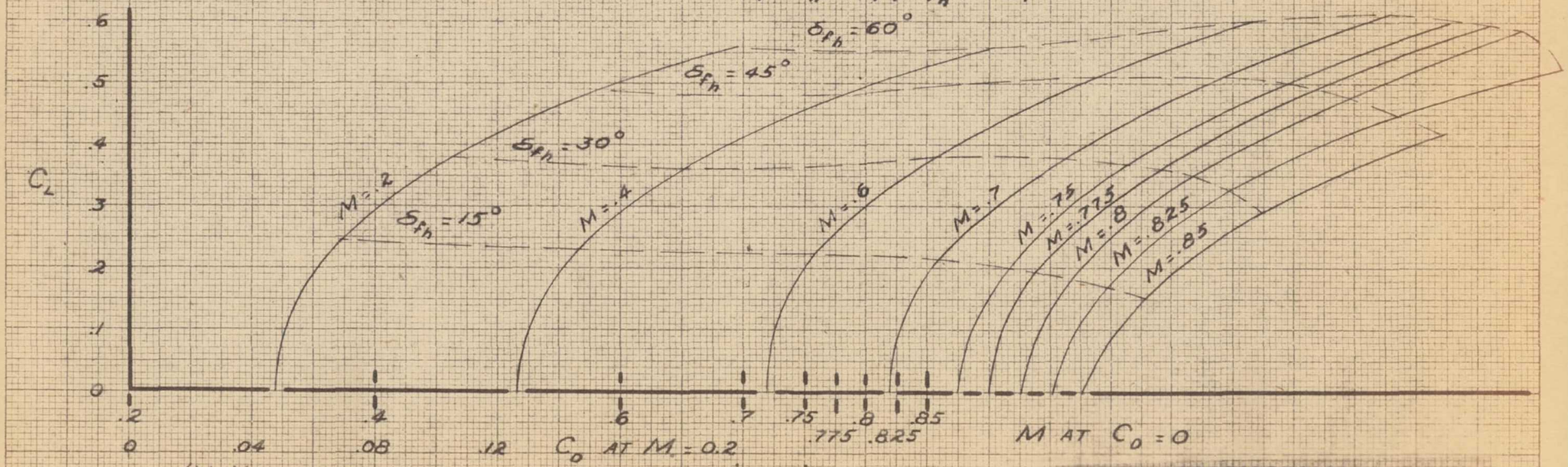

(b) VARIABLE FLAP DEFLECTION. α, i_{w_v}, i_{w_h}, δ_{f_v}, δ_t, 0°.

CONFIDENTIAL
NATIONAL ADVISORY COMMITTEE FOR AERONAUTICS

FIGURE 4. - VARIATION OF DRAG COEFFICIENT WITH LIFT COEFFICIENT FOR THE CONSOLIDATED VULTEE LARK.

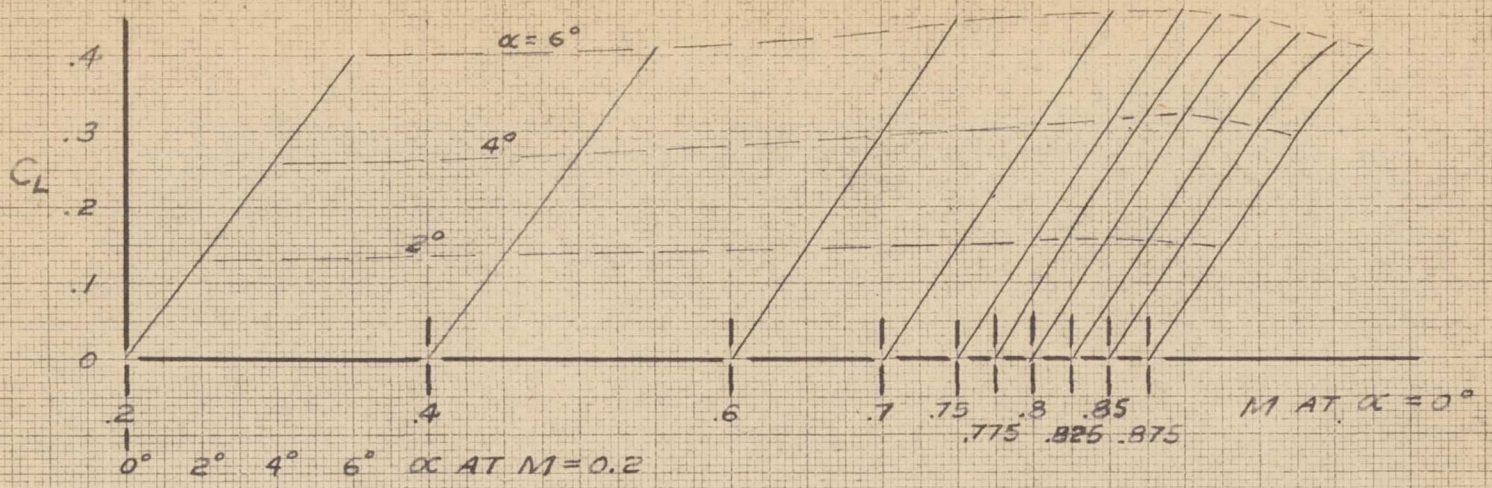

(a) VARIABLE ANGLE OF ATTACK. i_{W_v}, i_{W_h}, δ_{f_v}, δ_{f_h}, 0°.

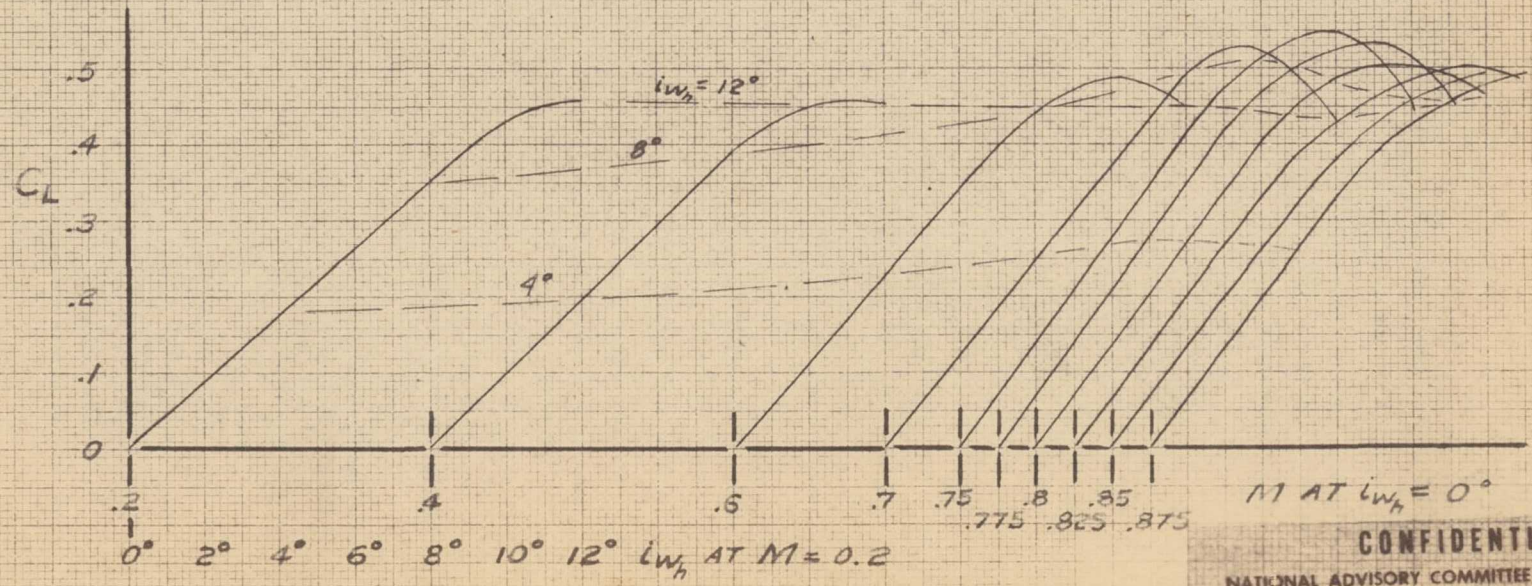

(b) VARIABLE HORIZONTAL WING INCIDENCE. α, i_{W_v}, δ_{f_v}, δ_{f_h}, 0°.

FIGURE 5.- VARIATION OF LIFT COEFFICIENT WITH ANGLE OF ATTACK, WING INCIDENCE, AND FLAP DEFLECTION FOR THE FULL-SCALE MODEL OF THE CONSOLIDATED VULTEE LARK, LESS TAIL.

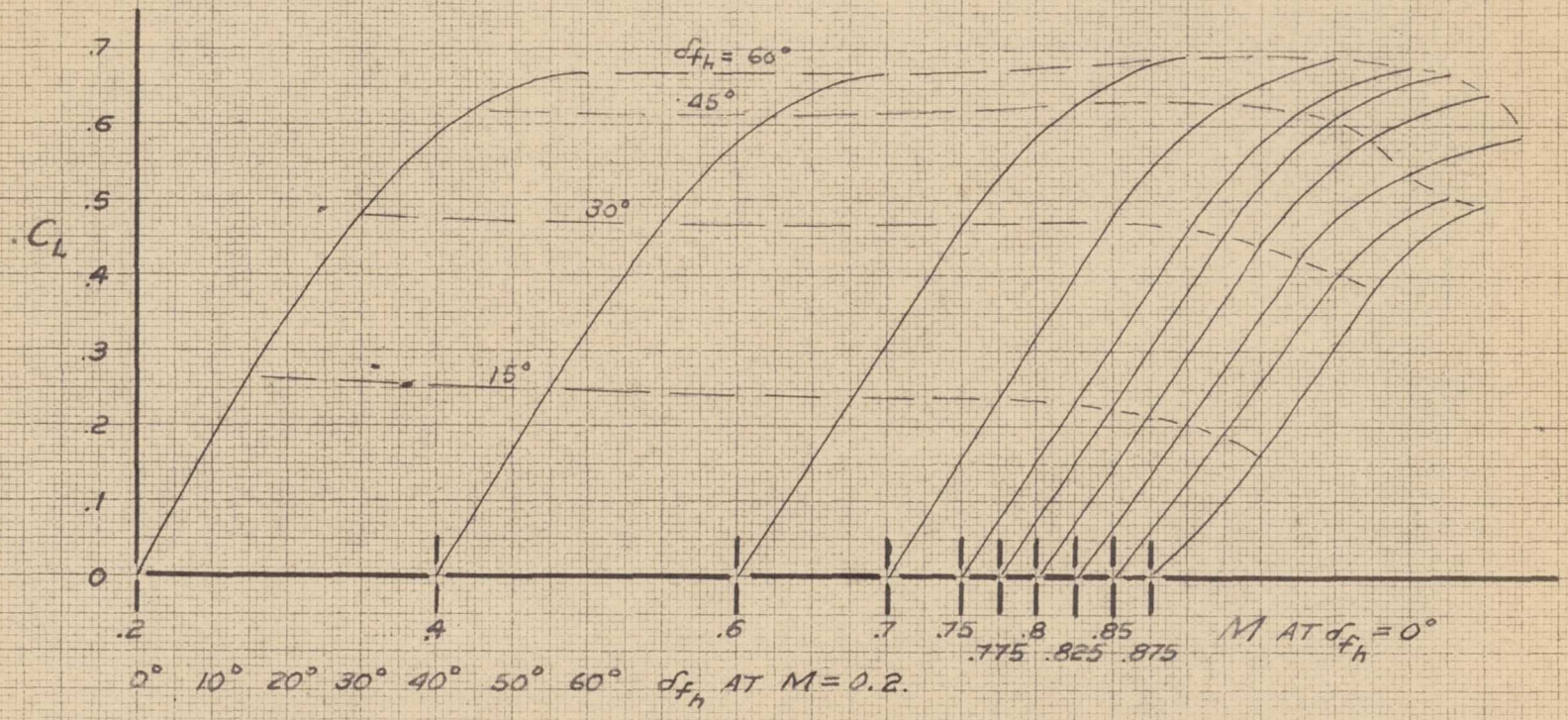

(c) VARIABLE HORIZONTAL WING FLAP DEFLECTION. $\alpha, i_{W_V}, i_{W_H}, df_V, 0°$

FIGURE 5.- CONCLUDED.

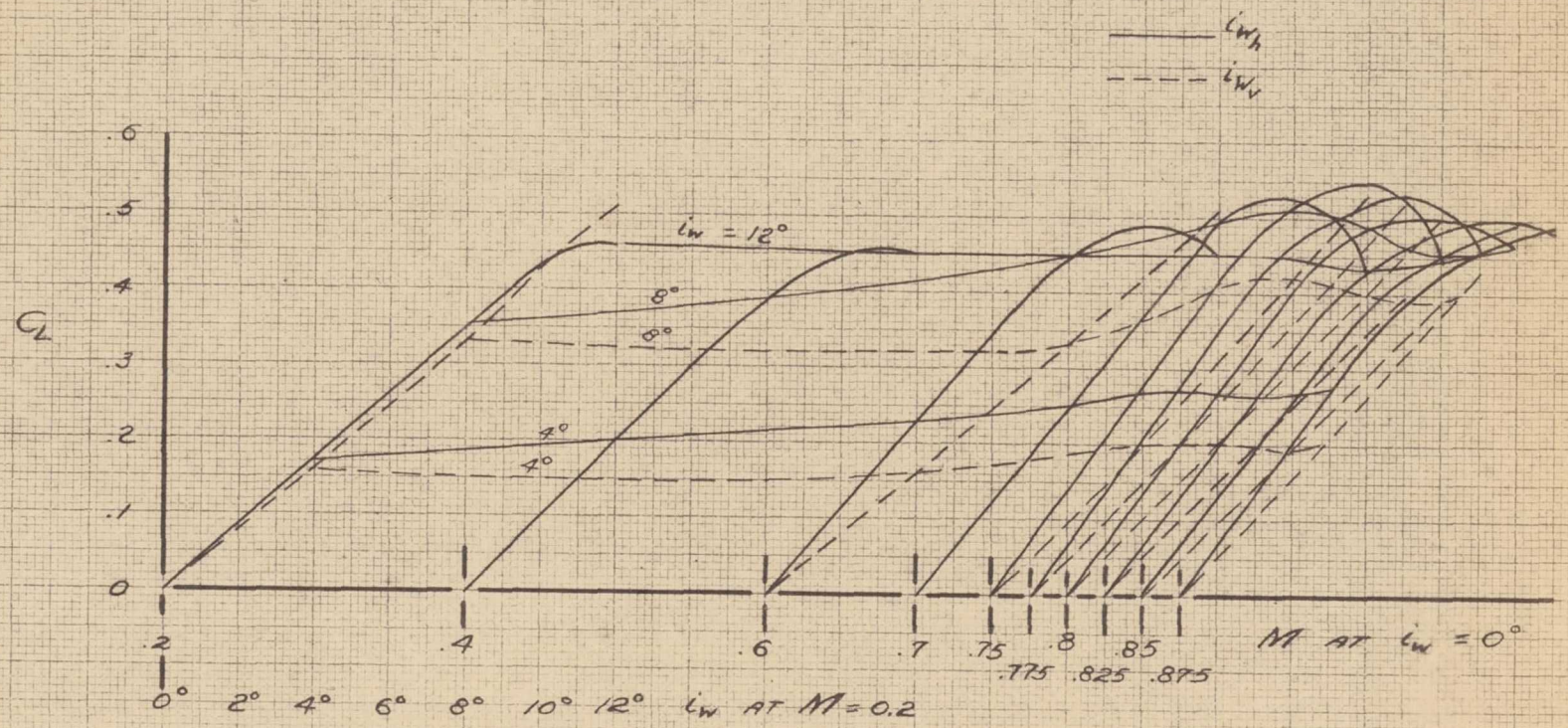

CONFIDENTIAL
NATIONAL ADVISORY COMMITTEE FOR AERONAUTICS

FIGURE 6.- COMPARISON OF THE LIFT CHARACTERISTICS OF THE HORIZONTAL AND VERTICAL WINGS OF THE FULL-SCALE MODEL OF THE CONSOLIDATED VULTEE LARK, LESS TAIL. α, δ_{f_v}, δ_{f_h}, 0°.

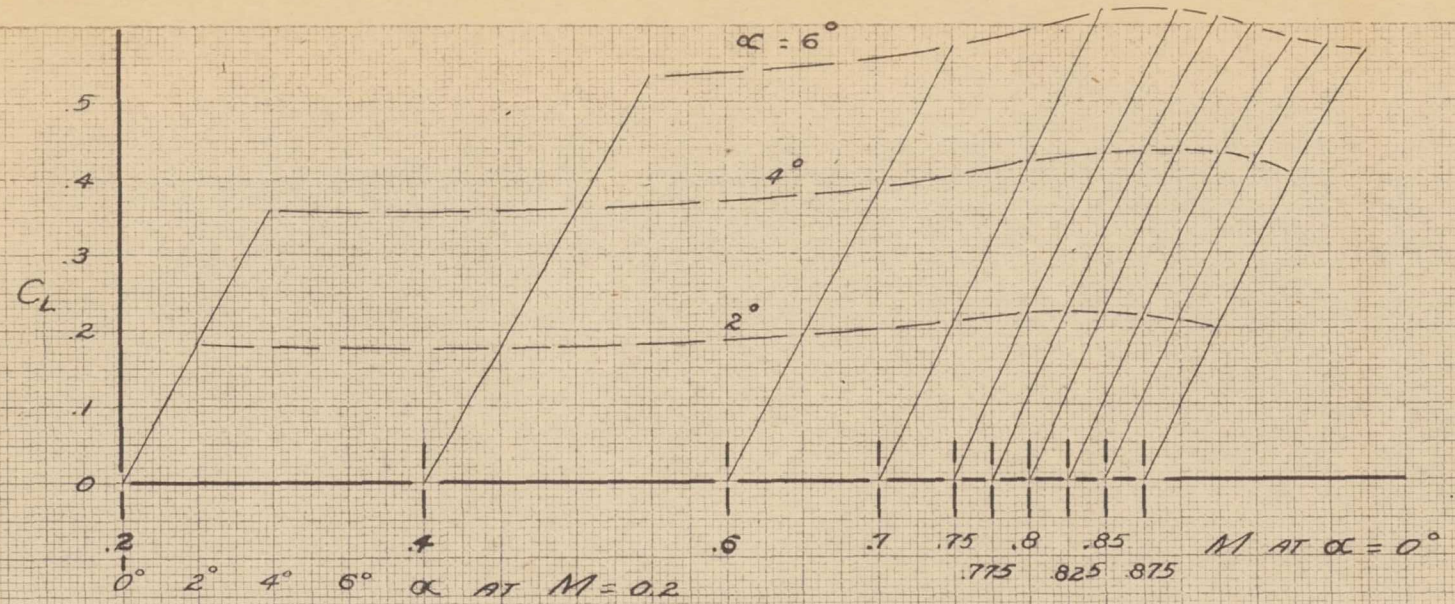

(a) VARIABLE ANGLE OF ATTACK. i_{W_V}, i_{W_H}, δ_{f_V}, δ_{f_H}, δ_t, 0°.

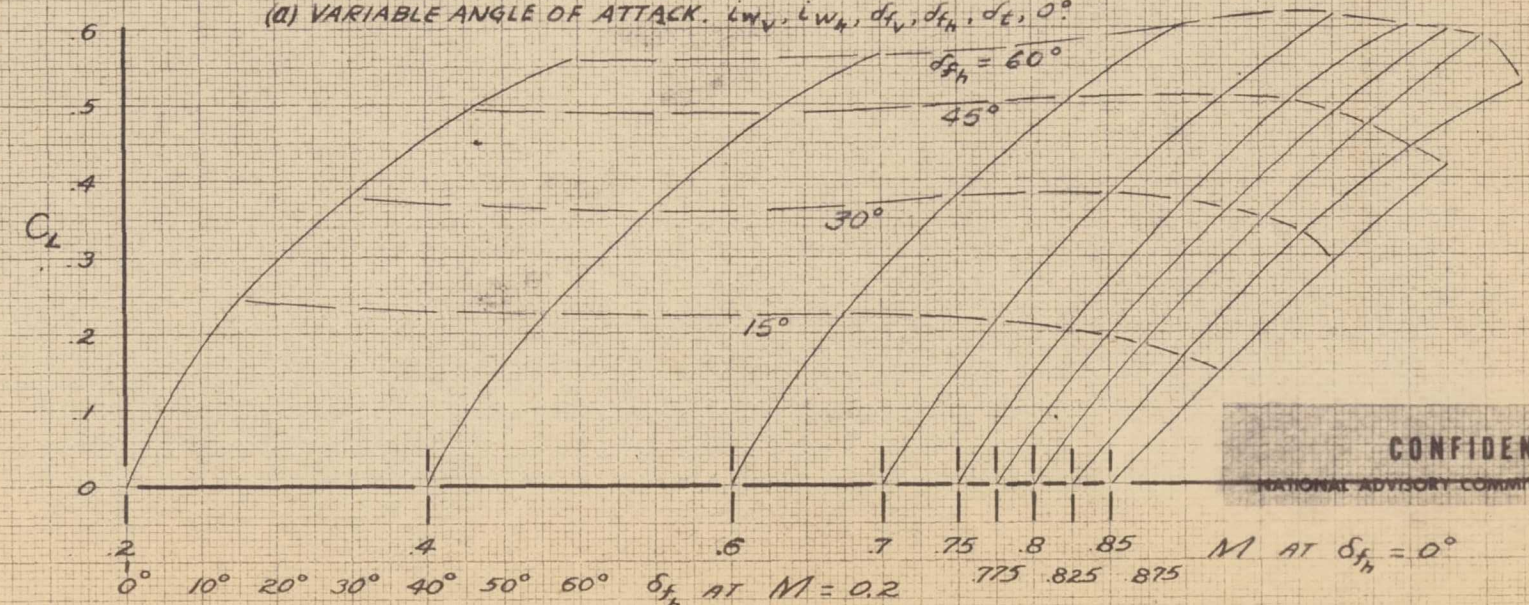

(b) VARIABLE HORIZONTAL WING FLAP DEFLECTION. α, i_{W_V}, i_{W_H}, δ_{f_V}, δ_t, 0°.

FIGURE 7. - VARIATION OF LIFT COEFFICIENT WITH ANGLE OF ATTACK, HORIZONTAL WING FLAP DEFLECTION, AND TAIL SETTING FOR THE FULL-SCALE MODEL OF THE CONSOLIDATED VULTEE LAEK.

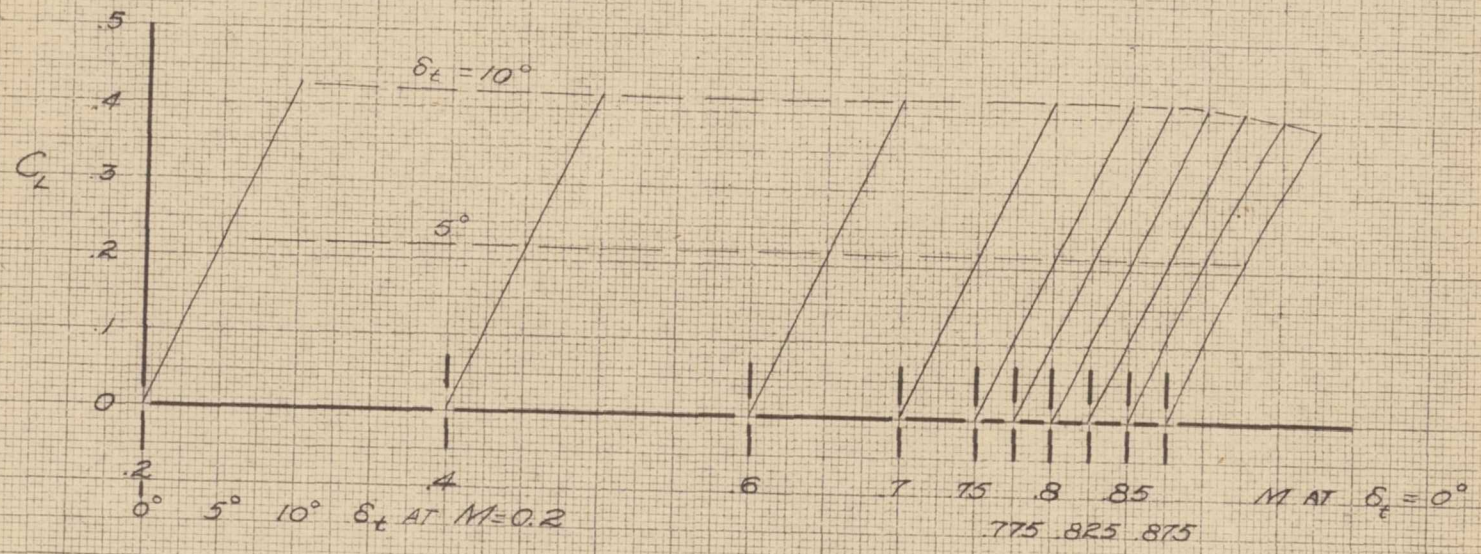

(c) VARIABLE TAIL SETTING. α, i_{W_V}, i_{W_H}, d_{f_V}, d_{f_H}, 0°.

FIGURE 7.- CONCLUDED.

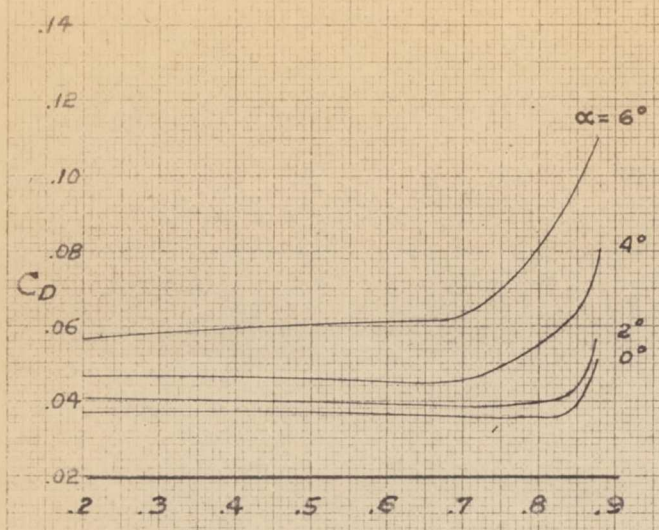

(a) VARIABLE ANGLE OF ATTACK.
i_{w_v}, i_{w_h}, δ_{f_v}, δ_{f_h}, 0°

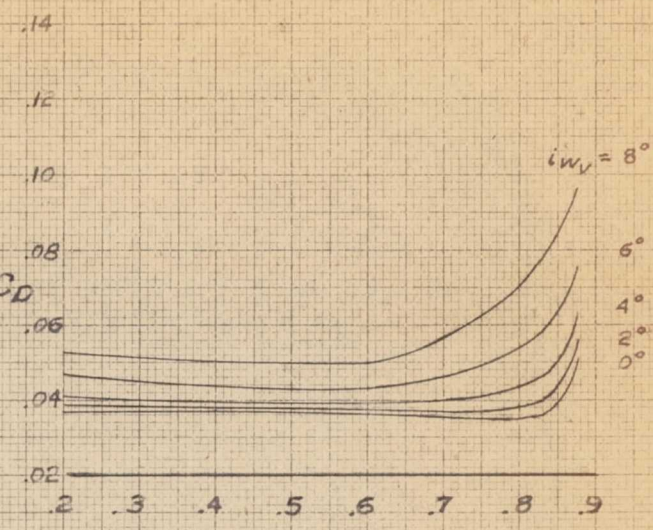

(b) VARIABLE WING INCIDENCE.
α, i_{w_h}, δ_{f_v}, δ_{f_h}, 0°.

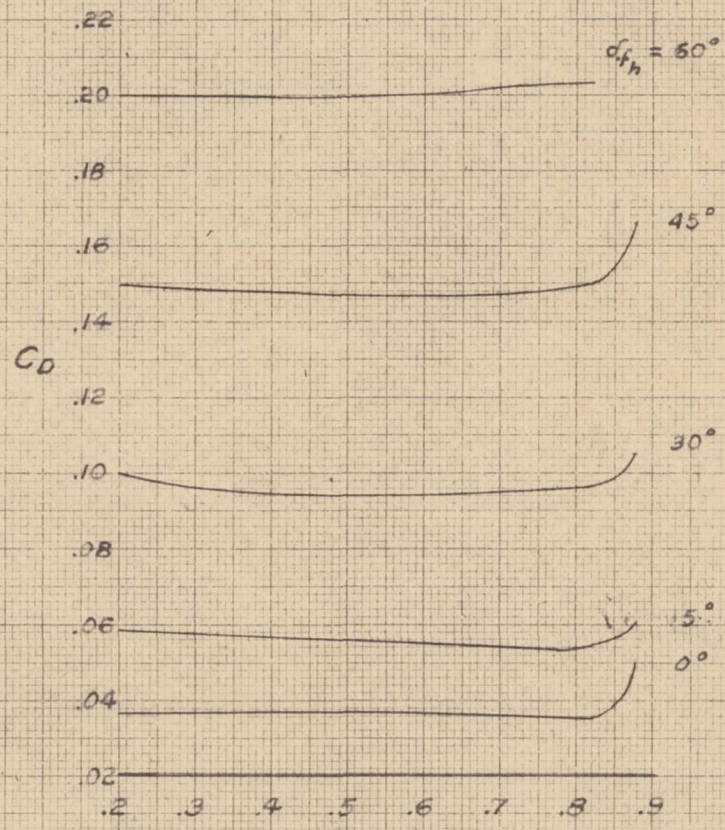

(c) VARIABLE FLAP DEFLECTION.
α, i_{w_v}, i_{w_h}, δ_{f_v}, 0°

FIGURE 8.- VARIATION OF DRAG COEFFICIENT WITH MACH NUMBER FOR THE FULL-SCALE MODEL OF THE CONSOLIDATED VULTEE LARK, LESS TAIL.

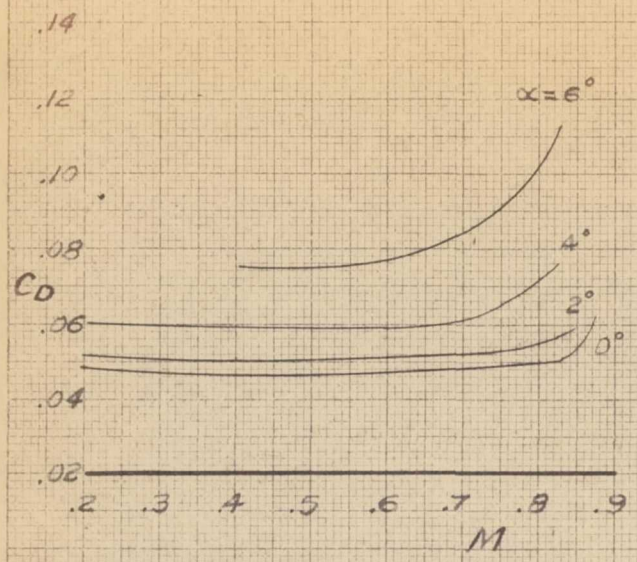

(a) VARIABLE ANGLE OF ATTACK.
i_{w_v}, i_{w_h}, δ_{f_v}, δ_{f_h}, δ_t, 0°.

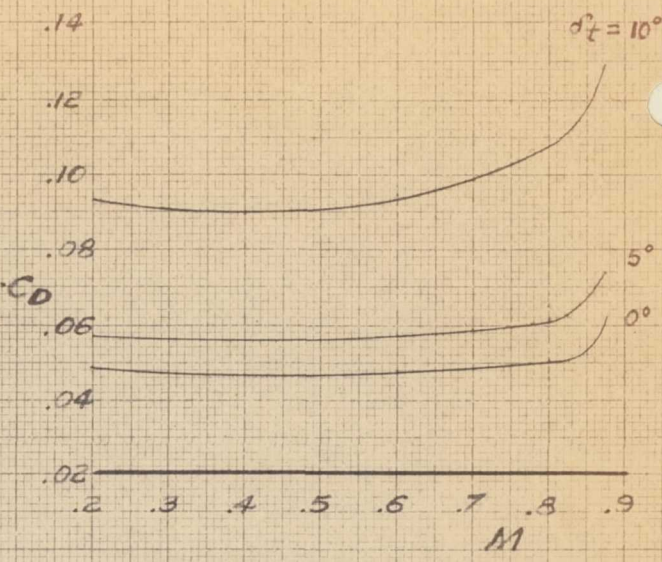

(b) VARIABLE TAIL SETTING.
α, i_{w_v}, i_{w_h}, δ_{f_v}, δ_{f_h}, 0°.

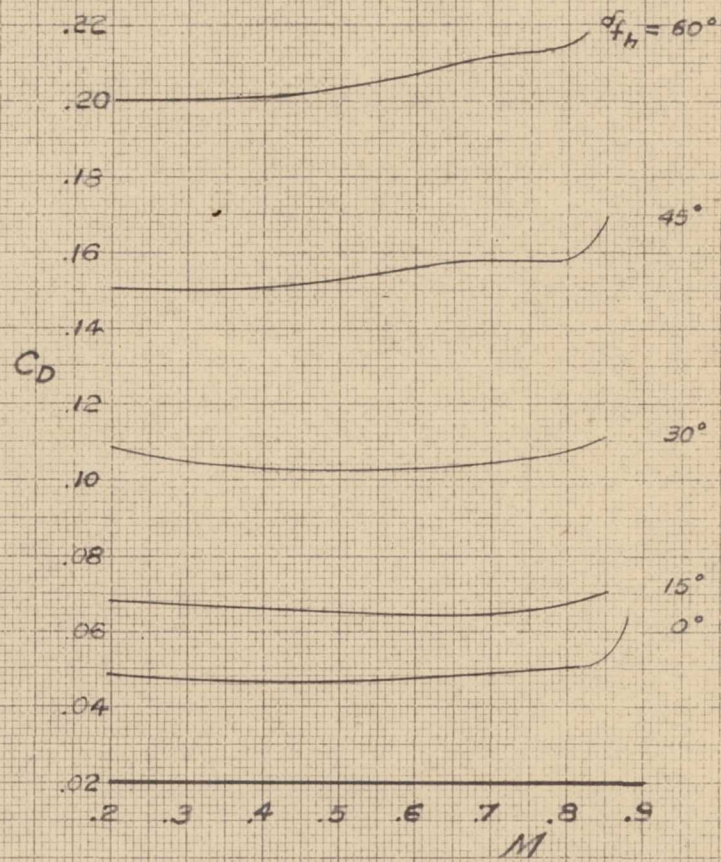

(c) VARIABLE FLAP DEFLECTION.
α, i_{w_v}, i_{w_h}, δ_{f_v}, δ_t, 0°.

FIGURE 9.- VARIATION OF DRAG COEFFICIENT WITH MACH NUMBER FOR THE FULL-SCALE MODEL OF THE CONSOLIDATED VULTEE LARK.

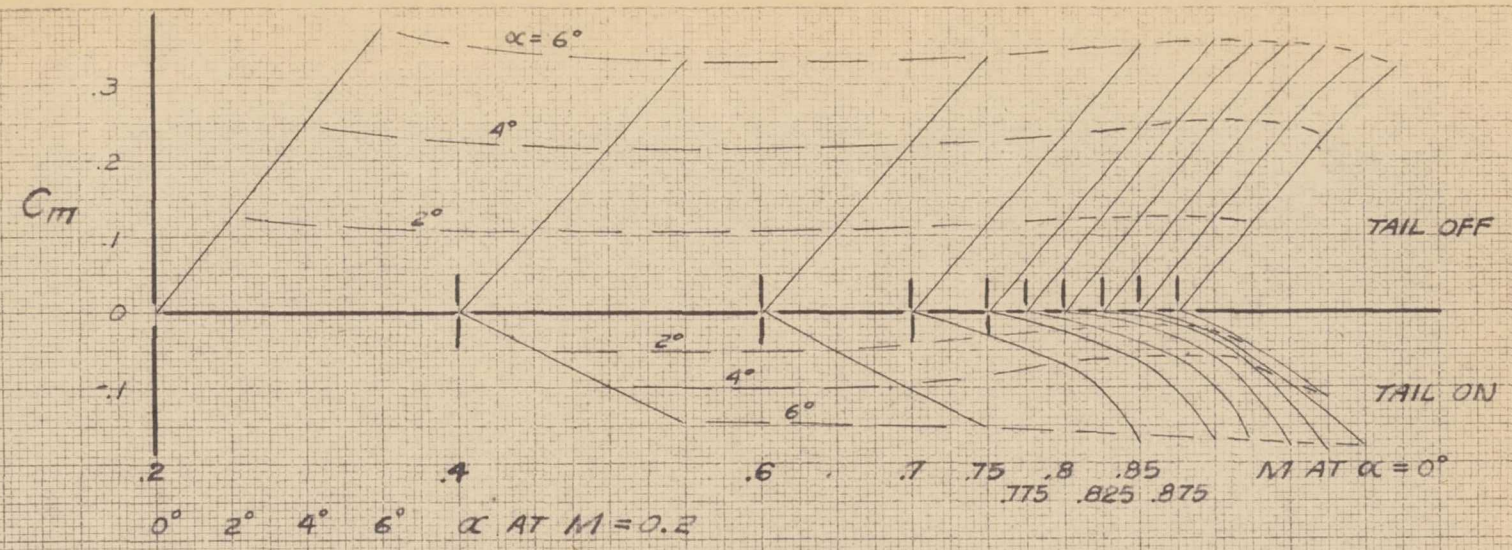

(a) VARIABLE ANGLE OF ATTACK. i_{w_v}, i_{w_h}, δ_{f_v}, δ_{f_h}, δ_t, 0°.

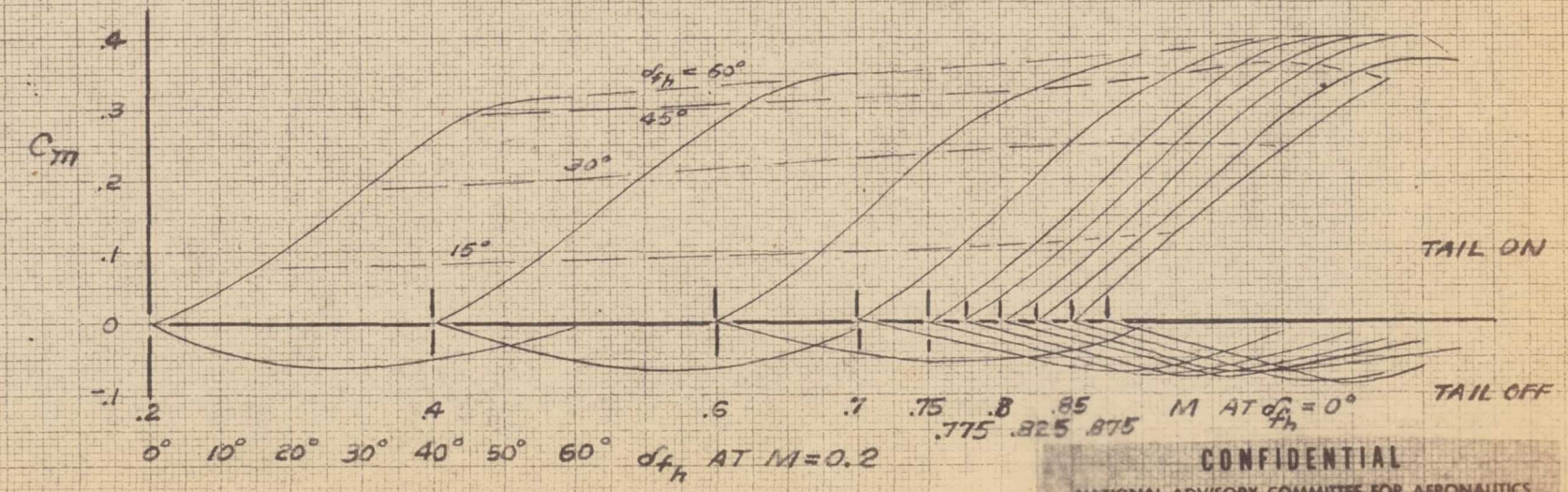

(b) VARIABLE HORIZONTAL WING FLAP DEFLECTION. α, i_{w_v}, i_{w_h}, δ_{f_v}, δ_t, 0°.

FIGURE 10.- EFFECTS OF ANGLE OF ATTACK AND HORIZONTAL WING-FLAP DEFLECTION ON THE PITCHING-MOMENT COEFFICIENT OF THE FULL-SCALE MODEL OF THE CONSOLIDATED VULTEE LARK.

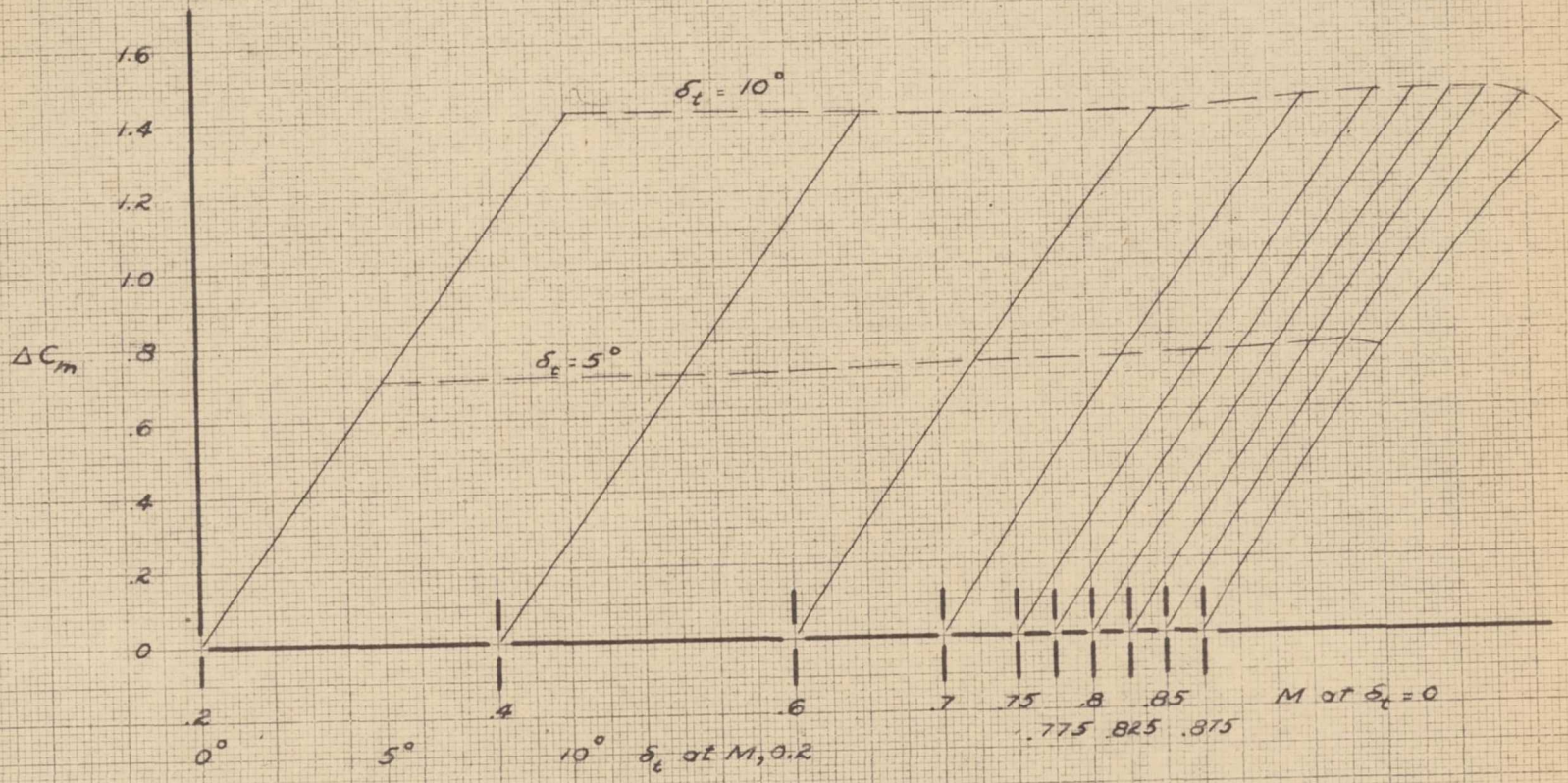

CONFIDENTIAL
NATIONAL ADVISORY COMMITTEE FOR AERONAUTICS

FIGURE 11.- VARIATION OF PITCHING MOMENT COEFFICIENT WITH TAIL DEFLECTION FOR THE FULL-SCALE MODEL OF THE CONSOLIDATED VULTEE LARK. α, i_{w_v}, i_{w_h}, δ_{f_v}, δ_{f_h}, 0°.

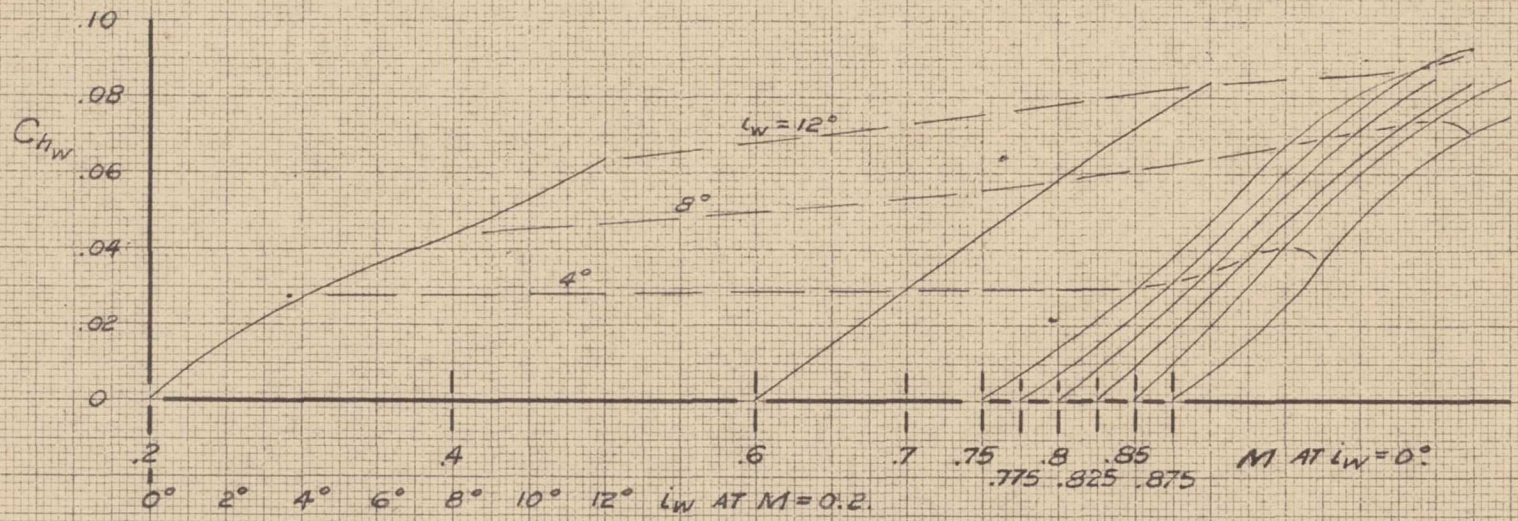

FIGURE 12 - VARIATION OF WING HINGE-MOMENT COEFFICIENT WITH WING INCIDENCE FOR THE VERTICAL WING OF THE FULL-SCALE MODEL OF THE CONSOLIDATED VULTEE LARK. α, i_{w_h}, δ_{f_v}, δ_{f_h}, 0°.

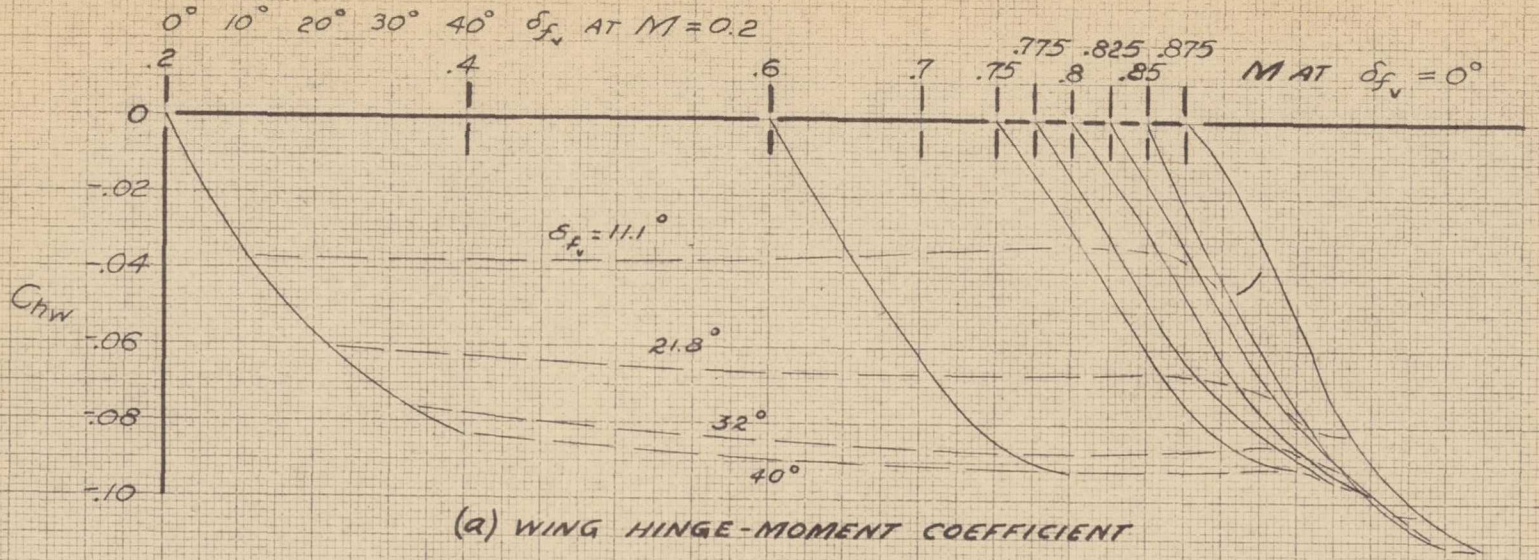

(a) WING HINGE-MOMENT COEFFICIENT

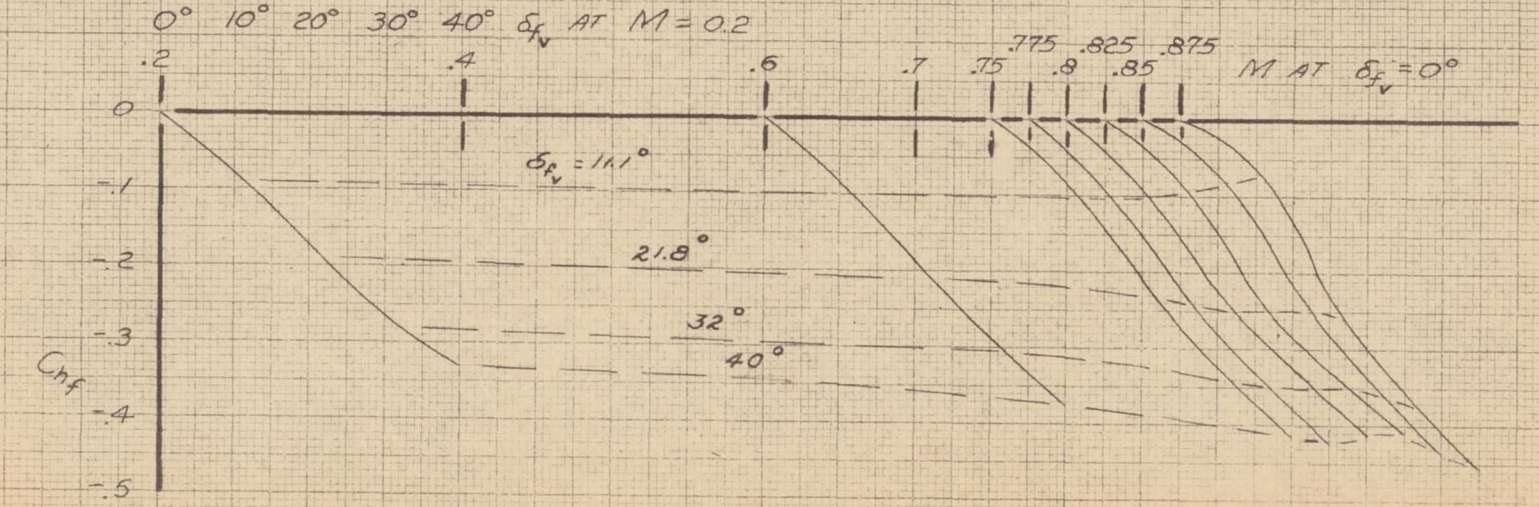

(b) FLAP HINGE-MOMENT COEFFICIENT

FIGURE 13.- VARIATIONS OF WING AND FLAP HINGE-MOMENT COEFFICIENTS WITH FLAP DEFLECTION FOR THE VERTICAL WING OF THE FULL-SCALE MODEL OF THE CONSOLIDATED VULTEE LARK. α, i_{w_v}, i_{w_h}, δ_{f_h}, 0°.

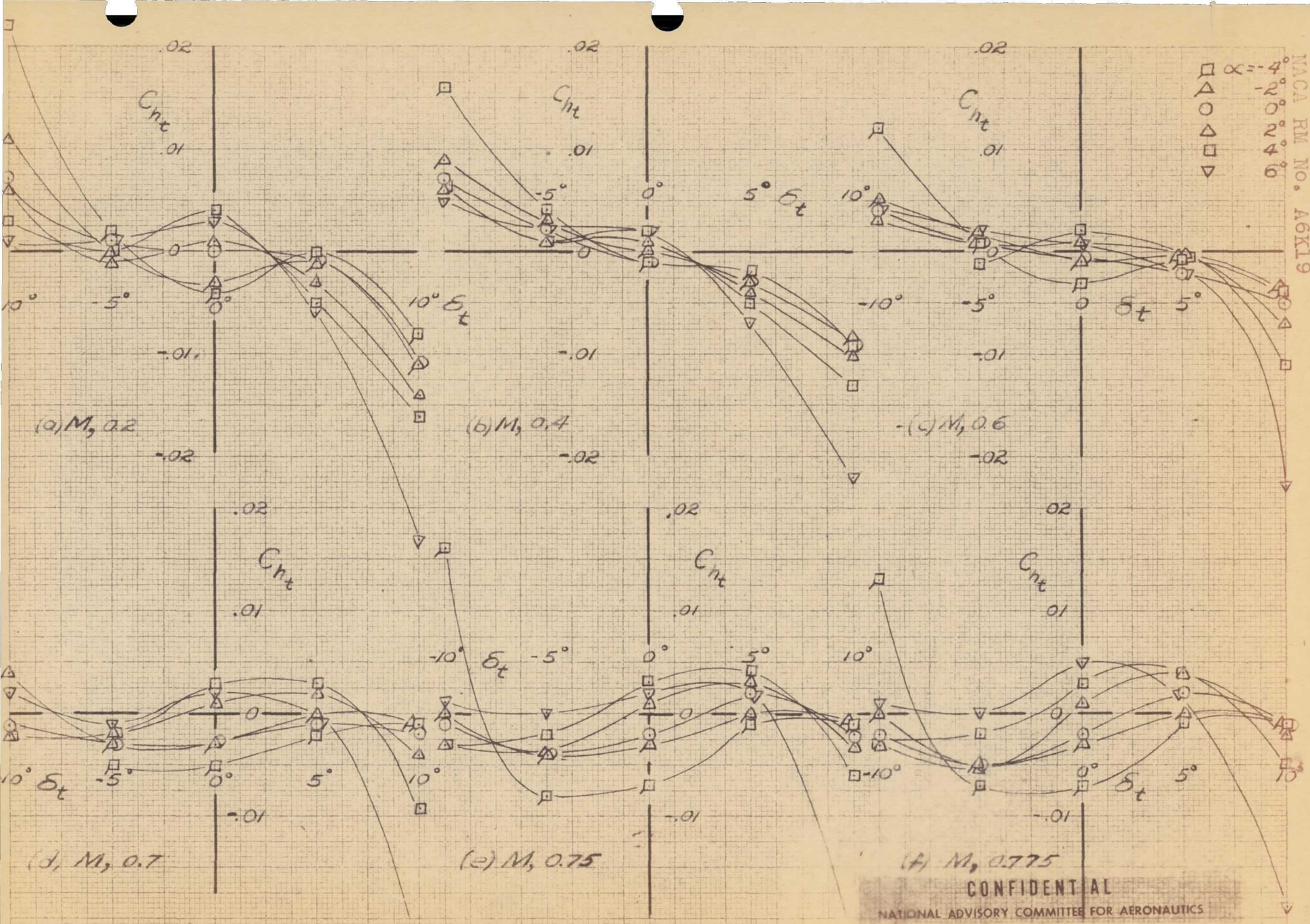

FIGURE 14.- VARIATION OF TAIL HINGE-MOMENT COEFFICIENT WITH TAIL DEFLECTION AT VARIOUS ANGLES OF ATTACK FOR THE FULL-SCALE MODEL OF THE CONSOLIDATED VULTEE LARK. i_{w_v}, i_{w_h}, δ_{f_v}, δ_{f_h}, 0°

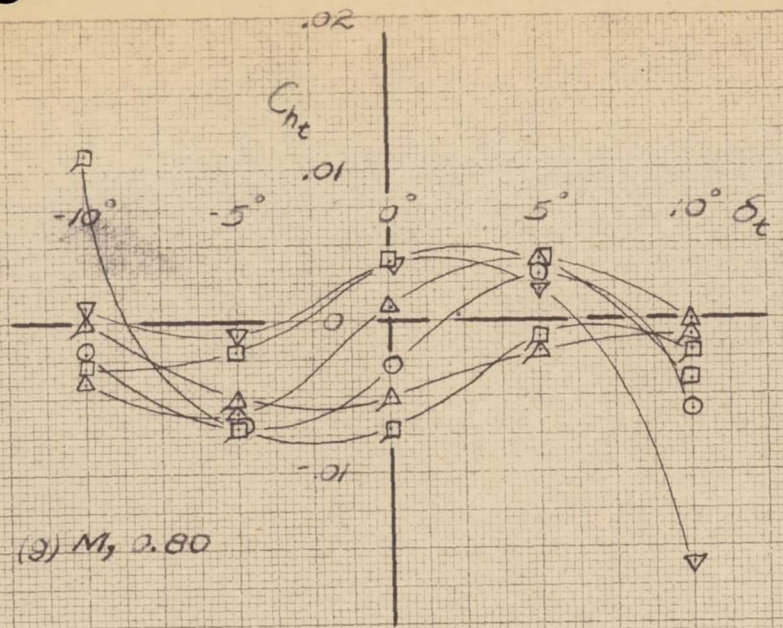

(g) M, 0.80

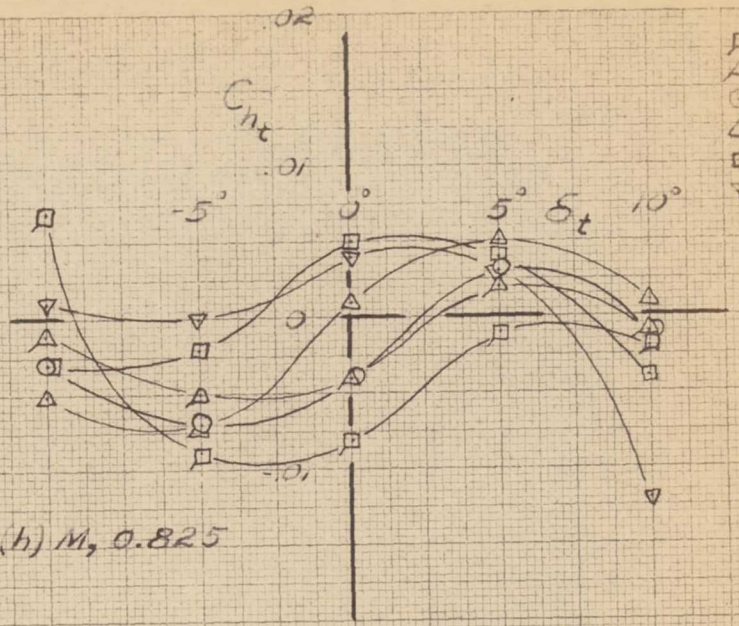

(h) M, 0.825

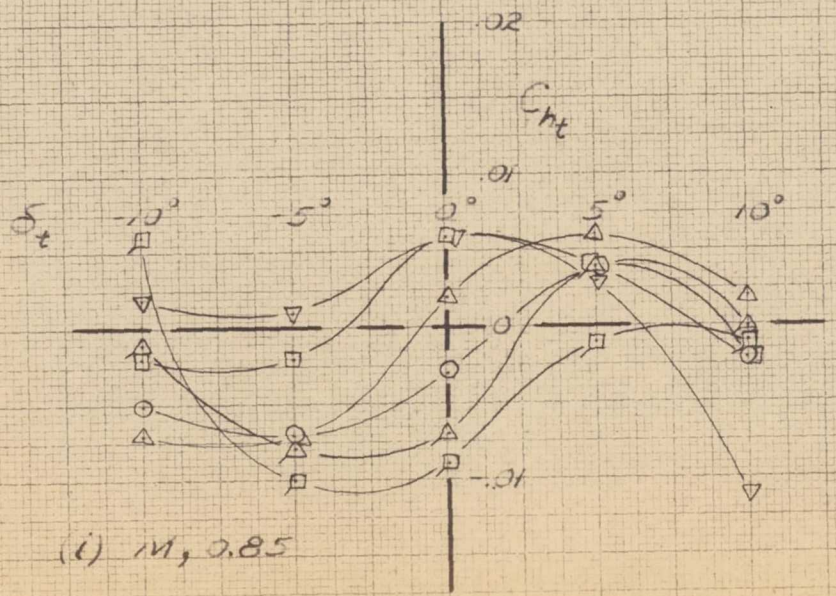

(i) M, 0.85

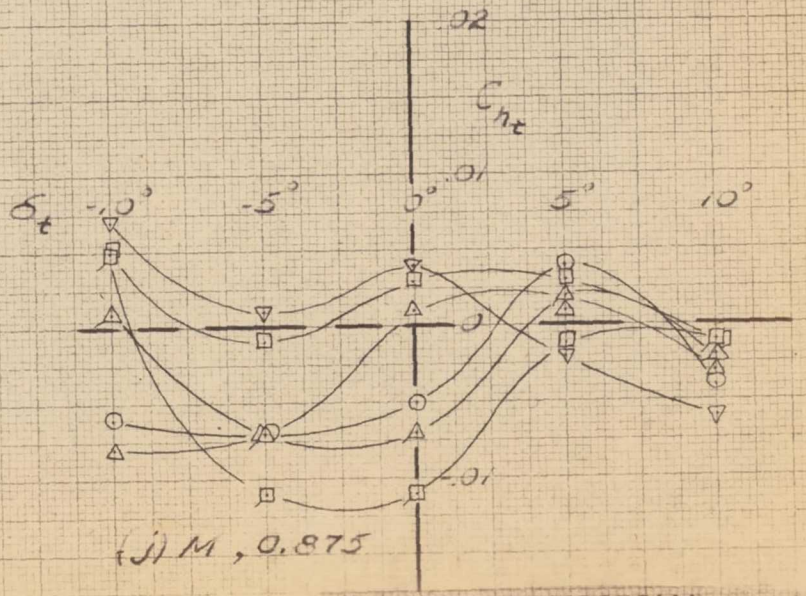

(j) M, 0.875

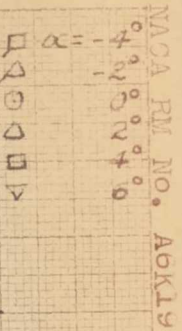

FIGURE 14.- CONCLUDED.

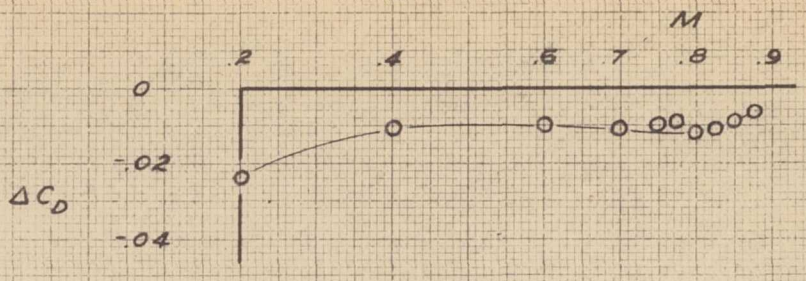

(a) TAIL CONE

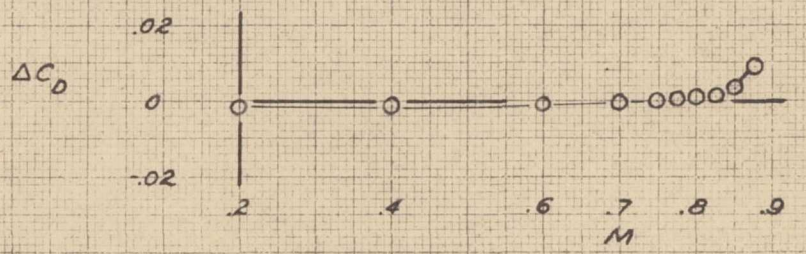

(b) CONTROL FAIRINGS

FIGURE 15. - VARIATIONS OF THE DRAG INCREMENTS OF THE TAIL CONE AND OF THE CONTROL FAIRINGS WITH MACH NUMBER FOR THE FULL-SCALE MODEL OF THE CONSOLIDATED VULTEE LARK.
α, i_{w_v}, i_{w_h}, δ_{f_v}, δ_{f_h}, δ_t, 0°.

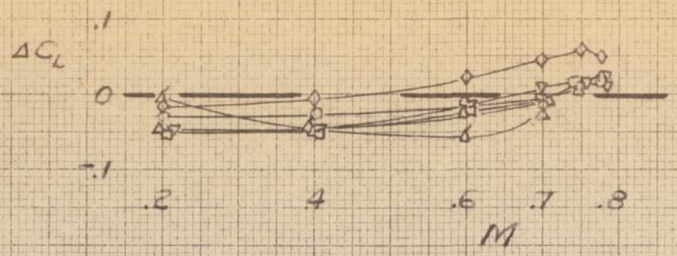

(a) LIFT COEFFICIENT

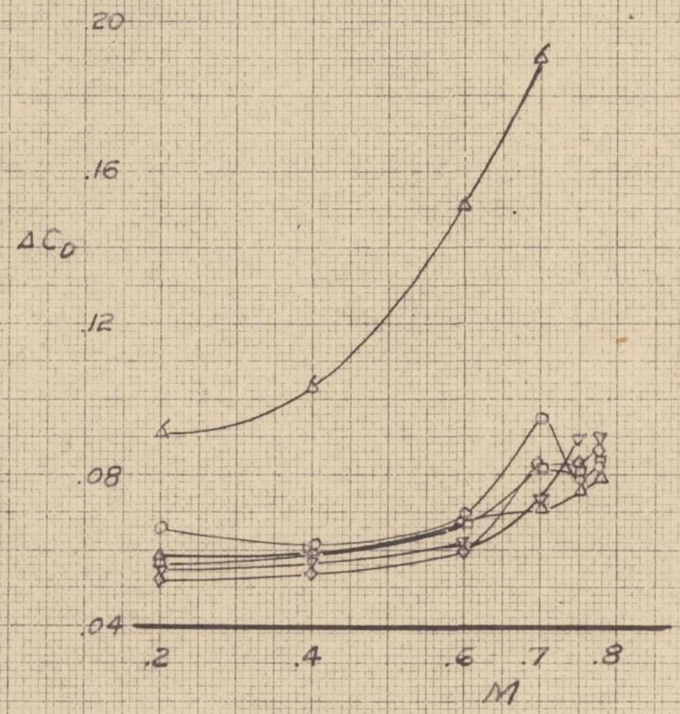

(b) DRAG COEFFICIENT

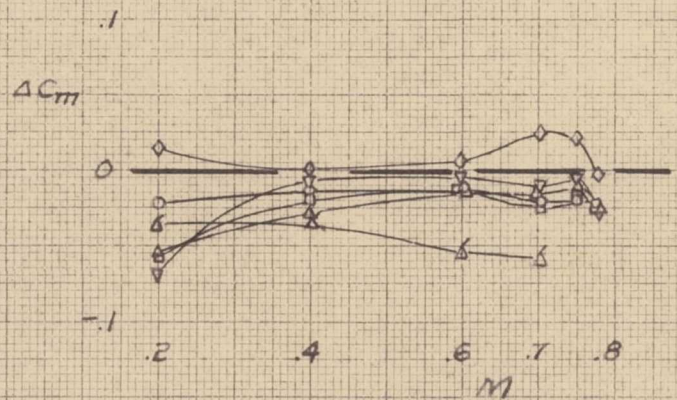

(c) PITCHING-MOMENT COEFFICIENT

CONFIDENTIAL

NATIONAL ADVISORY COMMITTEE FOR AERONAUTICS

FIGURE 16.- VARIATION OF THE INCREMENTS OF LIFT, DRAG, AND PITCHING-MOMENT COEFFICIENTS WITH MACH NUMBER DUE TO THE JATOS ON THE FULL-SCALE MODEL OF THE CONSOLIDATED VULTEE LARK, LESS TAIL. i_{W_h}, δ_{f_h}, 0°.

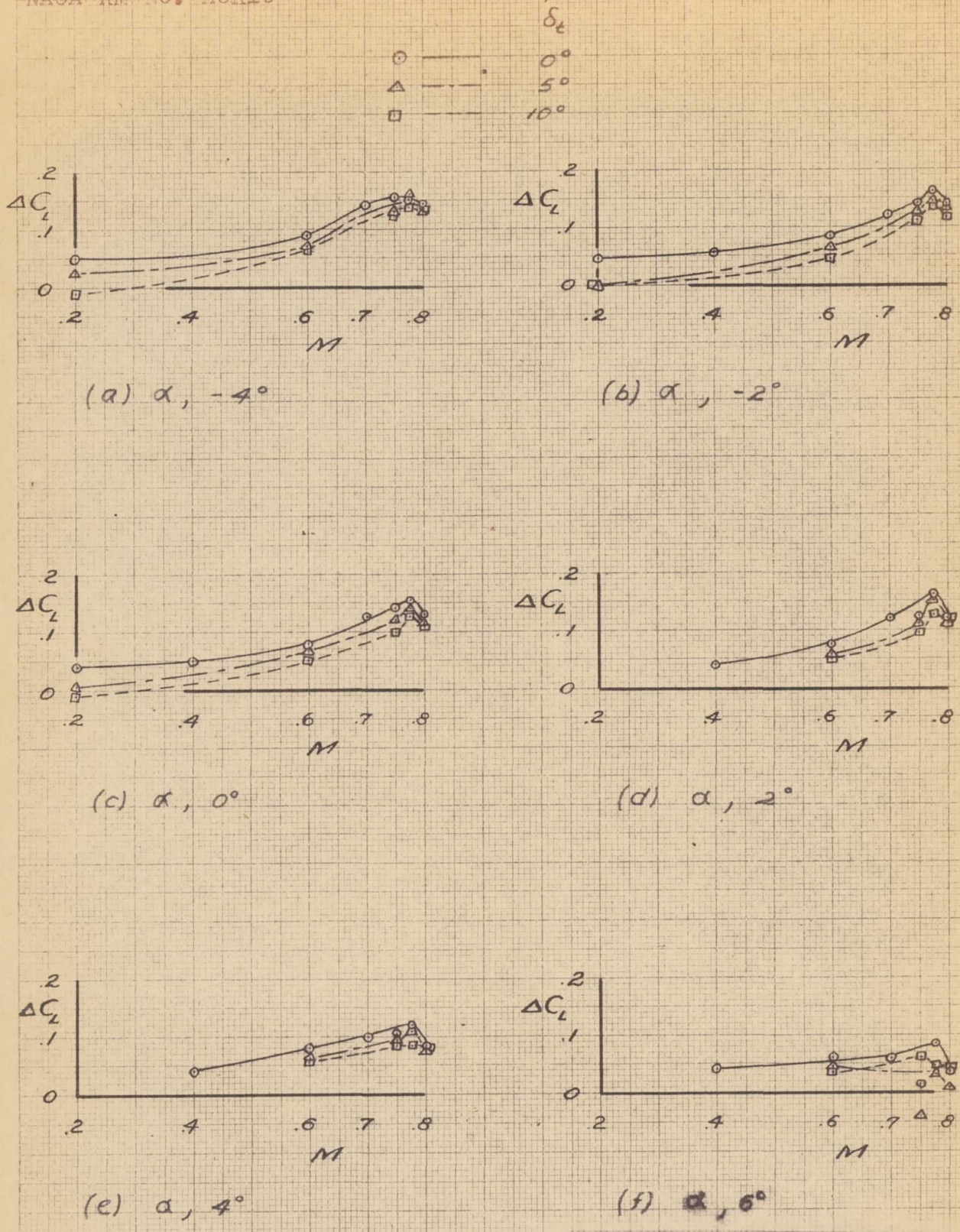

FIGURE 17.- VARIATION OF THE INCREMENTS OF LIFT COEFFICIENT WITH NUMBER DUE TO THE JATOS ON THE FULL-SCALE MODEL OF THE CONSOLIDATED VULTEE LARK. i_{w_v}, i_{w_h}, δ_{f_v}, δ_{f_h}, 0°.

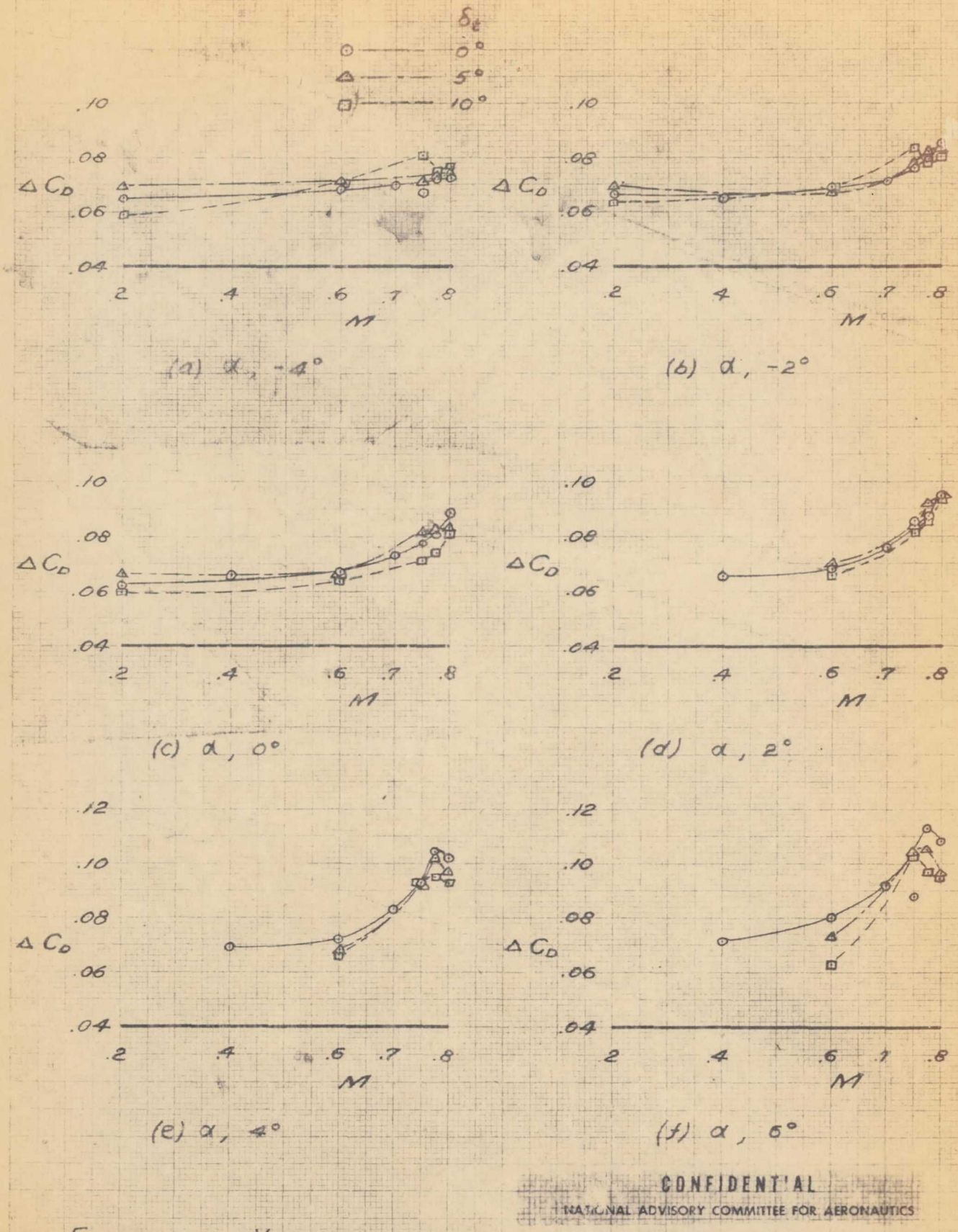

FIGURE 18. - VARIATION OF THE INCREMENTS OF DRAG COEFFICIENT WITH MACH NUMBER DUE TO THE JATOS ON THE FULL-SCALE MODEL OF THE CONSOLIDATED VULTEE LARK. i_{w_o}, i_{w_i}, δ_{f_o}, δ_{f_i}, 0°.

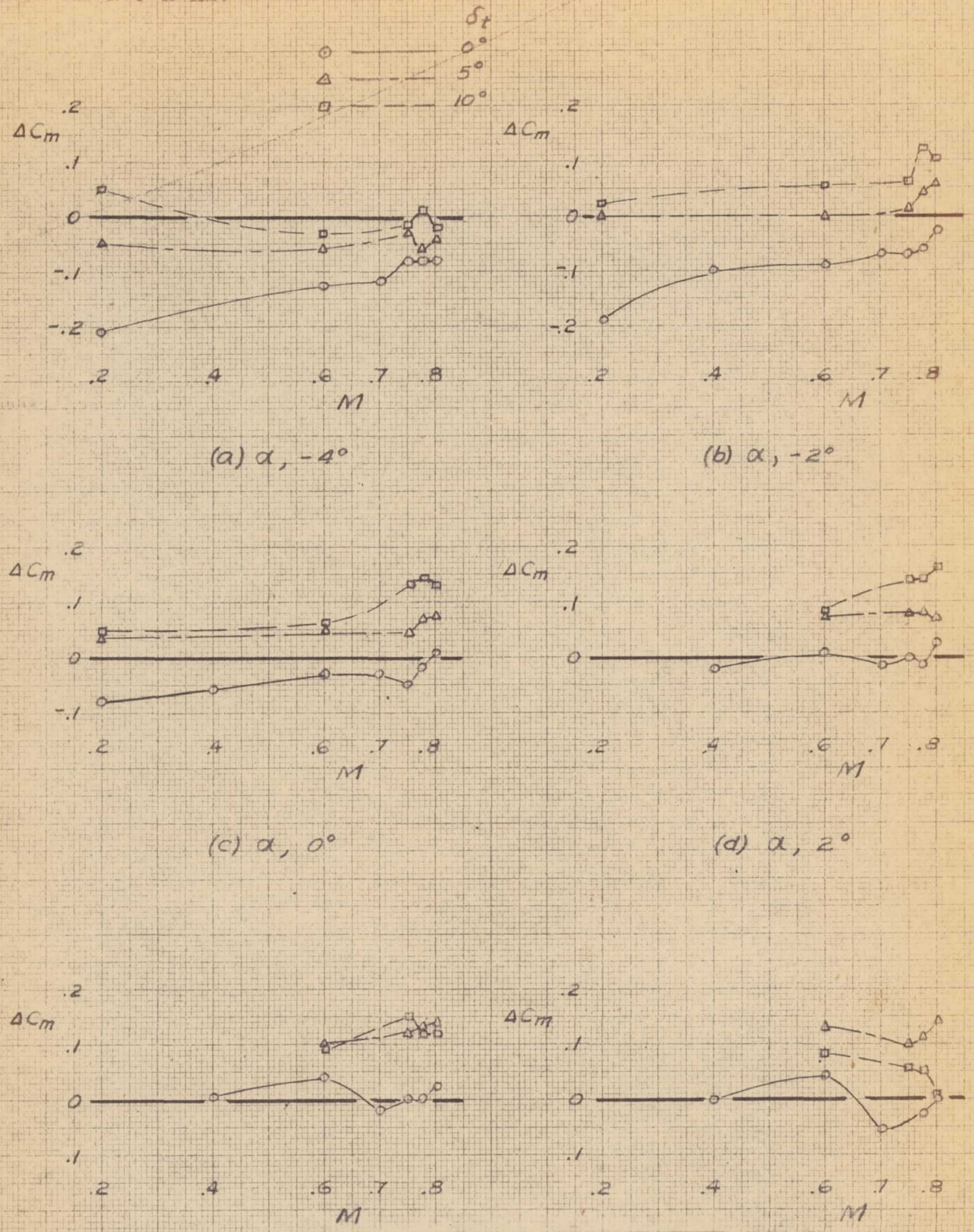

FIGURE 19. - VARIATION OF THE INCREMENTS OF PITCHING-MOMENT COEFFICIENT WITH MACH NUMBER DUE TO THE JATOS ON THE FULL-SCALE MODEL OF THE CONSOLIDATED VULTEE LARK. i_{w_1}, i_{w_2}, δ_{f_1}, δ_{f_2}, 0°.

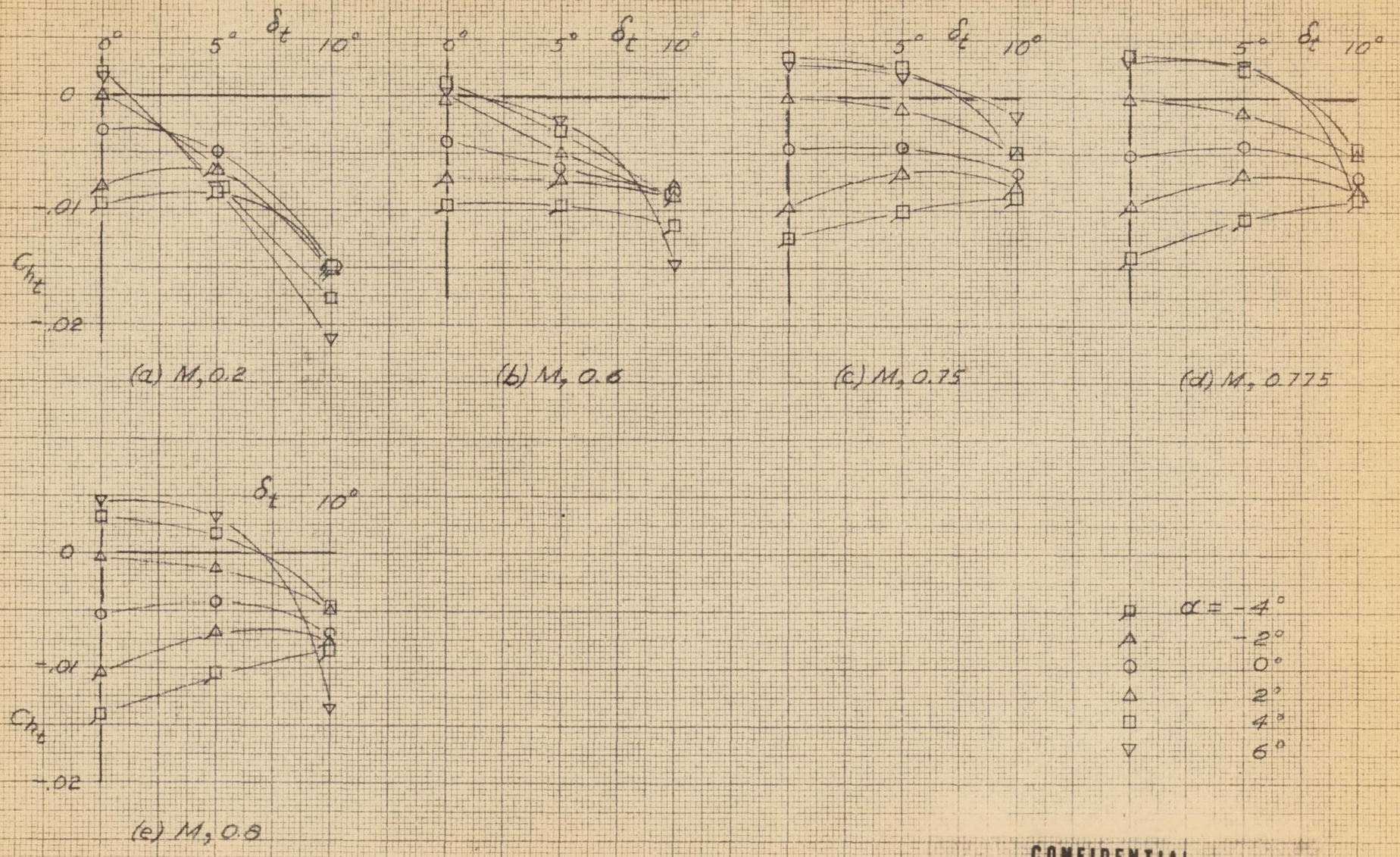

FIGURE 20- VARIATION OF TAIL HINGE-MOMENT COEFFICIENT WITH TAIL DEFLECTION FOR THE FULL-SCALE MODEL OF THE CONSOLIDATED VULTEE LARK WITH JATOS.

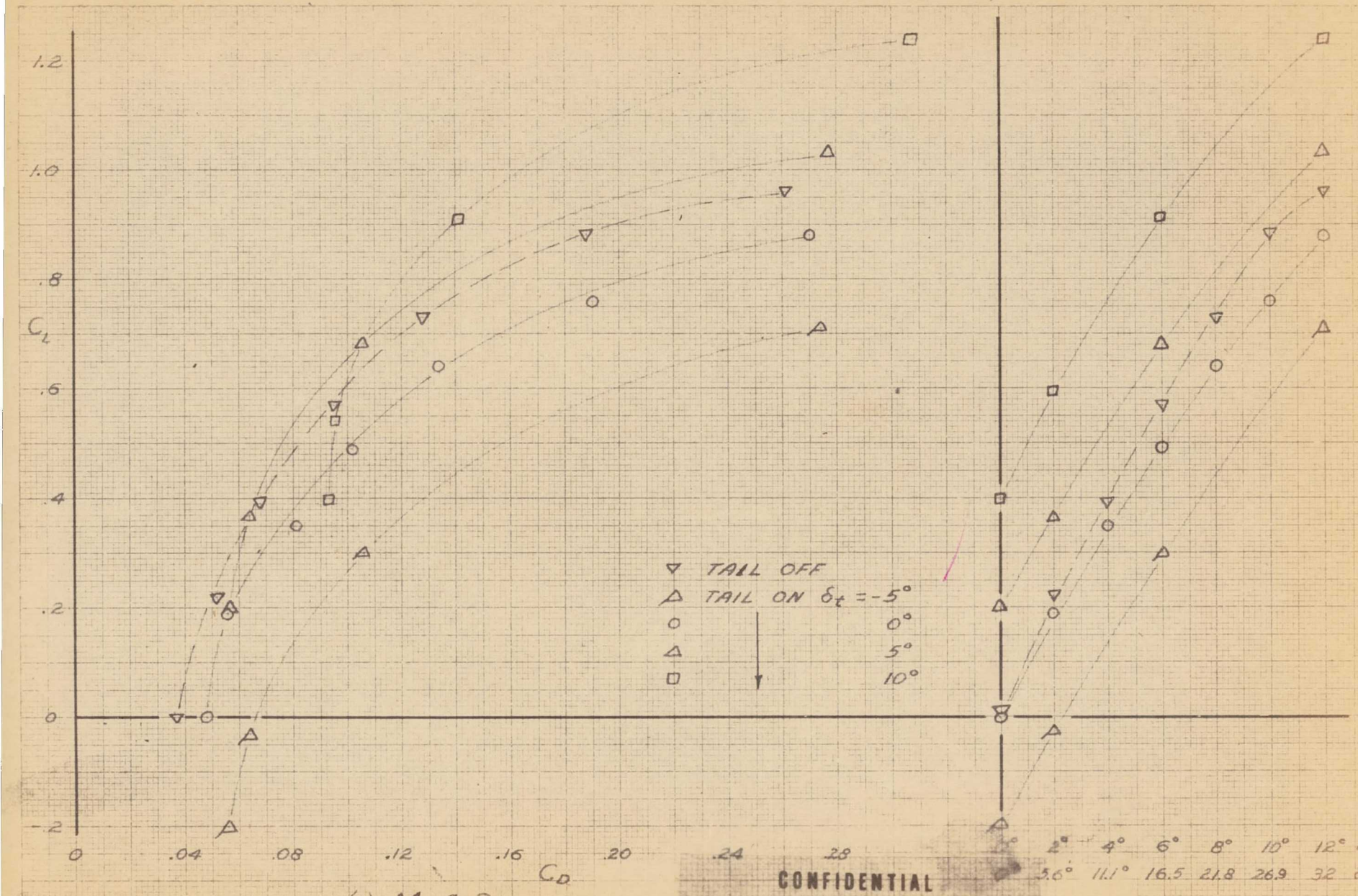

(a) M_1 0.2

FIGURE 21. – VARIATION OF LIFT COEFFICIENT WITH DRAG COEFFICIENT AND WITH LINKED DEFLECTIONS OF THE HORIZONTAL WING AND FLAPS FOR THE FULL-SCALE MODEL OF THE CONSOLIDATED VULTEE LARK. α, i_{W_V}, δ_{f_V}, 0°.

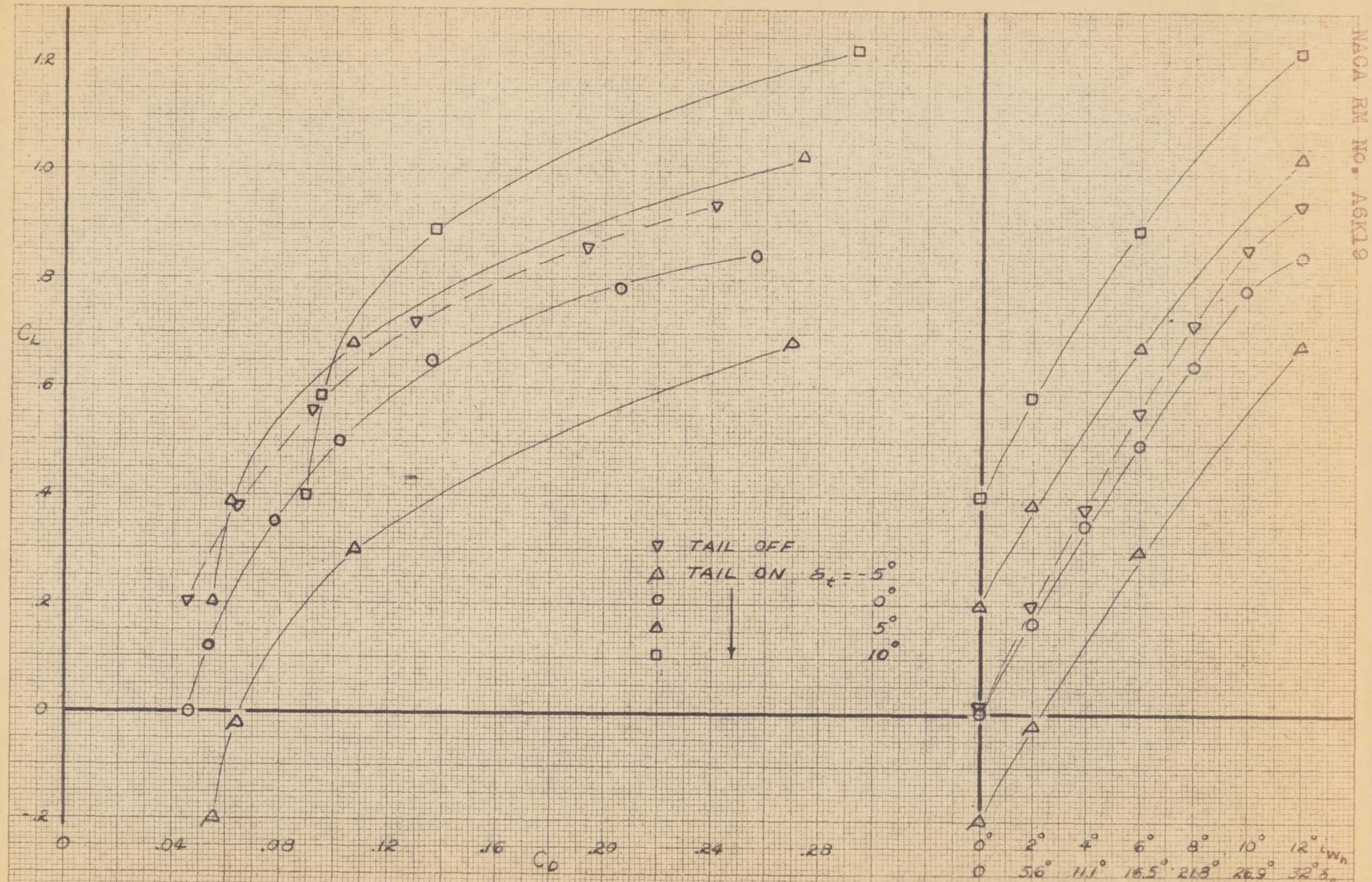

(b) M_o 0.4

FIGURE 21. - CONTINUED

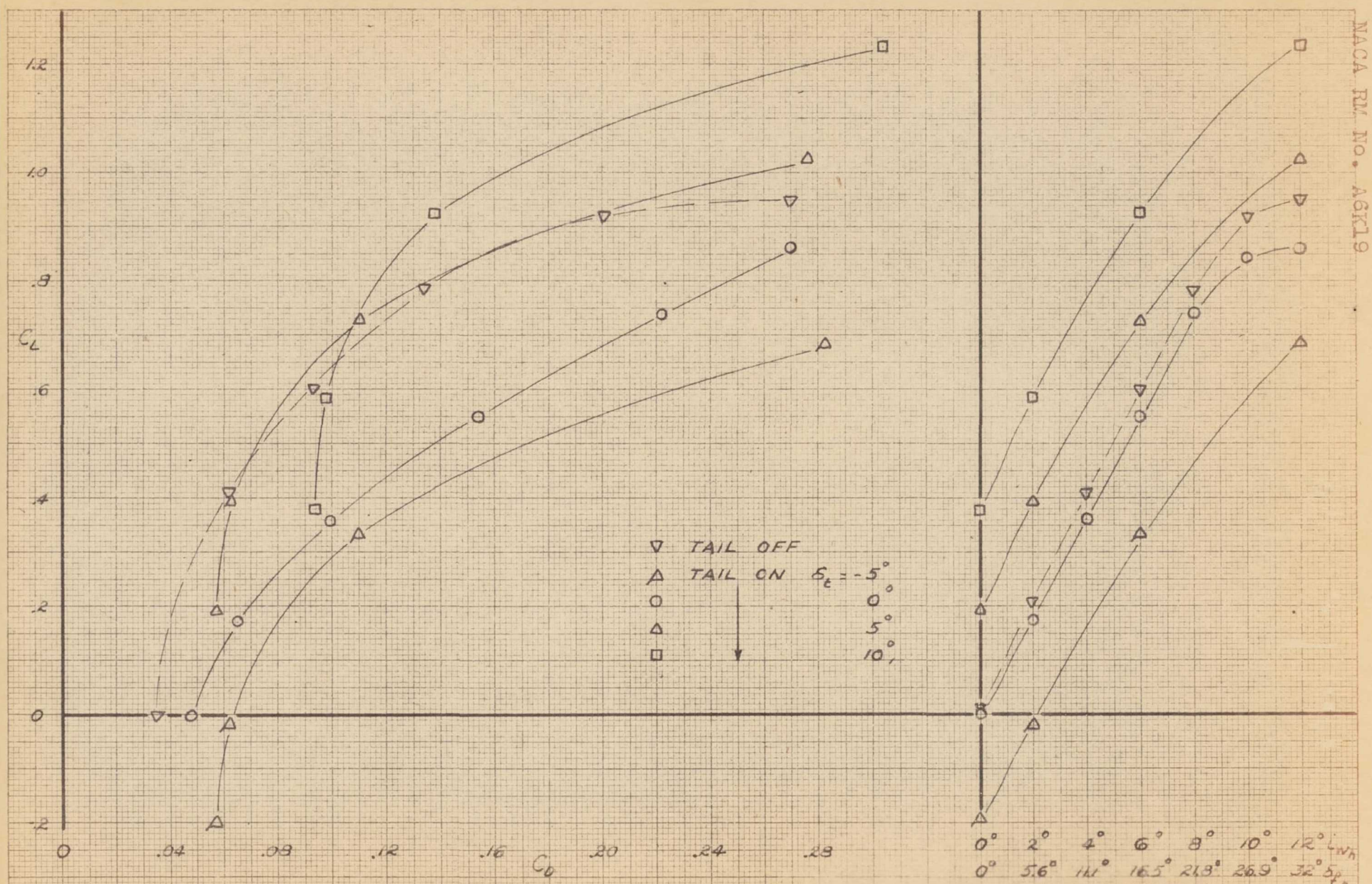

(c) M, 0.6

FIGURE 21.- CONTINUED

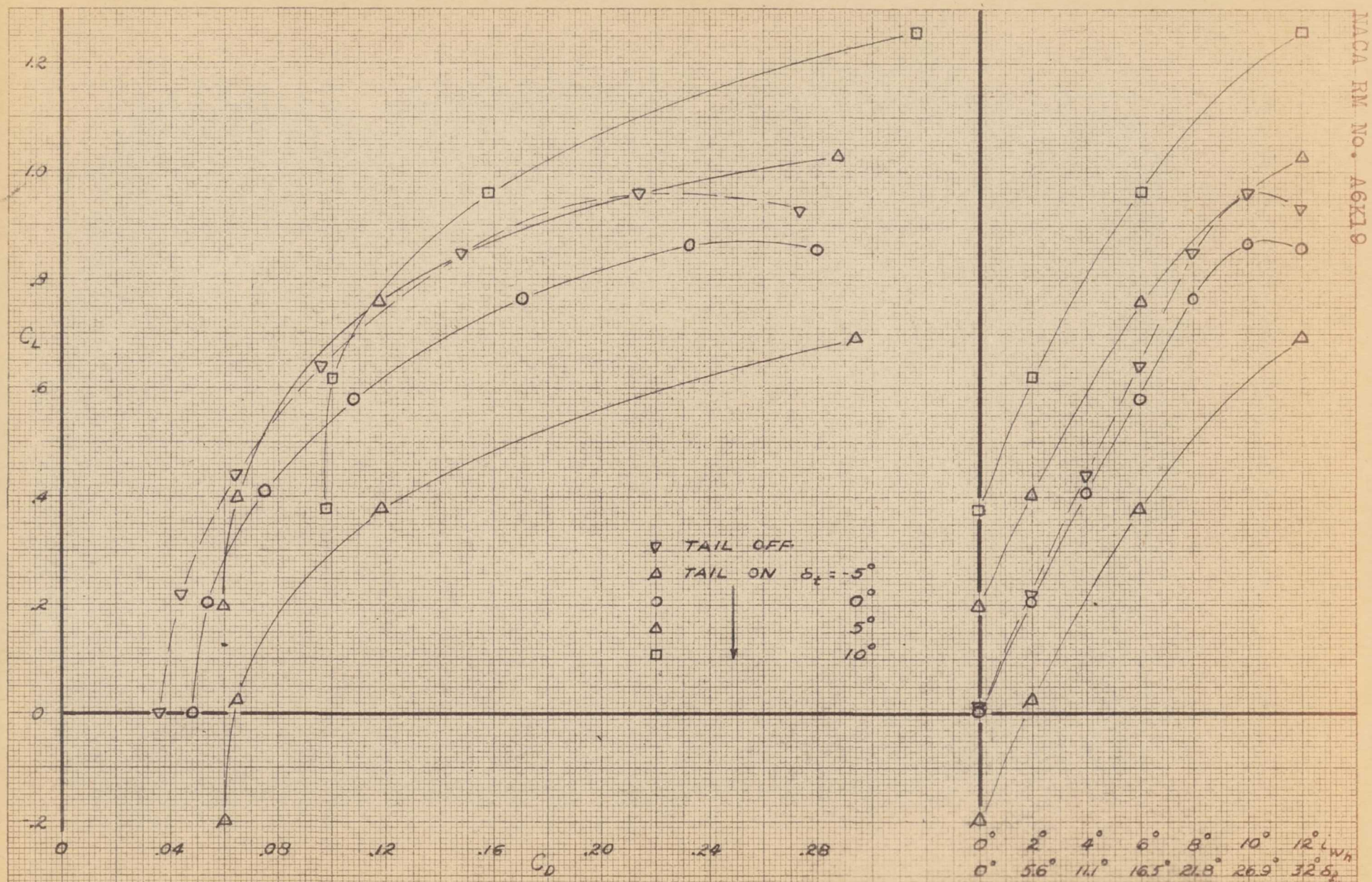

(d) M, 0.7

FIGURE 21.- CONTINUED.

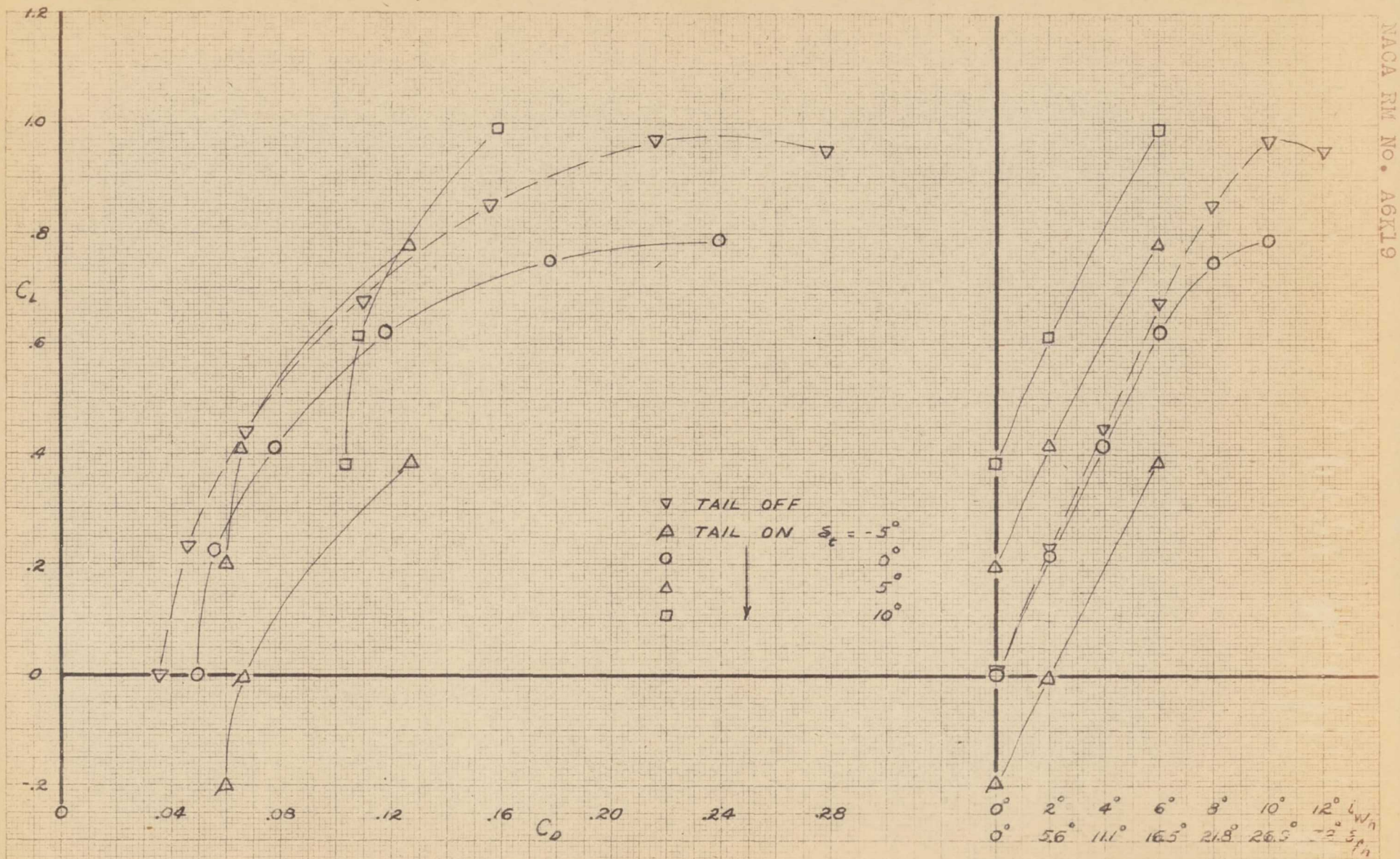

(e) M, 0.25

FIGURE 21. - CONTINUED.

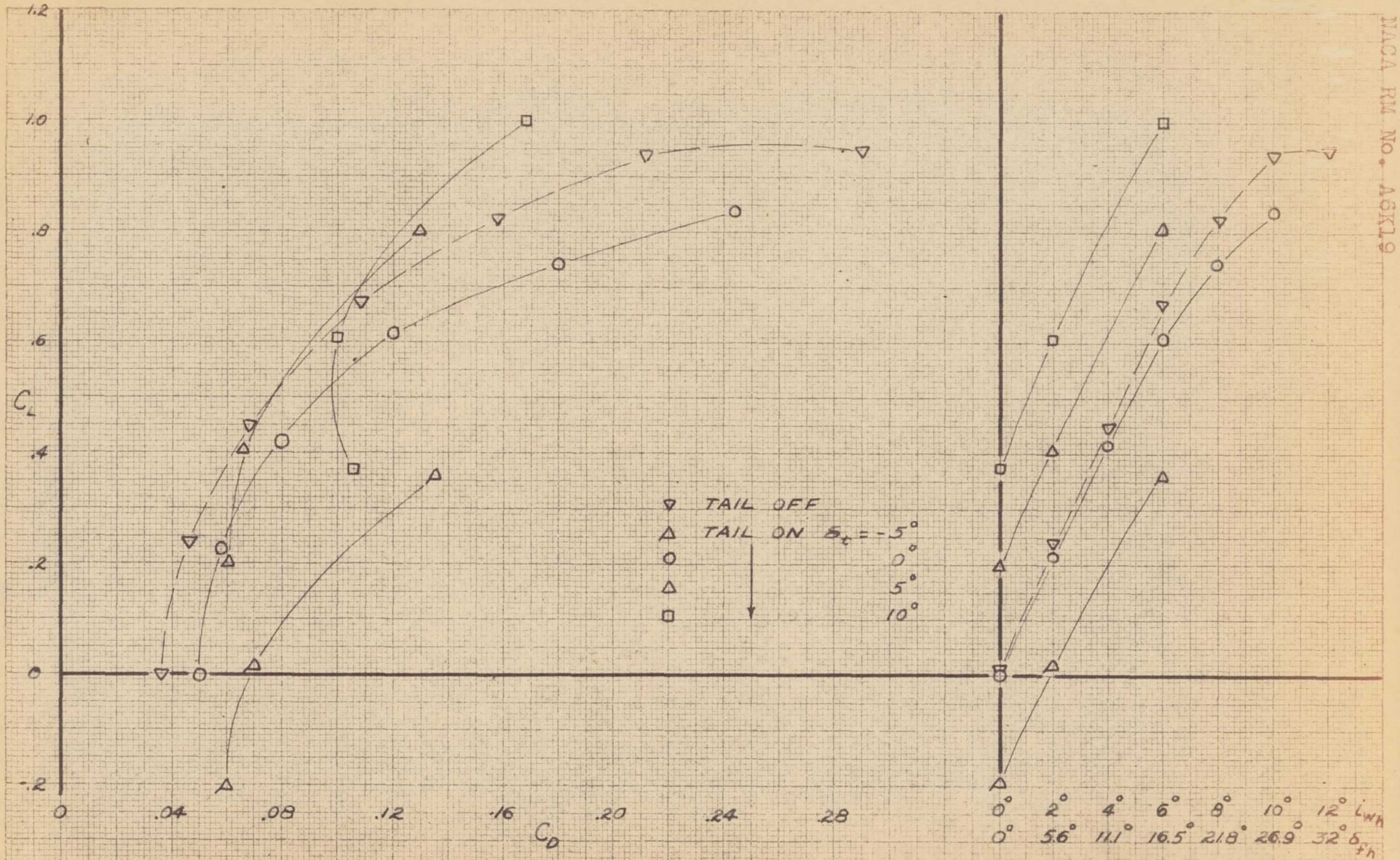

(f) M, 0.775

FIGURE 21.- CONTINUED

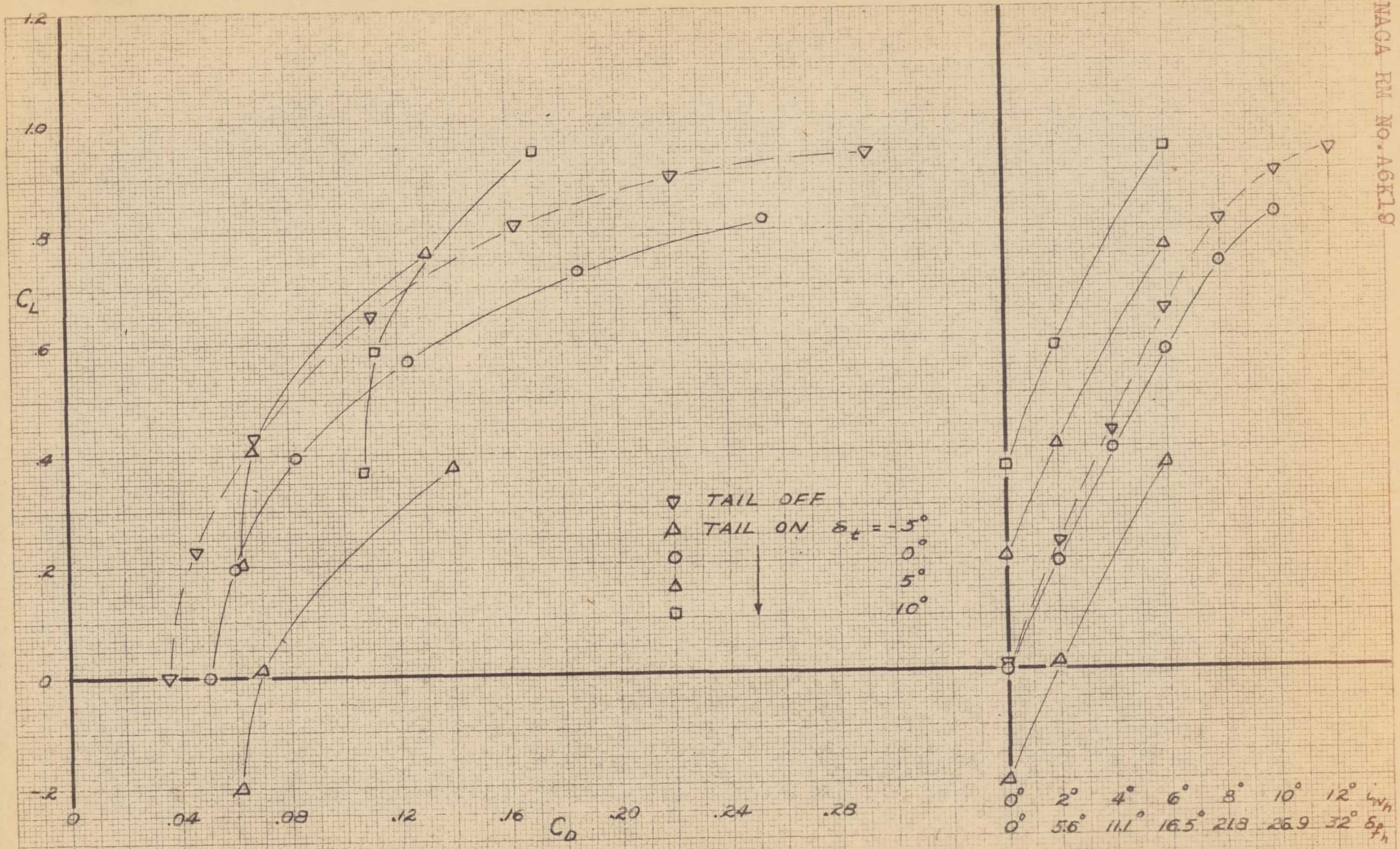

(g) M, 0.8

FIGURE 21. - CONTINUED.

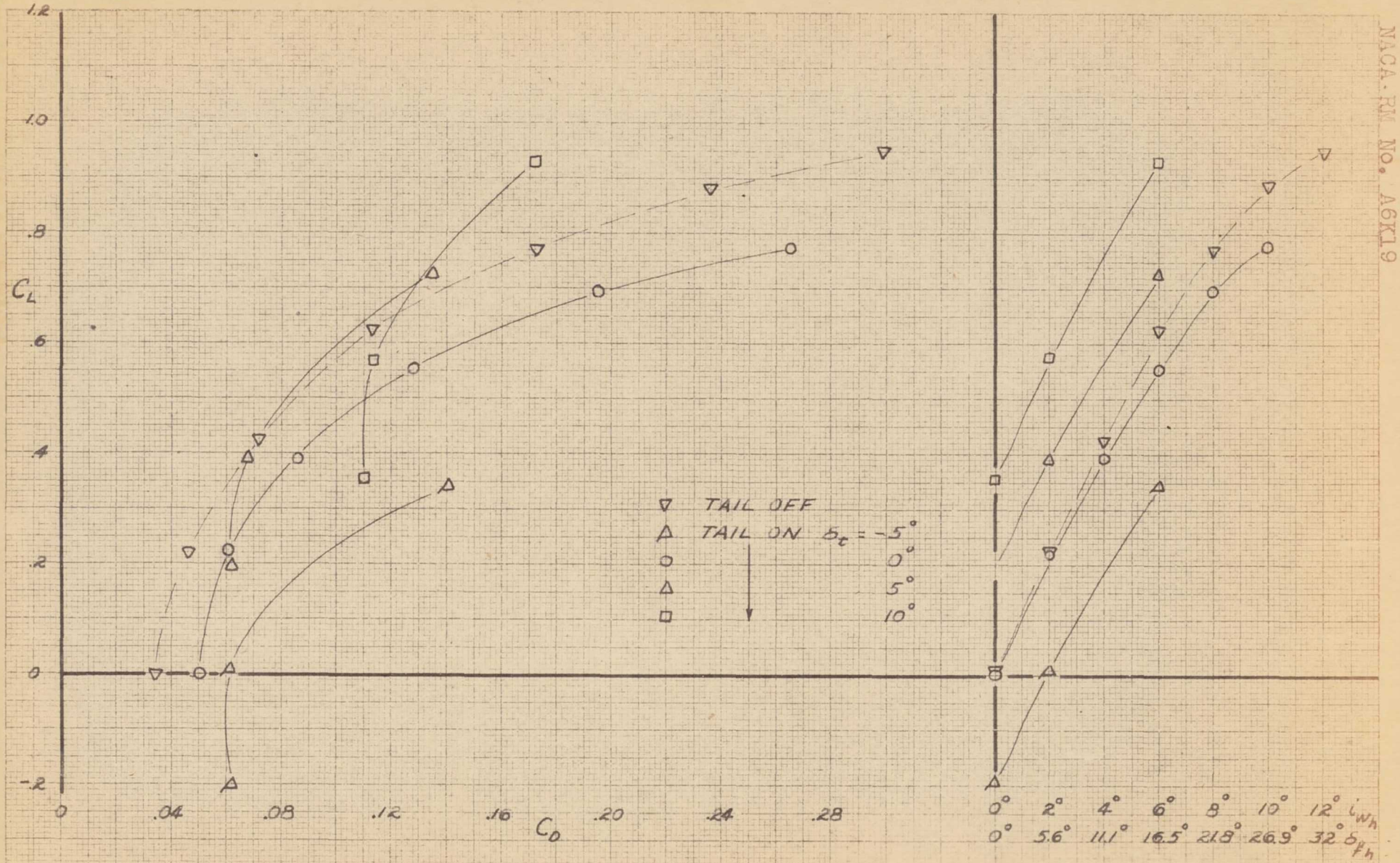

(b) M, 0.825

FIGURE 21. - CONTINUED.

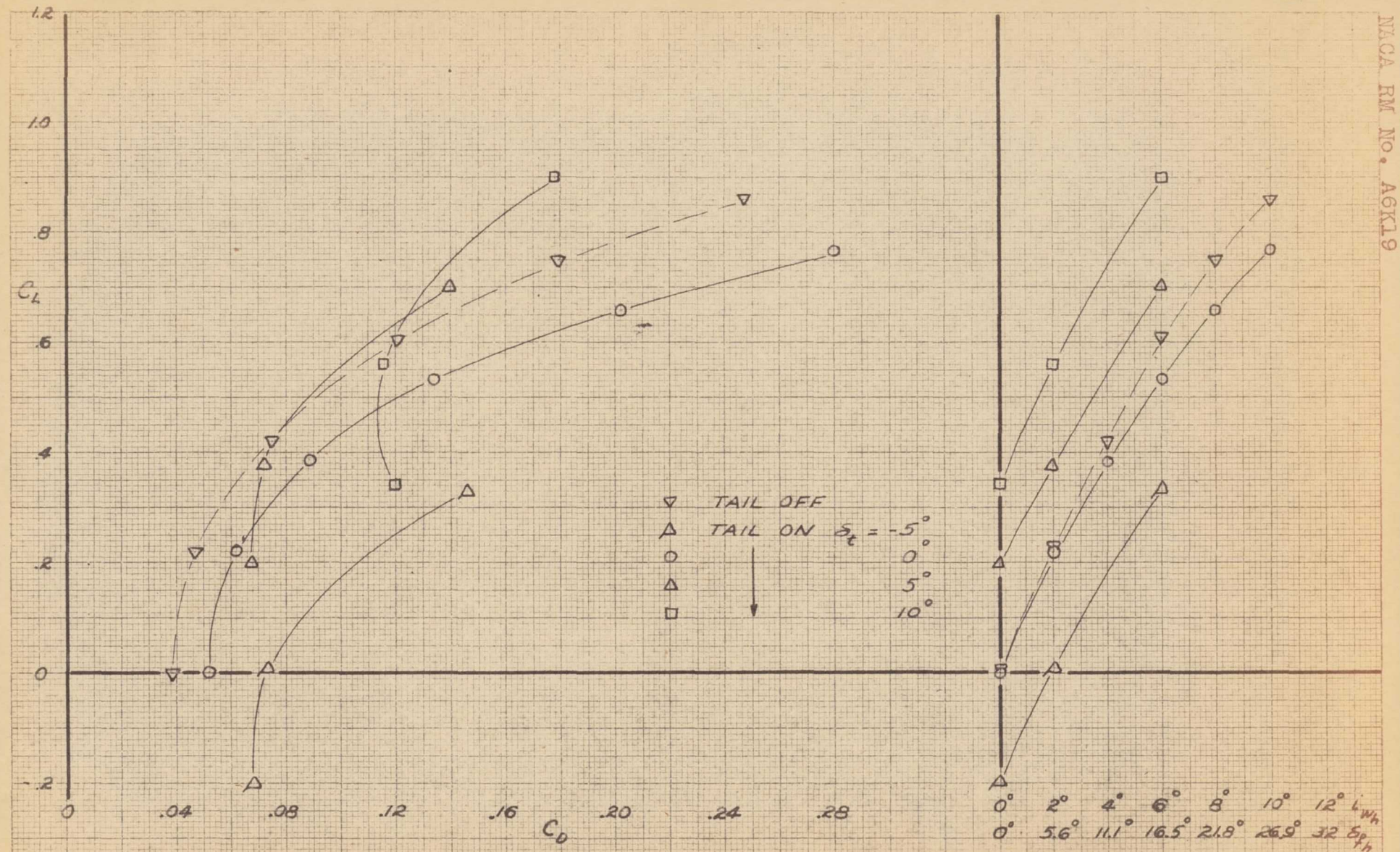

(i) M, 0.85

FIGURE 21. - CONTINUED.

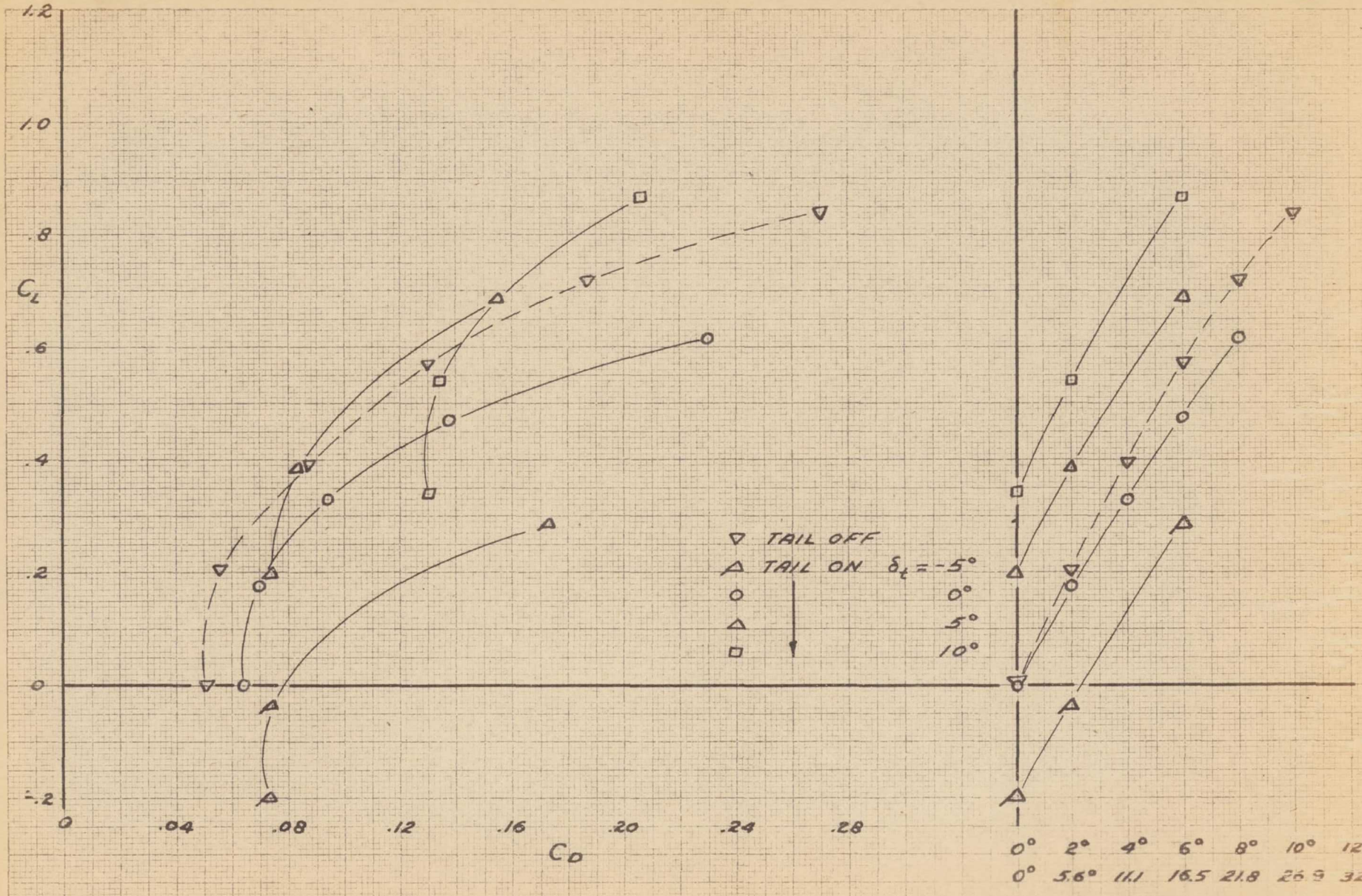

(j) M, 0.875

FIGURE 21.- CONCLUDED

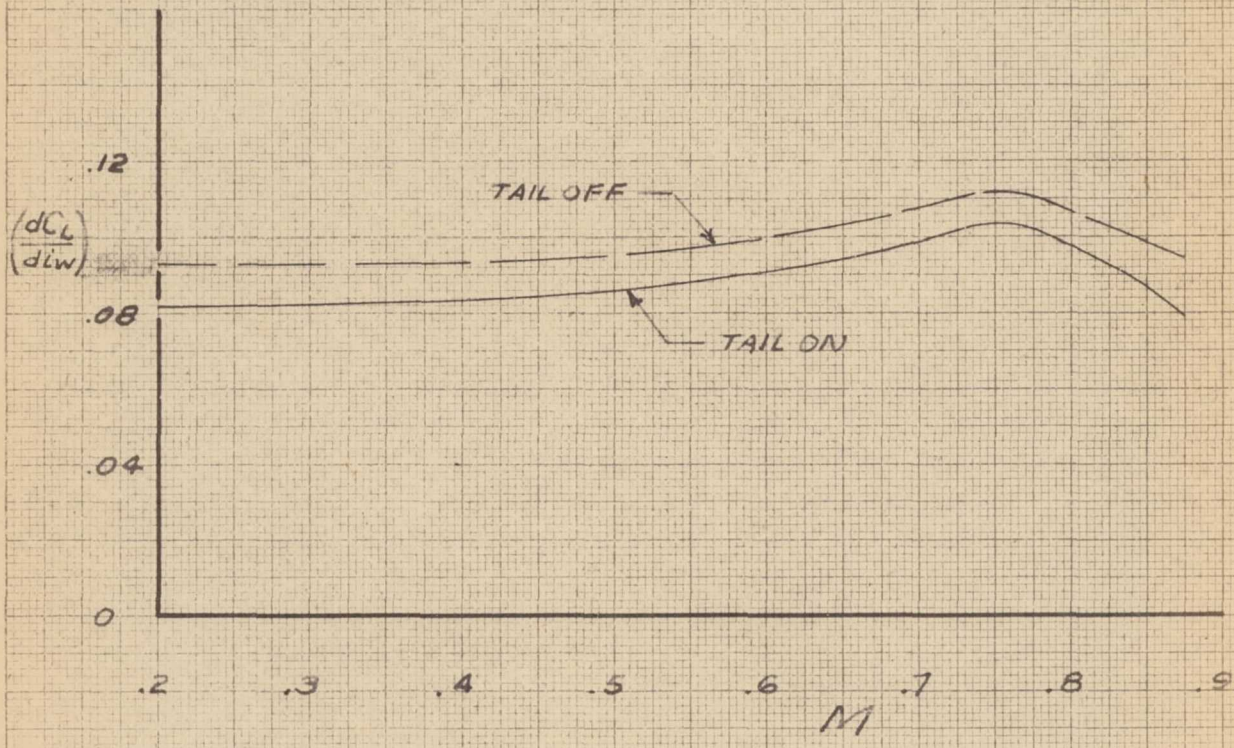

FIGURE 22.- VARIATION WITH MACH NUMBER OF THE LIFT-CURVE SLOPE FOR LINKED DEFLECTIONS OF THE HORIZONTAL WING AND FLAPS FOR THE FULL-SCALE MODEL OF THE CONSOLIDATED VULTEE LARK $\alpha, i_{W_h}, \delta_{f_h}, 0°$.

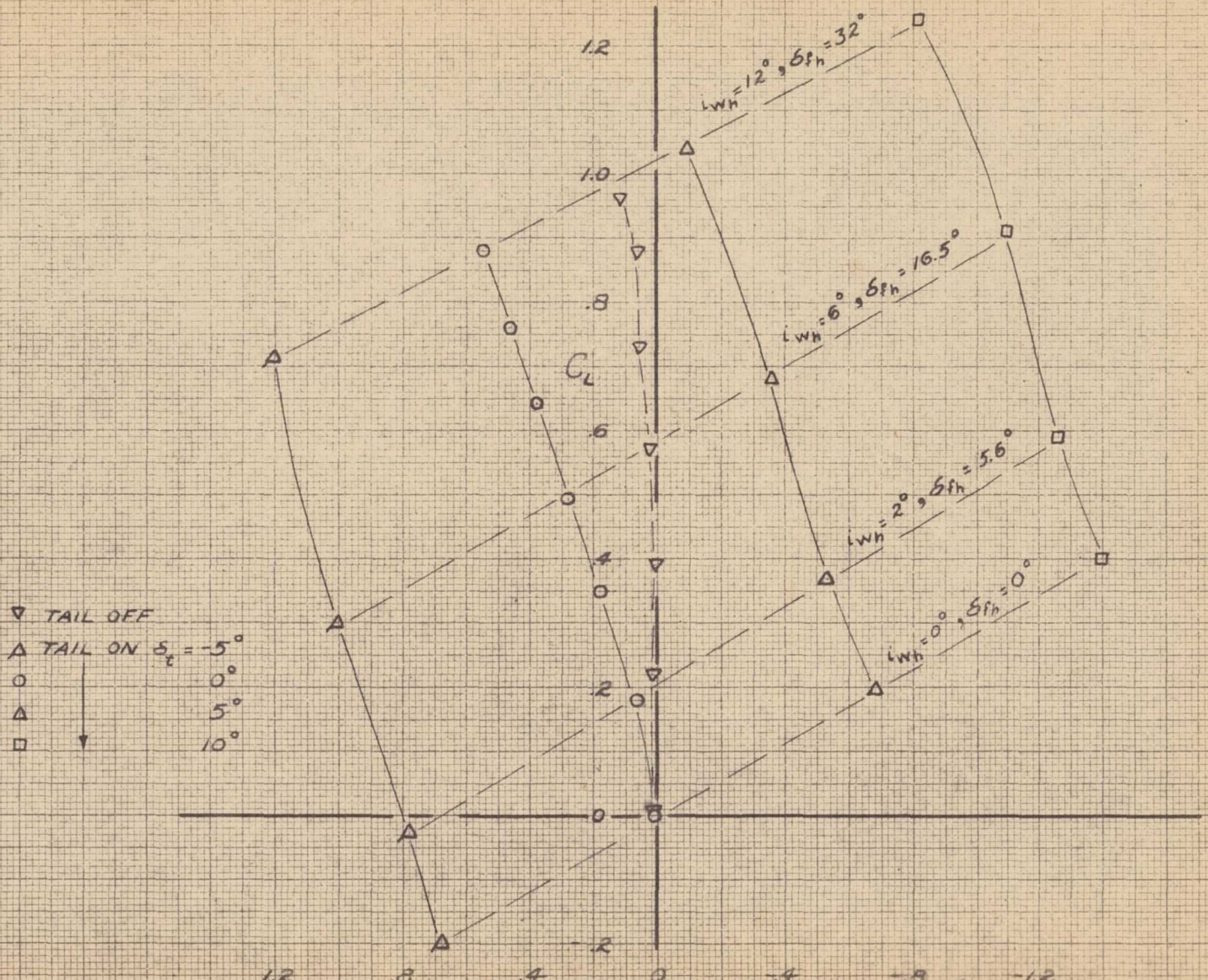

(a) M, 0.2

FIGURE 23. - VARIATION OF PITCHING-MOMENT COEFFICIENT WITH COEFFICIENT FOR LINKED DEFLECTIONS OF THE HORIZONTAL WING AND FLAPS OF THE FULL-SCALE MODEL OF THE CONSOLIDATED VULTEE LARK. α, i_{W_v}, δ_{f_v}, 0°.

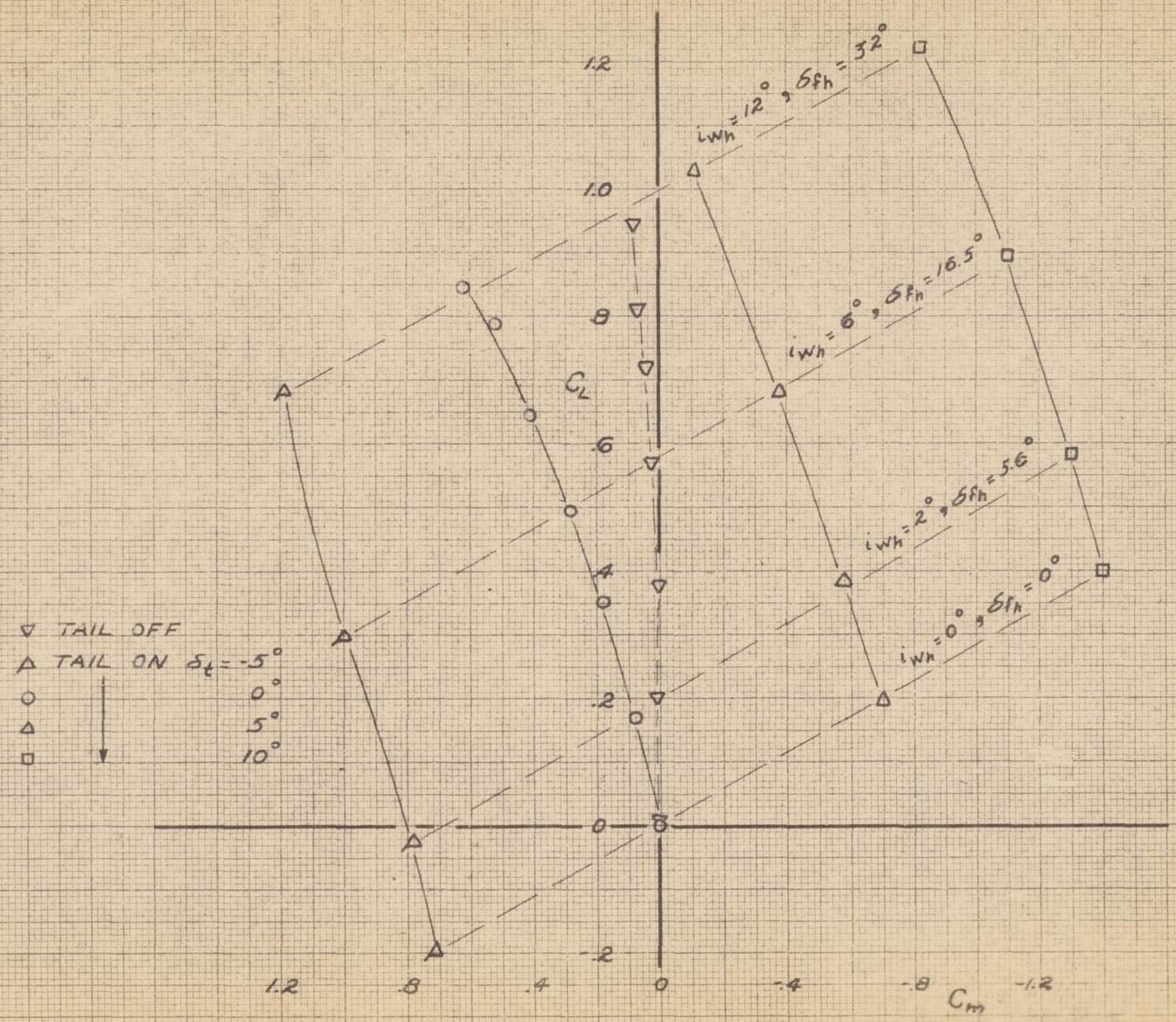

(b) M, 0.4

FIGURE 23.- CONTINUED.

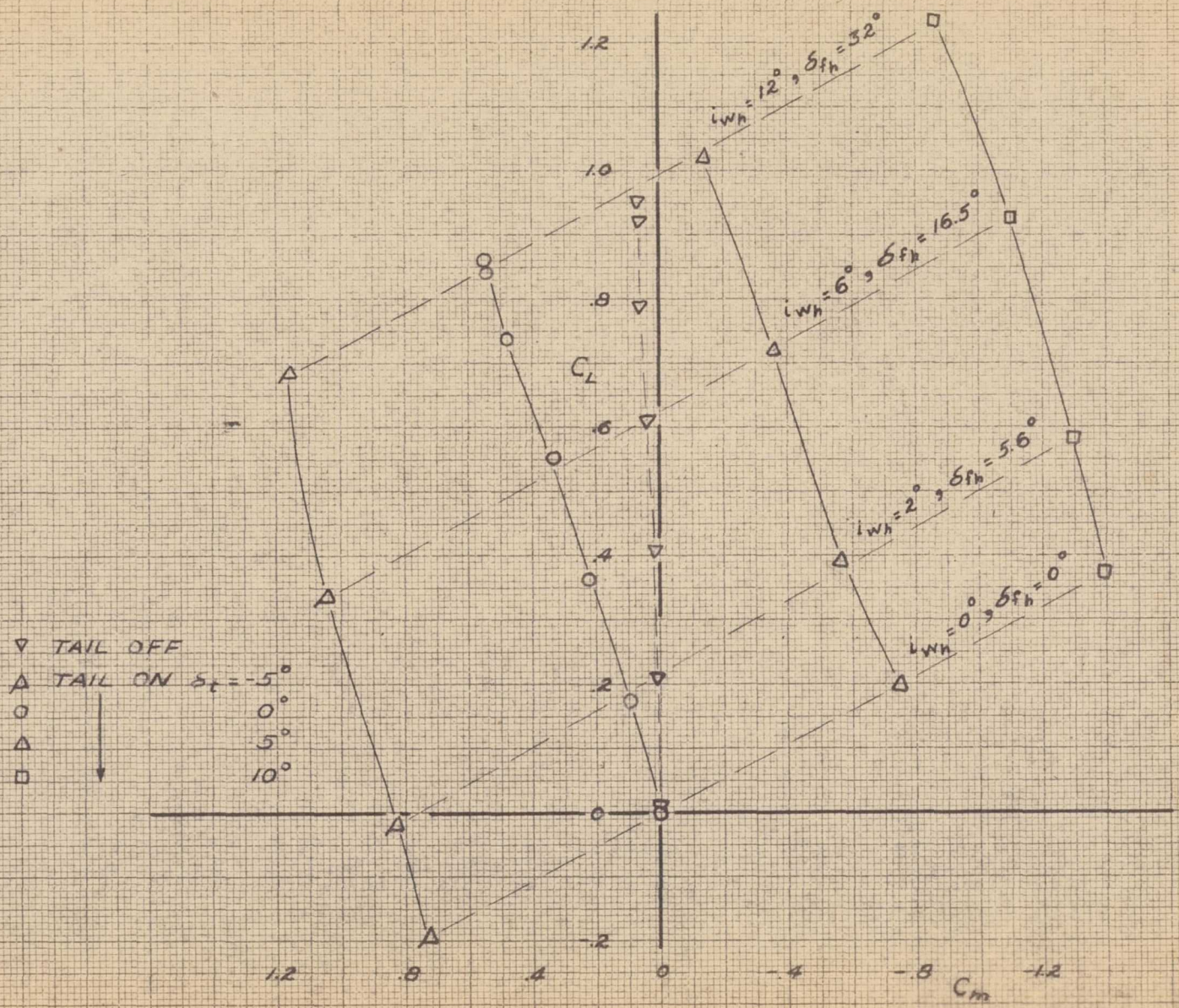

(c) M, 0.6

FIGURE 23.– CONTINUED.

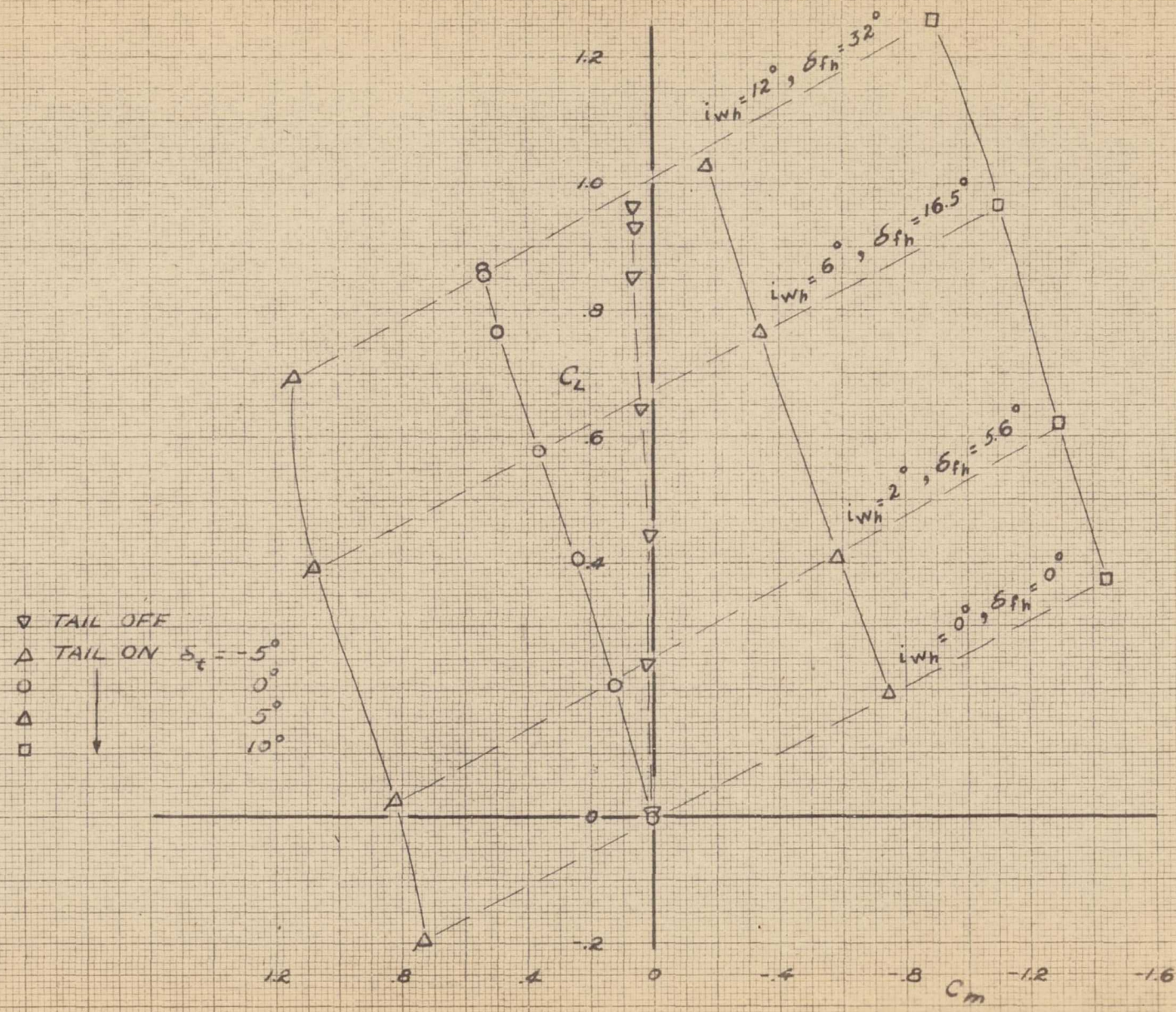

(d) M, 0.7

FIGURE 23.- CONTINUED.

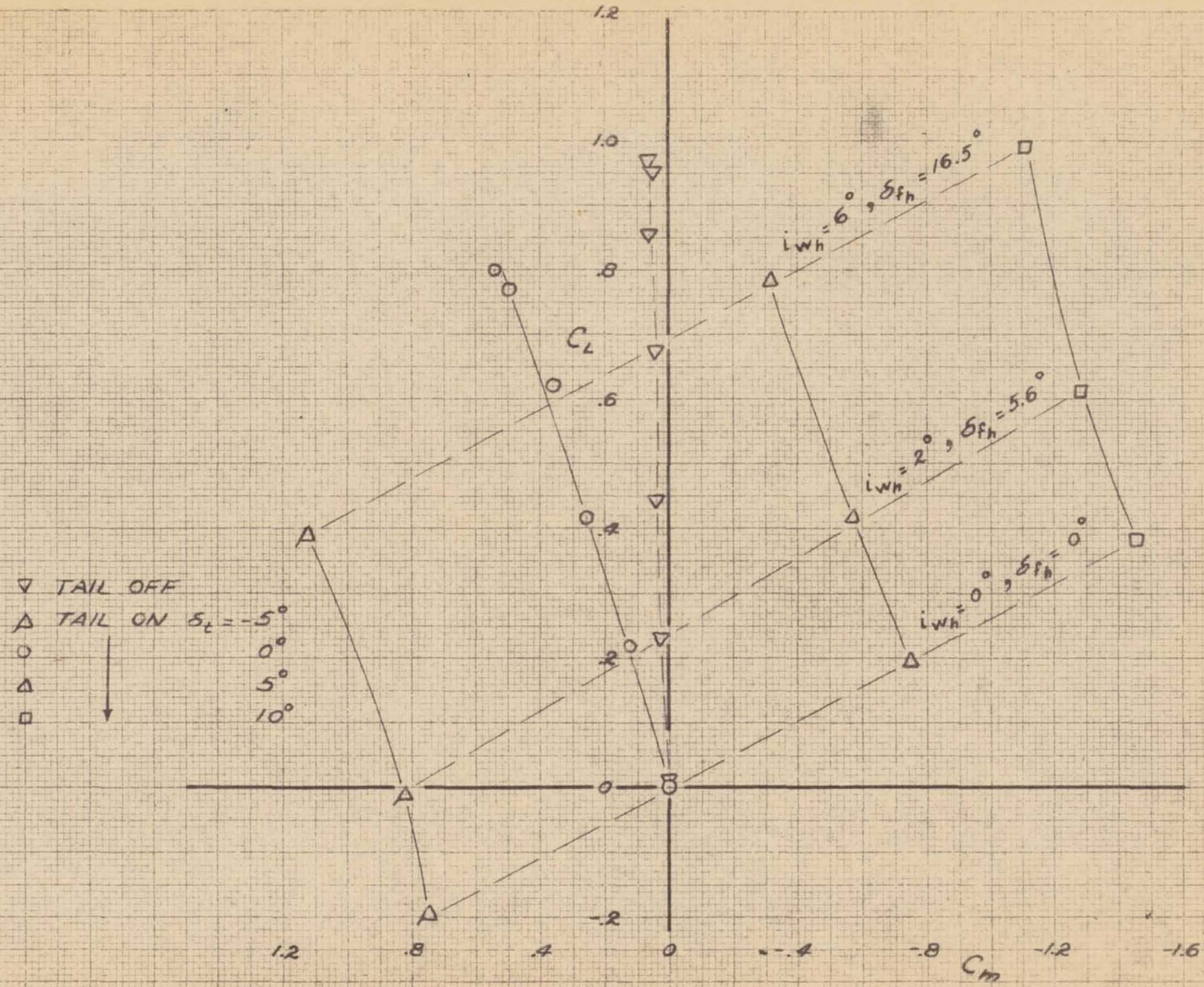

(e) M, 0.75

FIGURE 23.- CONTINUED.

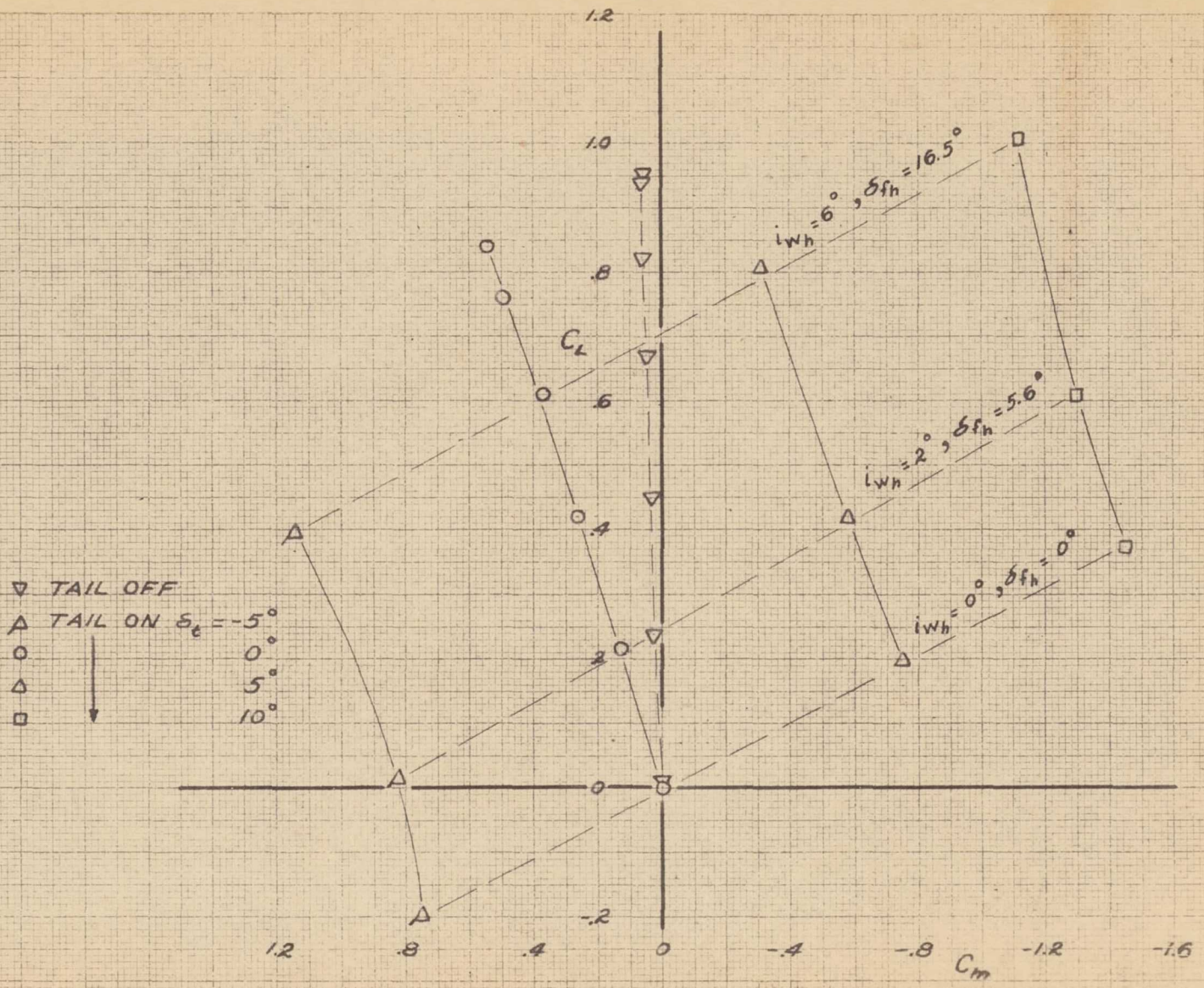

(f) M, 0.775

FIGURE 23.- CONTINUED.

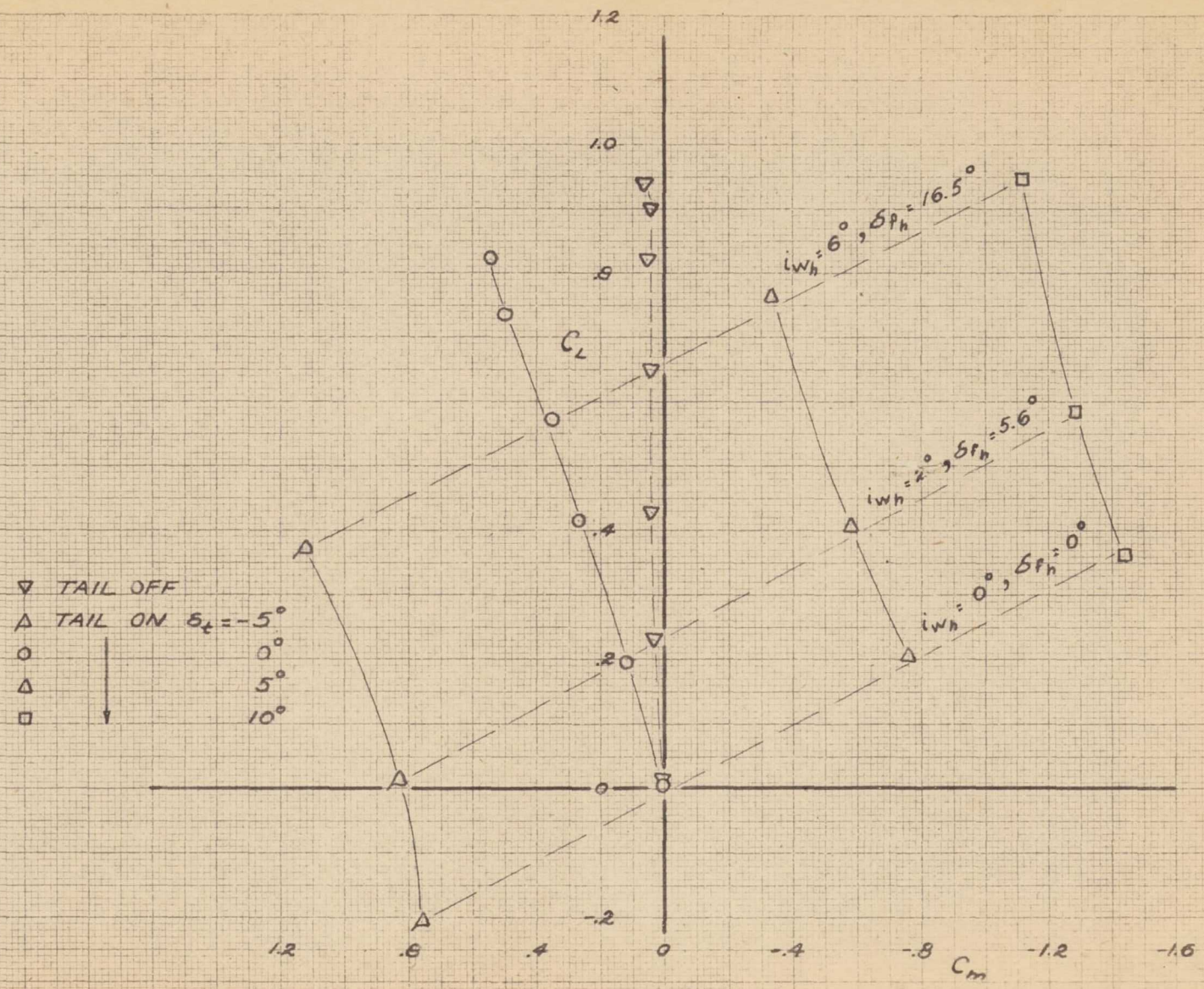

(g) M, 0.8

FIGURE 23.- CONTINUED.

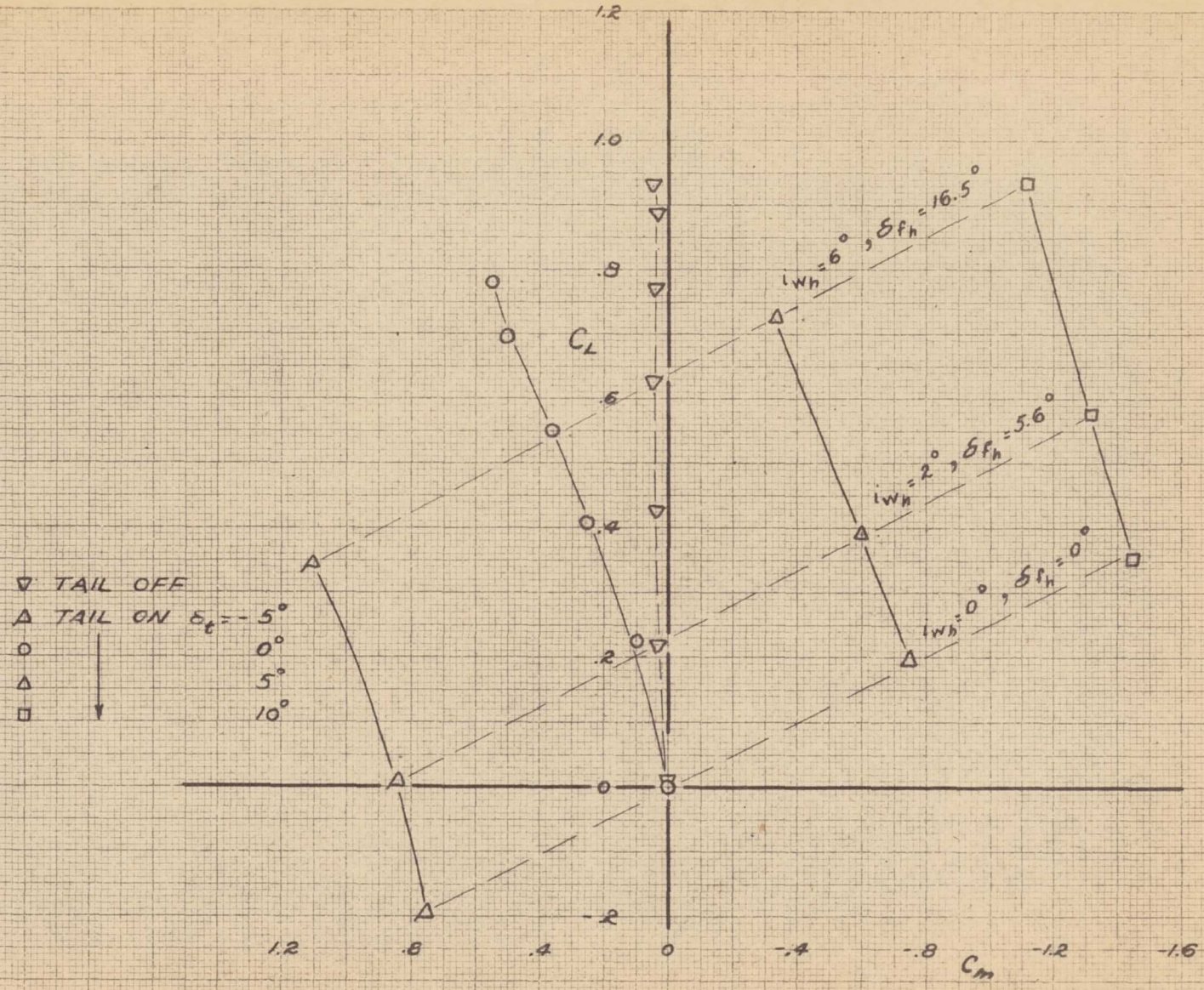

(h) M, 0.825

FIGURE 23.- CONTINUED.

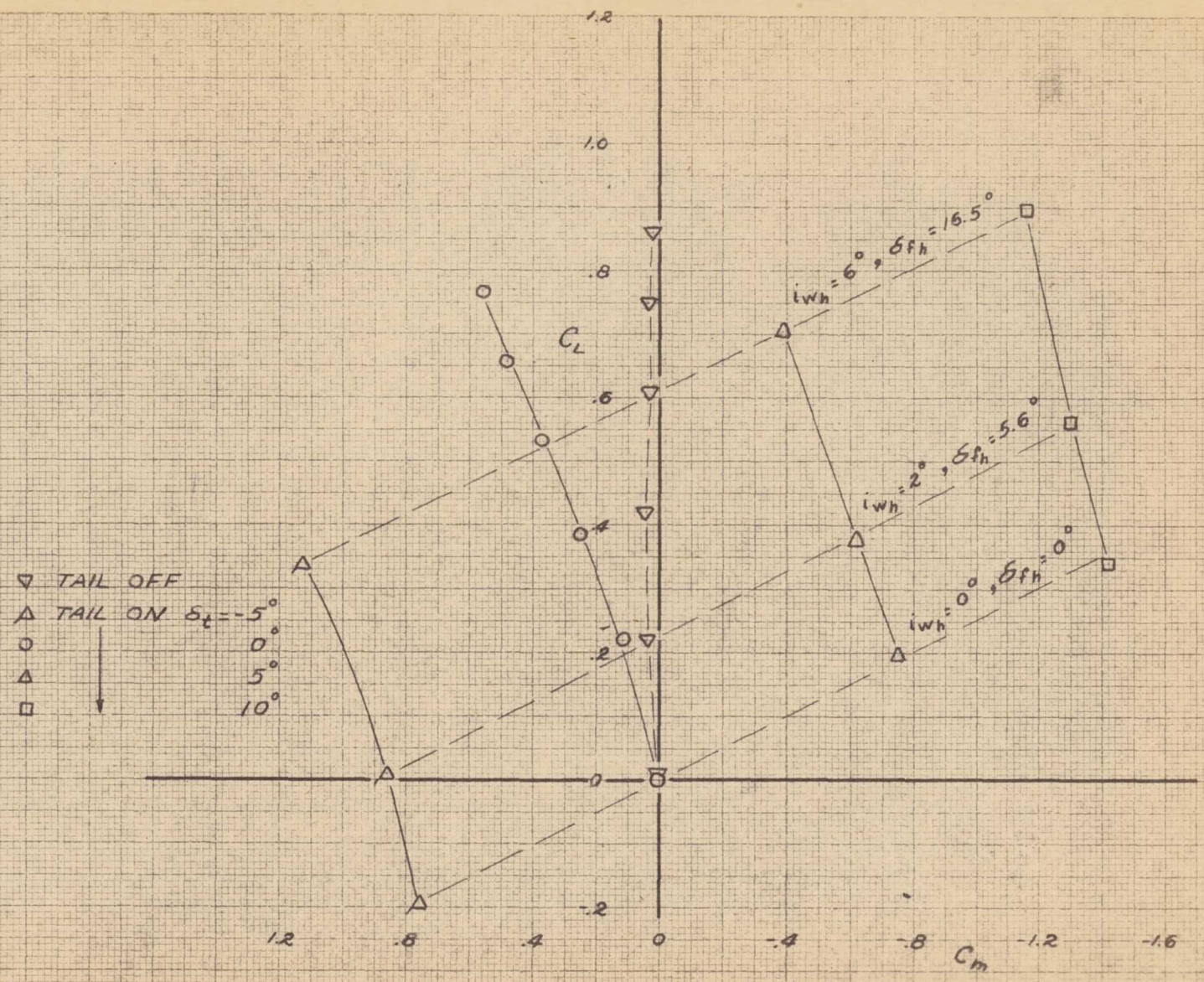

(i) M, 0.85

FIGURE 23.- CONTINUED.

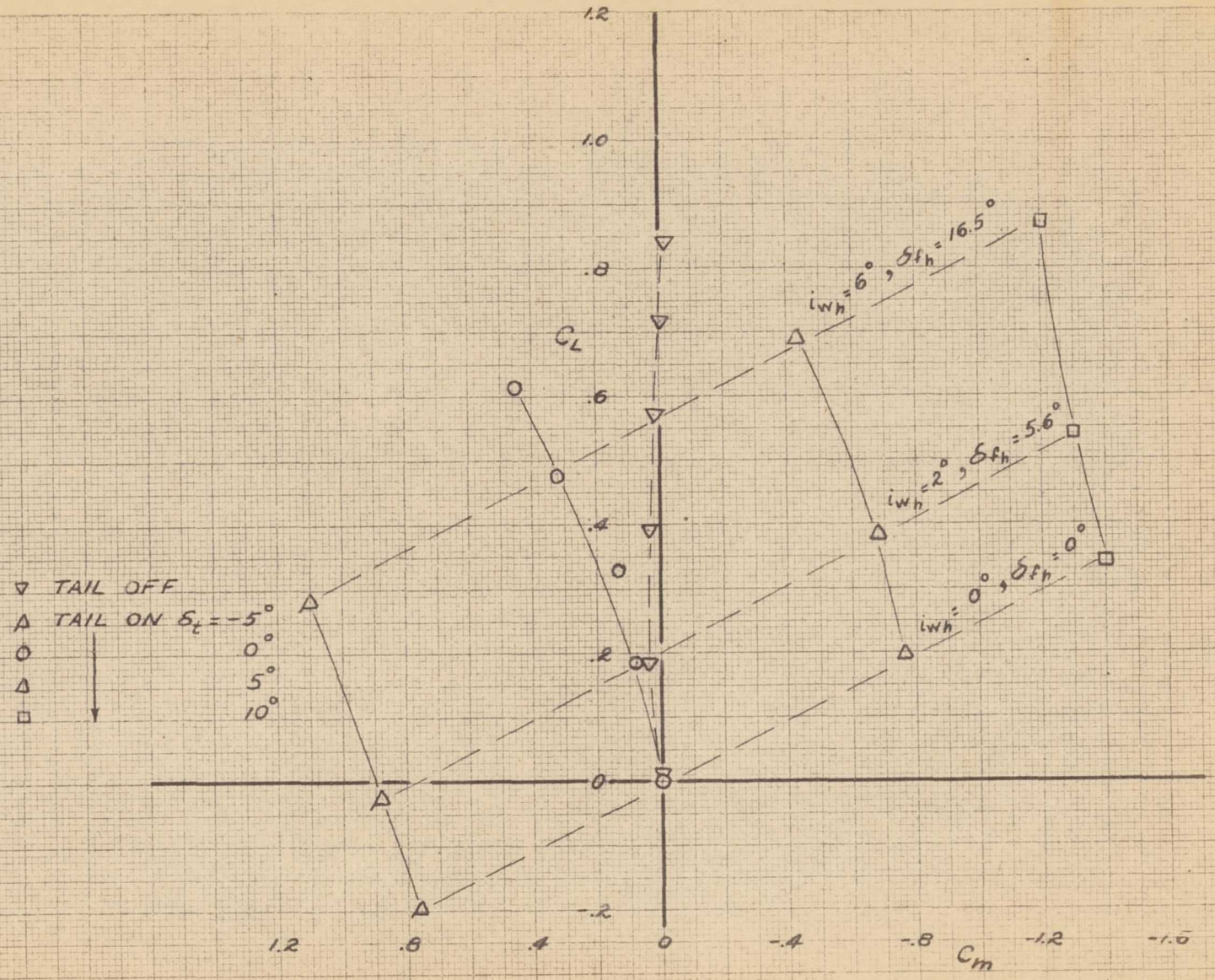

(j) M, 0.875

FIGURE 23.- CONCLUDED.

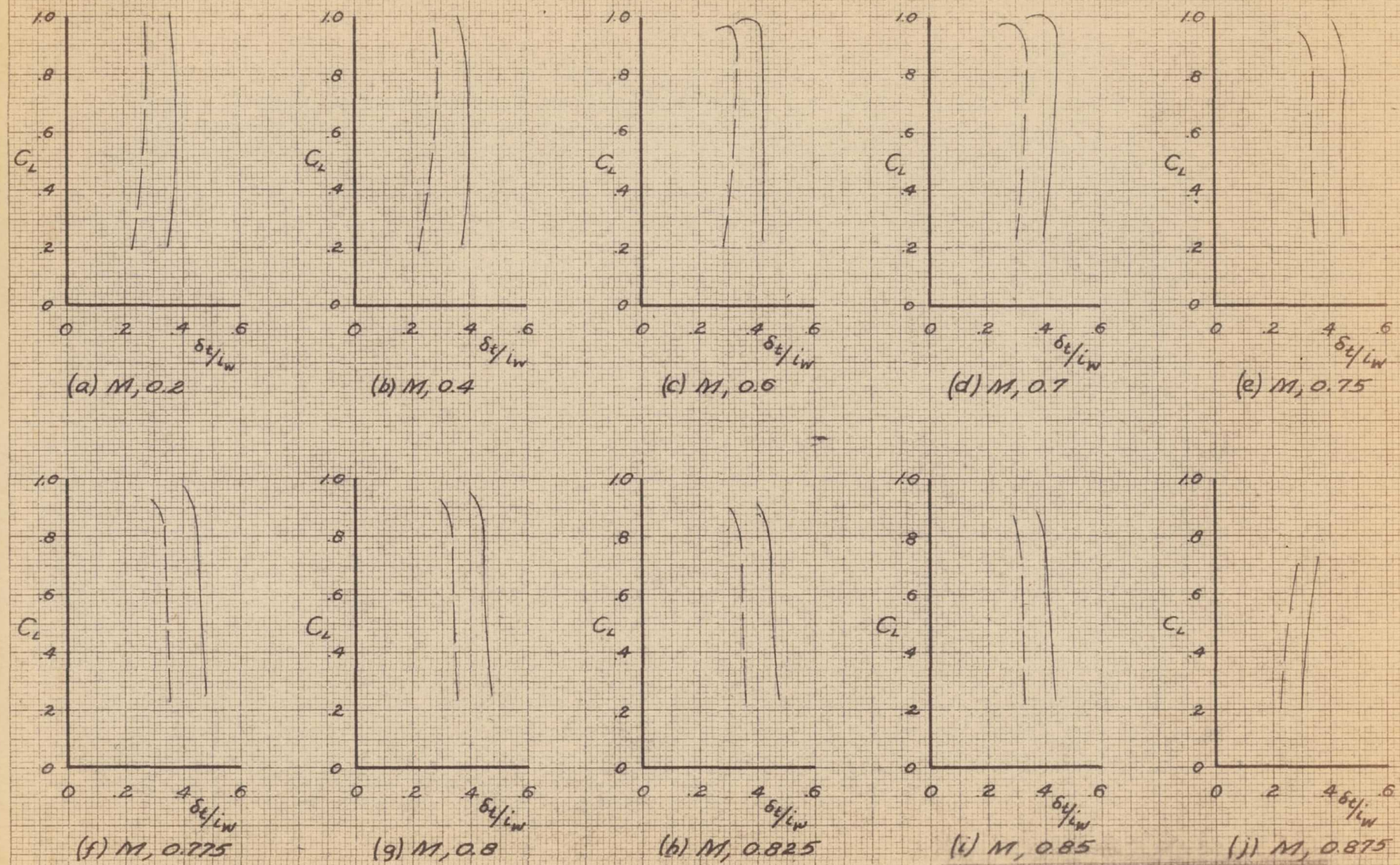

FIGURE 24.- VARIATION OF THE RATIO OF TAIL DEFLECTION TO WING DEFLECTION FOR BALANCE FOR THE FULL-SCALE MODEL OF THE CONSOLIDATED VULTEE LARK.

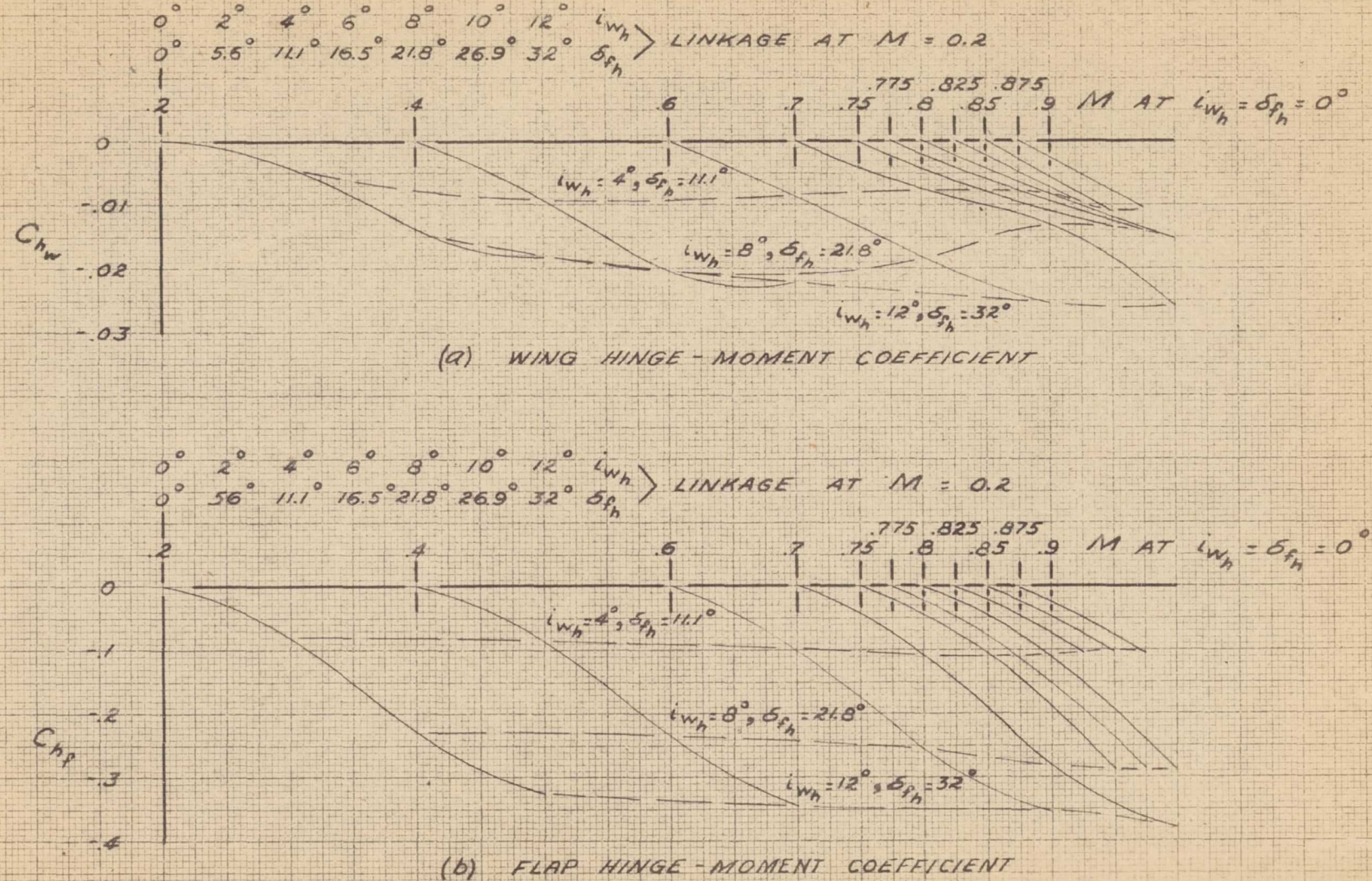

CONFIDENTIAL
NATIONAL ADVISORY COMMITTEE FOR AERONAUTICS

FIGURE 25.- VARIATION OF WING HINGE-MOMENT COEFFICIENT AND OF FLAP HINGE-MOMENT COEFFICIENT WITH LINKED DEFLECTIONS OF THE VERTICAL WING AND FLAPS FOR THE FULL-SCALE MODEL OF THE CONSOLIDATED VULTEE LARK. $\alpha, i_{w_h}, \delta_{f_h}, 0°$

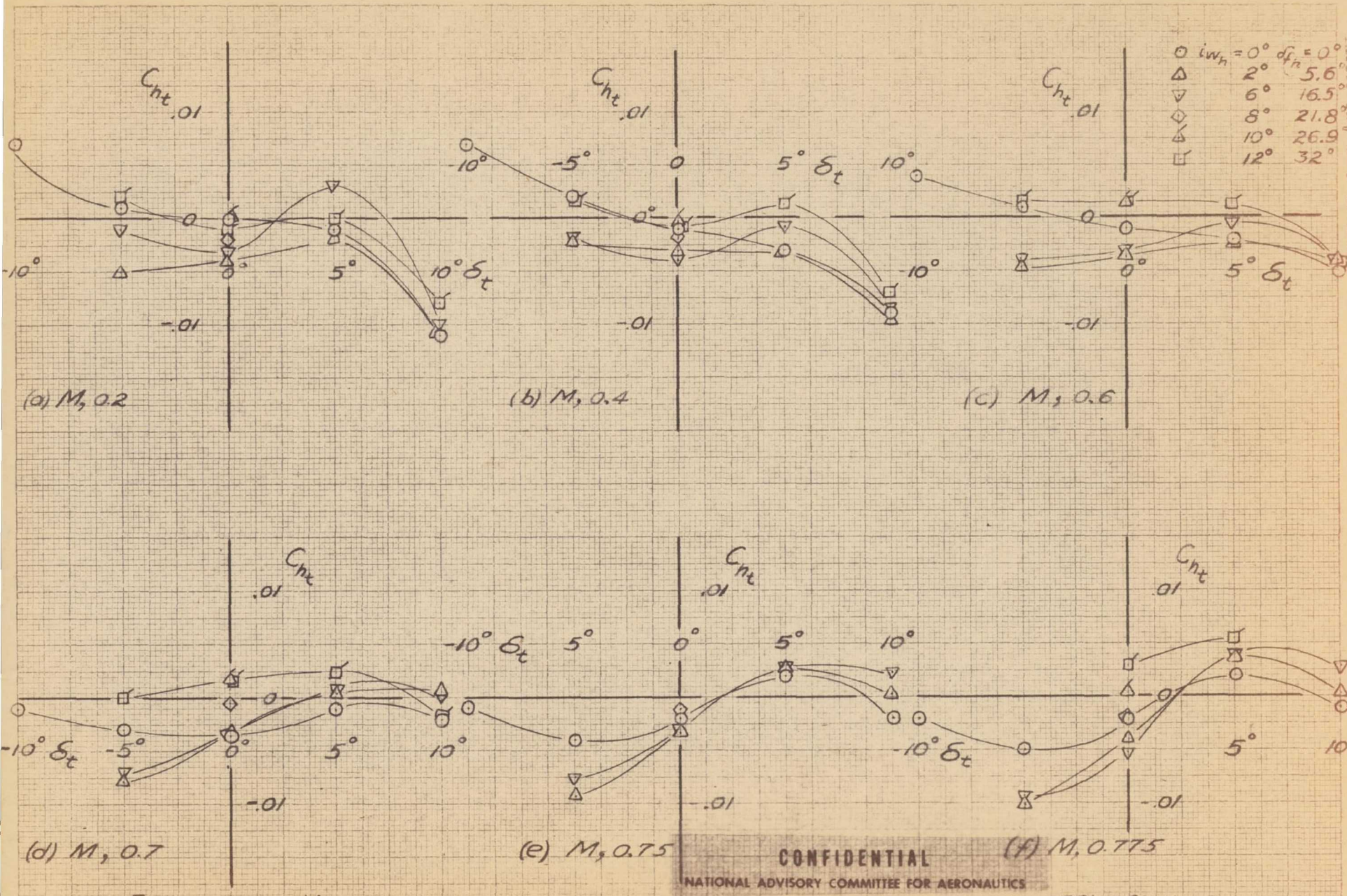

FIGURE 26. - VARIATION OF TAIL HINGE-MOMENT COEFFICIENT WITH TAIL DEFLECTION AT VARIOUS LINKED DEFLECTIONS OF THE HORIZONTAL WING AND FLAP OF THE FULL-SCALE MODEL OF THE CONSOLIDATED VULTEE LARK α, i_{w_h}, δ_{f_h}, 0°.

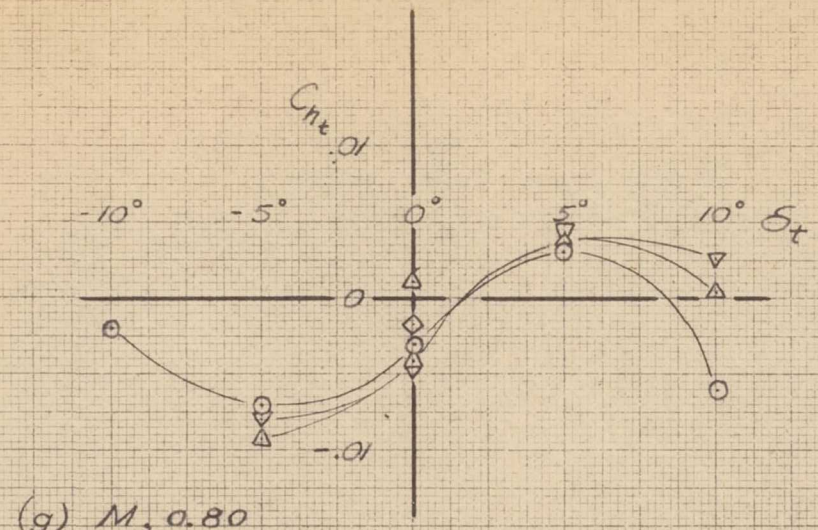

(g) M, 0.80

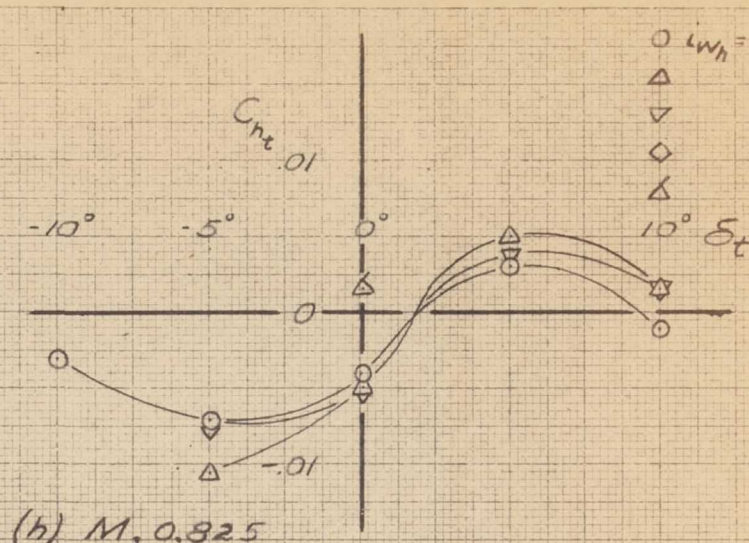

(b) M, 0.825

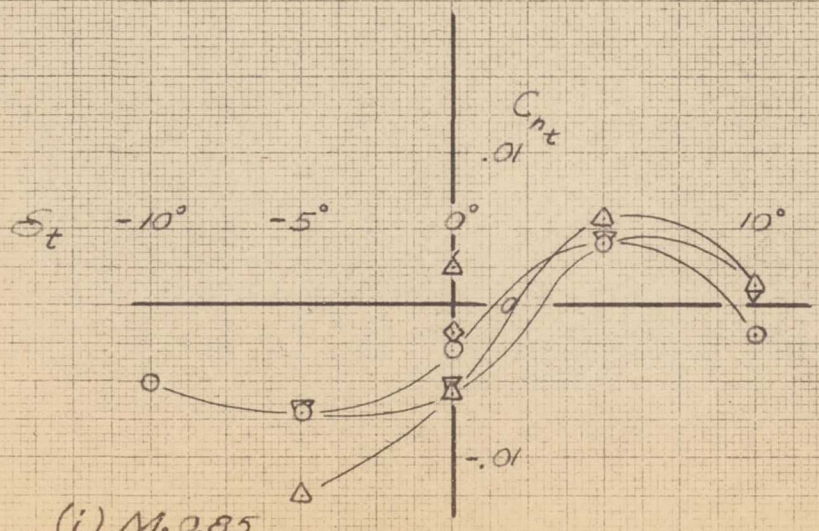

(i) M, 0.85

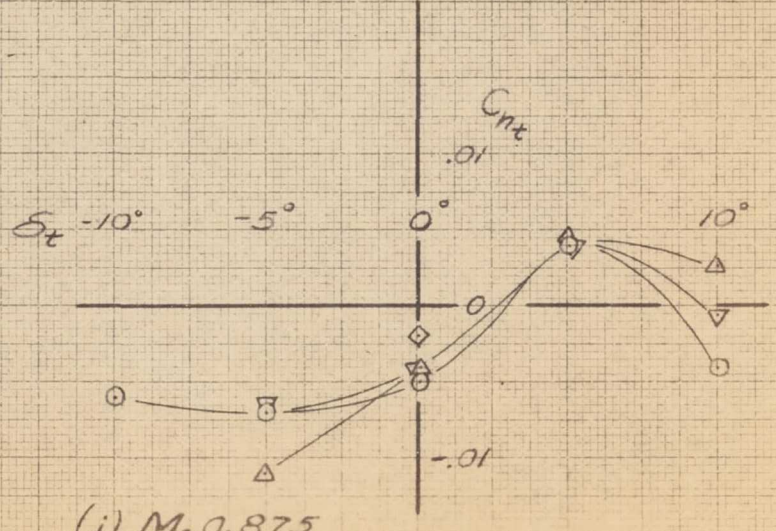

(j) M, 0.875

FIGURE 26. - CONCLUDED.

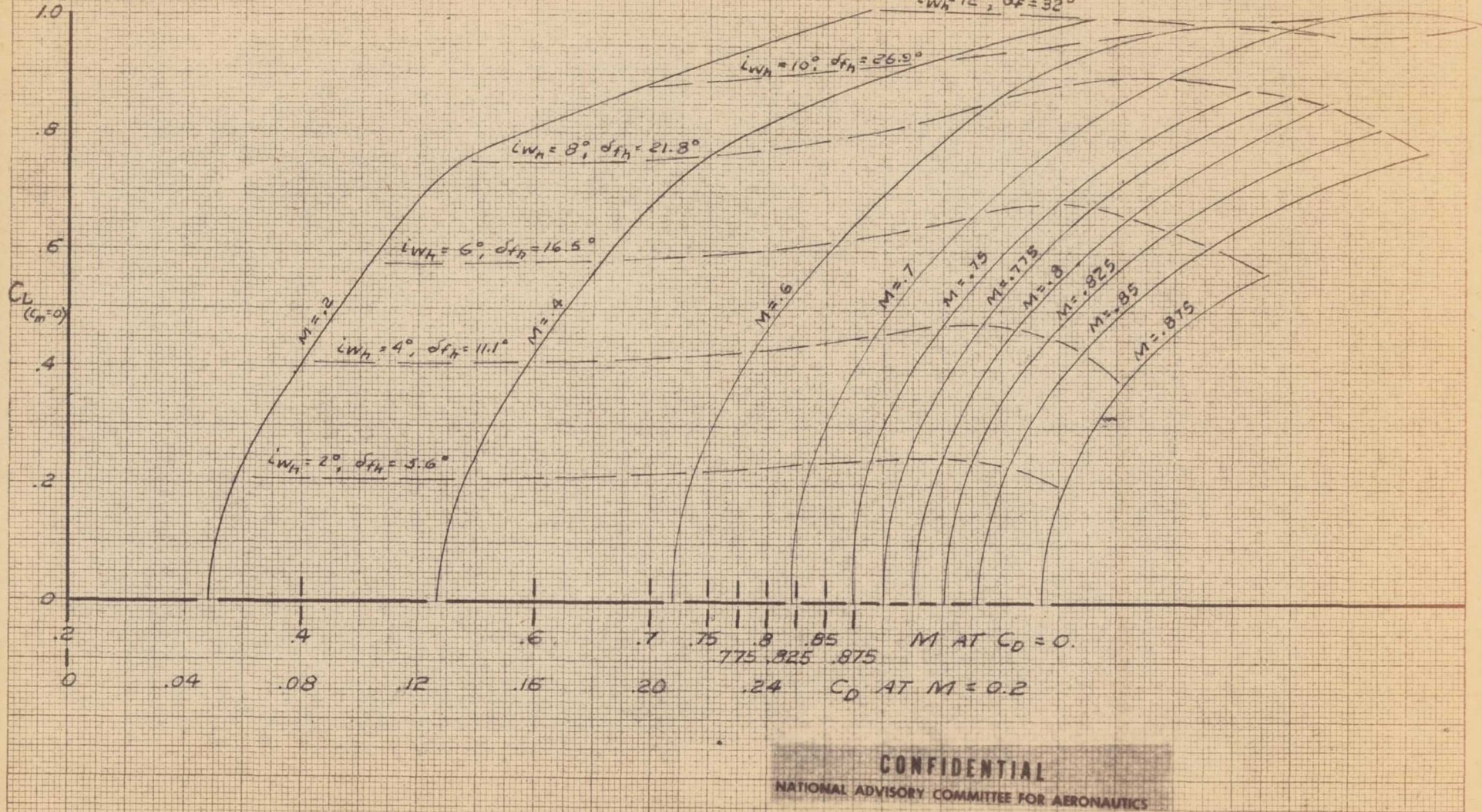

CONFIDENTIAL
NATIONAL ADVISORY COMMITTEE FOR AERONAUTICS

FIGURE 27.- VARIATION OF DRAG COEFFICIENT WITH LIFT COEFFICIENT AT BALANCE (C_m=0) WITH LINKED DEFLECTIONS OF THE HORIZONTAL WING AND FLAPS FOR THE FULL-SCALE MODEL OF THE CONSOLIDATED VULTEE LARK. α, i_{W_H}, δ_{f_H}, 0°.

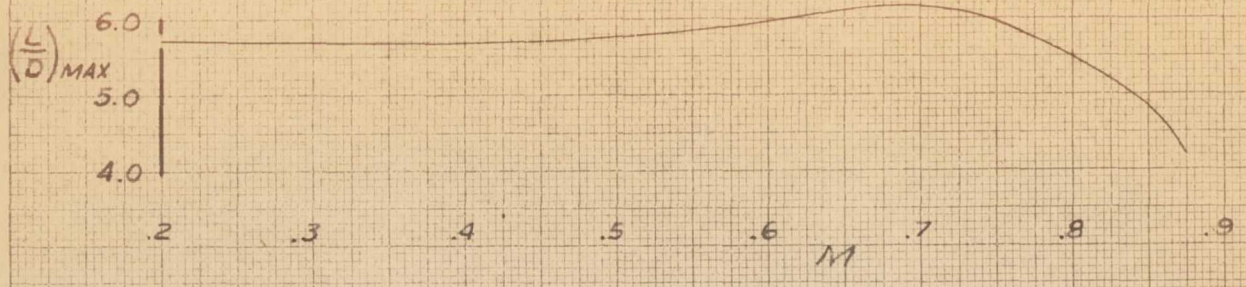

(a) MAXIMUM LIFT-TO-DRAG RATIO

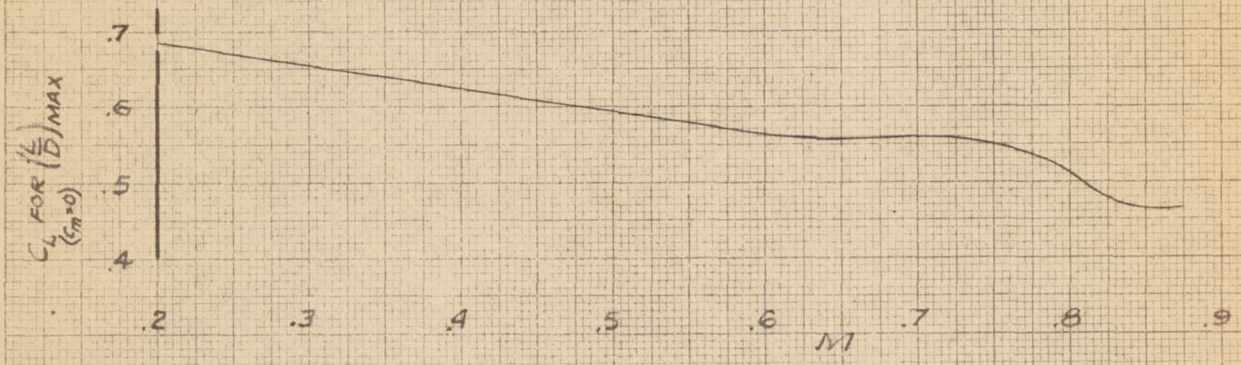

(b) LIFT COEFFICIENT FOR MAXIMUM LIFT-TO-DRAG RATIO.

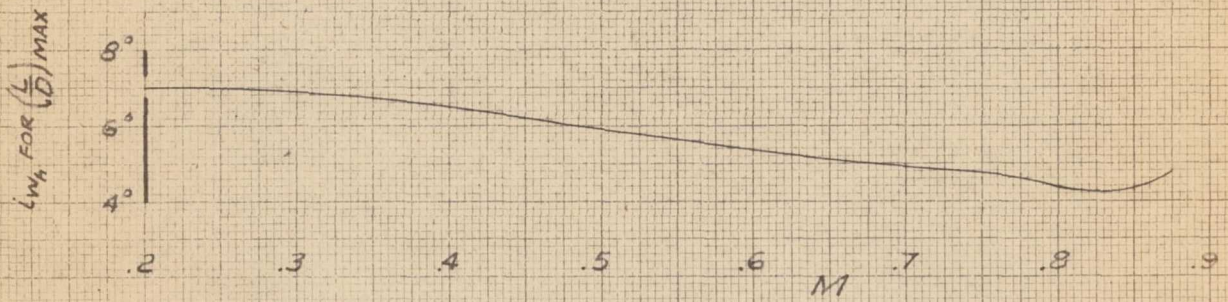

(c) WING INCIDENCE FOR MAXIMUM LIFT-TO-DRAG RATIO.

FIGURE 28.- VARIATION WITH MACH NUMBER OF THE MAXIMUM LIFT-TO-DRAG RATIOS AND THE CORRESPONDING LIFT COEFFICIENTS AND WING INCIDENCES AT BALANCE ($C_m=0$) FOR THE FULL-SCALE MODEL OF THE CONSOLIDATED VULTEE LARK WITH THE WING-FLAP LINKAGE. α, i_{W_V}, δ_{f_V}, 0°

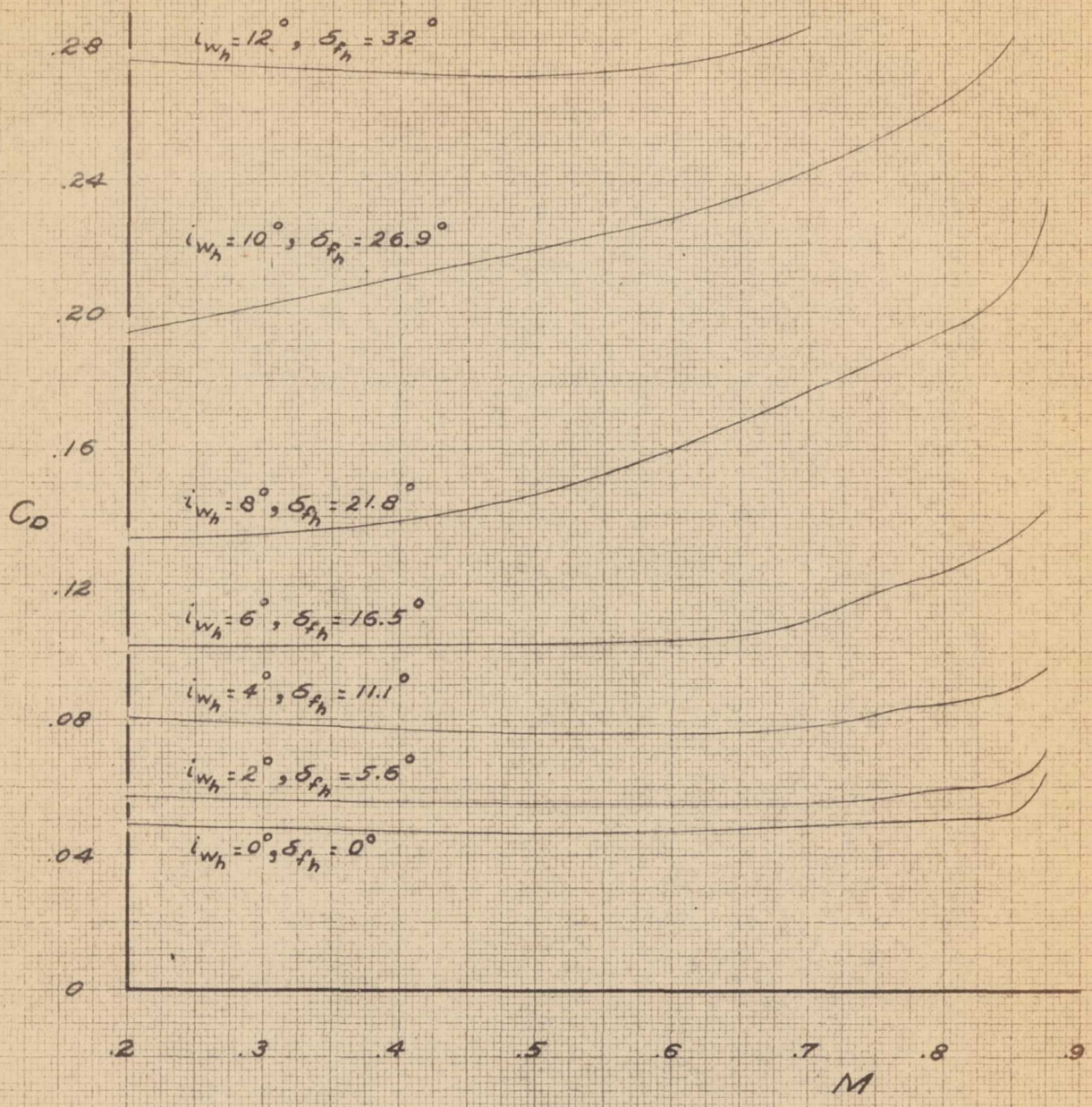

FIGURE 29.- VARIATION OF DRAG COEFFICIENT WITH MACH NUMBER AT BALANCE ($C_m = 0$) FOR LINKED DEFLECTIONS OF THE HORIZONTAL WING AND FLAPS FOR THE FULL-SCALE MODEL OF THE CONSOLIDATED VULTEE LARK. α, i_{w_h}, δ_{f_h}, 0°.

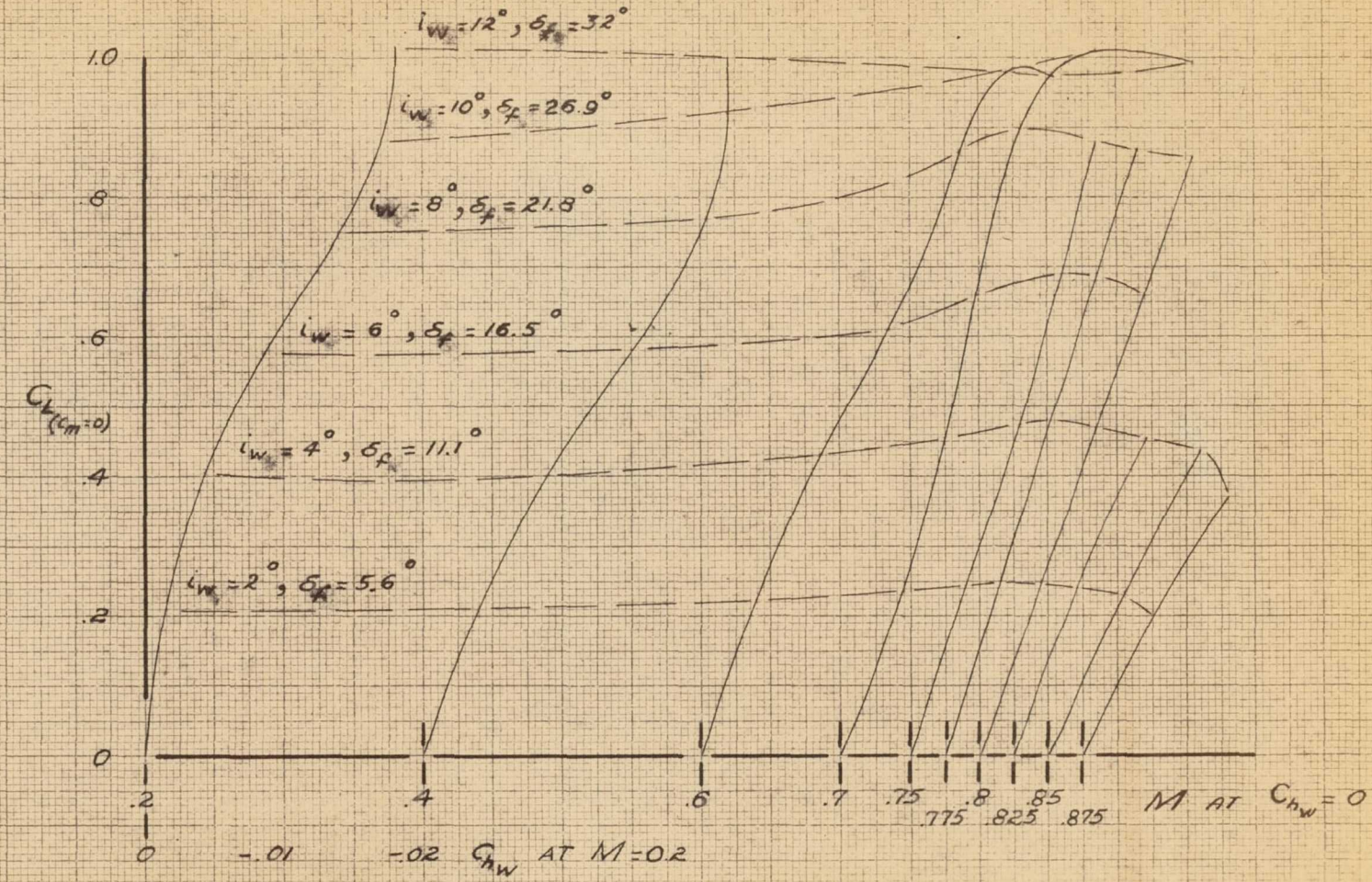

FIGURE 30.- VARIATION OF WING HINGE-MOMENT COEFFICIENT WITH LIFT COEFFICIENT AT BALANCE (PITCHING MOMENT = 0) FOR LINKED DEFLECTIONS OF HORIZONTAL WING AND FLAPS FOR THE FULL-SCALE MODEL OF THE CONSOLIDATED VULTEE LARK. $\alpha, i_{w_v}, \delta_{f_v}, 0°$.

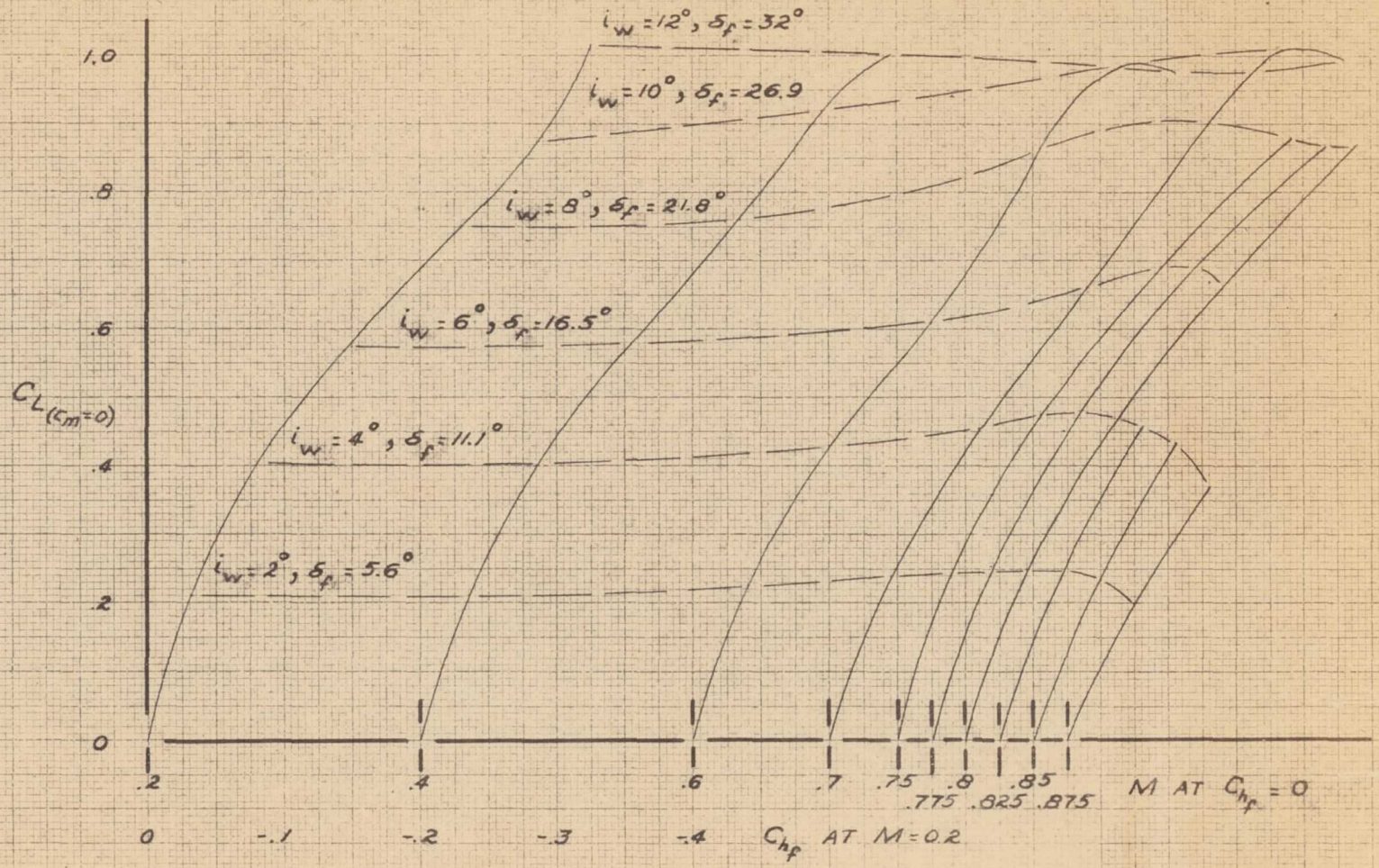

CONFIDENTIAL
NATIONAL ADVISORY COMMITTEE FOR AERONAUTICS

FIGURE 31.- VARIATION OF FLAP HINGE-MOMENT COEFFICIENT WITH LIFT COEFFICIENT AT BALANCE ($C_m = 0$) FOR LINKED DEFLECTIONS OF THE HORIZONTAL WING AND FLAPS OF THE FULL-SCALE MODEL OF THE CONSOLIDATED VULTEE LARK. $\alpha, i_{w_V}, \delta_{f_V}, 0°$.

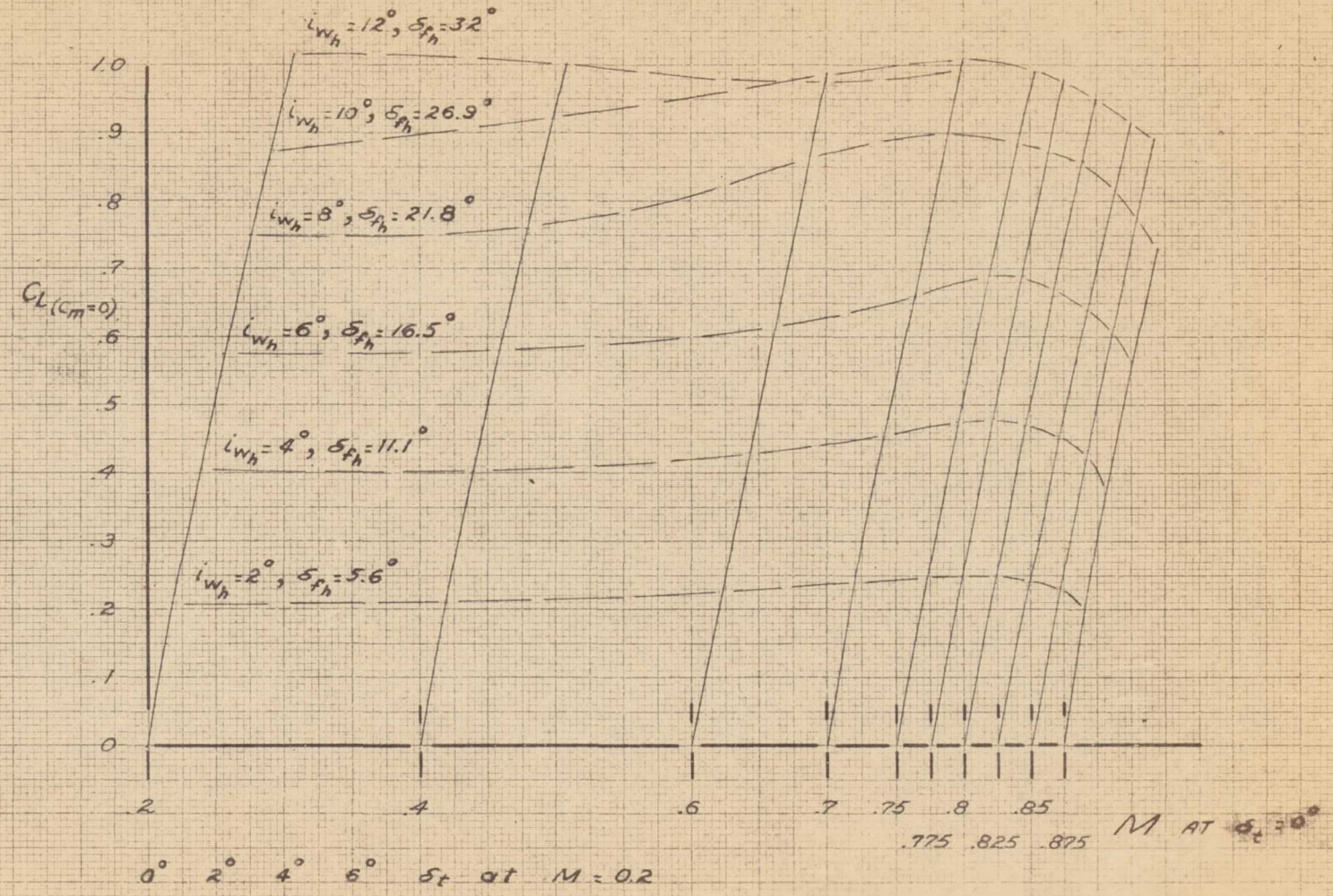

CONFIDENTIAL
NATIONAL ADVISORY COMMITTEE FOR AERONAUTICS

FIGURE 32.- VARIATION OF TAIL DEFLECTION WITH LIFT COEFFICIENT AT BALANCE ($C_m = 0$) WITH LINKED DEFLECTIONS OF THE HORIZONTAL WING AND FLAPS FOR THE FULL-SCALE MODEL OF THE CONSOLIDATED VULTEE LARK. α, i_{w_v}, δ_{f_v}, 0°.

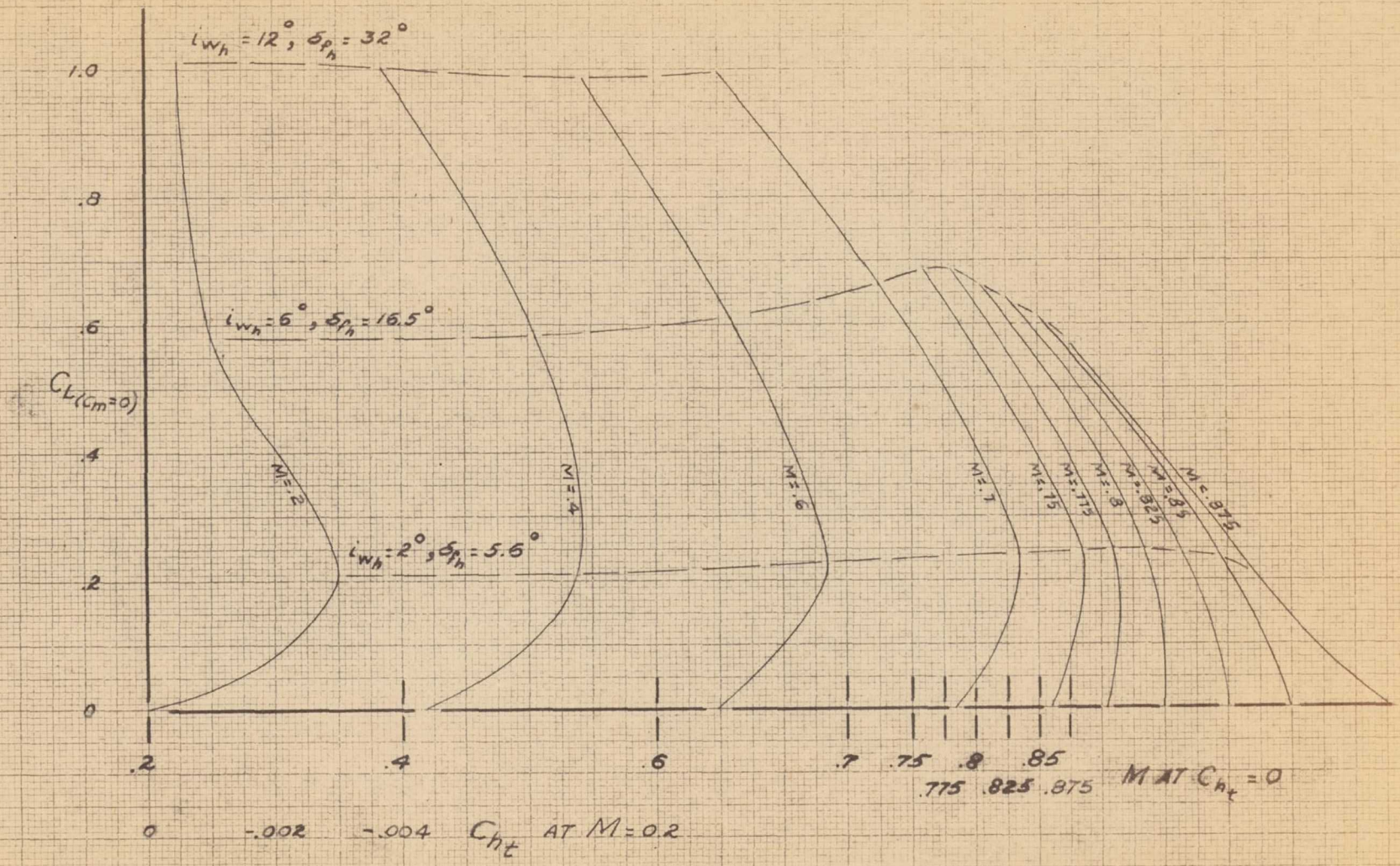

CONFIDENTIAL
NATIONAL ADVISORY COMMITTEE FOR AERONAUTICS

FIGURE 33.- VARIATION OF TAIL HINGE-MOMENT COEFFICIENT WITH LIFT COEFFICIENT AT BALANCE ($C_m = 0$) WITH LINKED DEFLECTIONS OF THE HORIZONTAL WING AND FLAPS FOR THE FULL-SCALE MODEL OF THE CONSOLIDATED VULTEE LARK. α, i_{w_V}, δ_{f_V}, 0°.

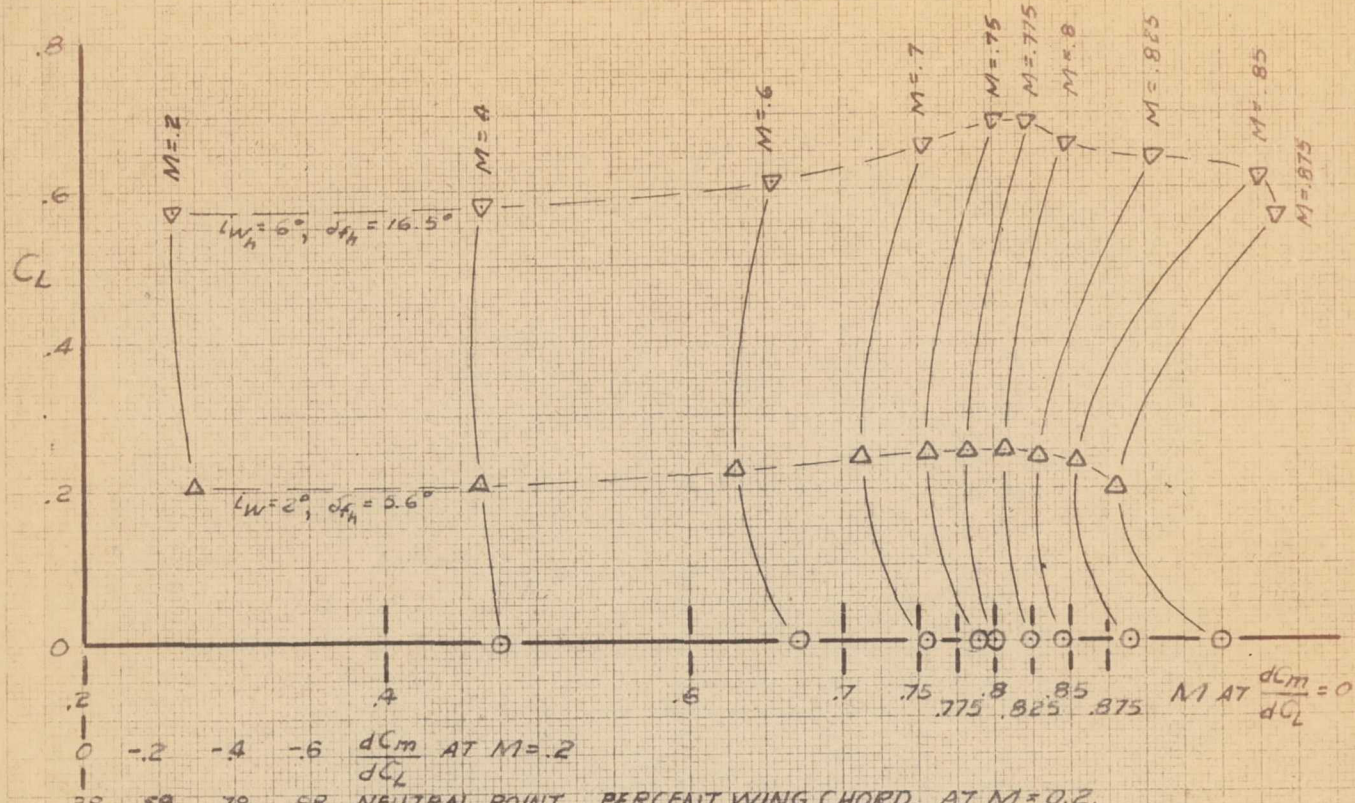

(a) VARIATION WITH LIFT COEFFICIENT

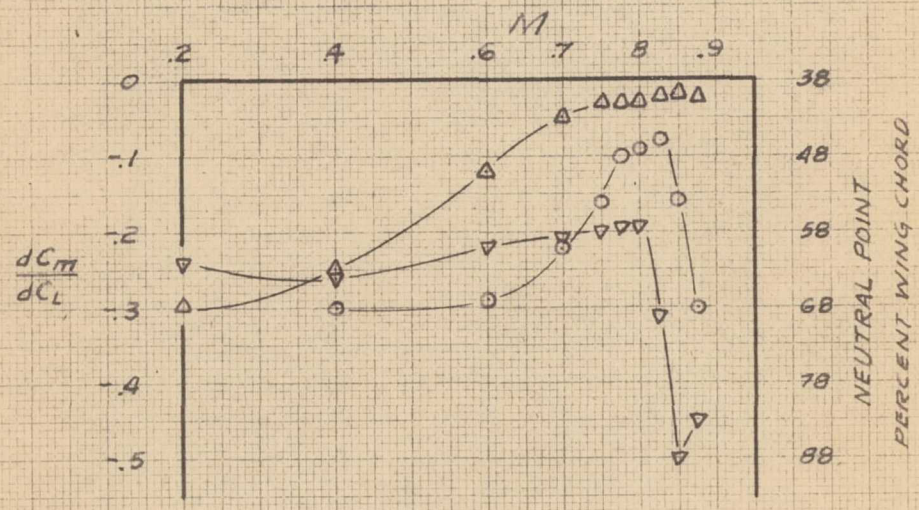

(b) VARIATION WITH MACH NUMBER

FIGURE 34.- STATIC LONGITUDINAL STABILITY AND NEUTRAL-POINT LOCATION AT BALANCE (C_m=0) FOR THE FULL-SCALE MODEL OF THE CONSOLIDATED VULTEE LARK. α, i_{W_V}, δ_{f_V}, 0°.